63-2-4

REPORT
of the
AD HOC PANEL ON
ELECTROMAGNETIC
PROPAGATION

ACAFSC: 103

ADVISORY COMMITTEE TO AIR FORCE SYSTEMS COMMAND
National Academy of Sciences
National Research Council

REPORT

of the

AD HOC PANEL ON
ELECTROMAGNETIC PROPAGATION

Final report - February 1963
~~1962~~

This work was supported by the
Air Force Systems Command
Under Contract AF 18 (600) - 1895

ERRATA*/

Report Title: "Report of the Ad Hoc Panel on Electromagnetic Propagation" ACAFSC: 103

Page	Line	Correction
i	5	ADD: Final Report-February 1963
i.a	--	Replace information concerning the draft status of the report with the following paragraphs:

PREFACE

The Chairman of the Ad Hoc Panel on Electromagnetic Propagation appointed Mr. David K. Barton as editor of the panel report. Mr. Barton compiled the report from contributions of the various panel members, including his own material.

The report was initially issued as a draft awaiting comments by the panel members. The inclusion of the Errata Sheets now permits issuance of this report in its final form, essentially endorsed by all panel members.

---

*/ Additional comments and suggestions by the authors which were not amenable to this format are on file in the office of the Advisory Committee to the Air Force Systems Command.

Page	Line	Correction
1	13	DELETE:...beginning to, if not already...
5	1	CHANGE: difference to differences
5	6	Section 2.2b: errors associated with mean atmosphere should be read as "bias errors."
22	9	CHANGE: $\sqrt{\csc B}$ to $\sqrt{\csc\theta_o}$
27	8	CHANGE: monotomically to monotonically
20	10	CHANGE: sporatic to sporadic
59	3	CHANGE: last term in equation (3-6) to $\frac{dn}{n_i}$
61	1	ADD: "the" to read,...evaluation of the integral...
61	11	CHANGE: second line of equation (3-12 to read, $\bar{n}_i = \ldots$
61	19	CHANGE: equation (3-15) to read $\theta_t = \theta_o - \delta$
62	9	CHANGE: equation (3-18) to read $h = r\left[\sqrt{\left(1 + \frac{h_s}{r}\right)^2 + \left(\frac{R}{r}\right)^2 + 2\left(1 + \frac{h_s}{r}\right)\frac{R}{r}\sin\theta_o} - 1\right]$
63	4	CHANGE: equation (3-21) to the following which was suggested by the author as being more precise.

Page	Line	Correction
63	4	$\phi = \frac{k}{r} \sum_{i=0}^{m} \int_{h_i}^{h_{i+1}} \frac{dh}{(1+h/r)\sqrt{n^2(1+h/r)^2 - k^2}}$ in which h_0 is the height of the radar and h_{m+1} is the target height.
63	14	ADD: "$+h_s$" to read $\overline{AC} = \frac{r+h_s}{\cos \phi}$
63	16	ADD: "$-h_s$" to read $\overline{CD} = (r+h) - \frac{r+h_s}{\cos \phi}$
64	3	ADD: "$+h_s$" to read $R_t = \frac{(r+h)\cos \phi - (r+h_s)}{\sin \theta_t}$
64	2	ADD: "$+h_s$" to read $\frac{\sin \phi_t}{(r+h)-r+h_s/\cos \phi}$
64	5	ADD: "$+h_s$" and "h_s/r" to read $\cot \theta_t = \frac{(r+h)\sin \phi}{(r+h)\cos \phi - (r+h_s)} = \frac{\sin \phi}{\cos \phi \frac{1+h_s/r}{1+h/r}}$
64	13	ADD: "using (3-19) and (3-25)" to read and <u>using (3-19) and (3-25)</u>, (3-21) becomes...
66	12	DELETE: paragraph beginning "From a computational..." and all that follows through page 68.
66	12	ADD: the following:

*/ The author feels the standard refraction correction method given here to be better than the form originally suggested.

It appears that equation (3-24) for small values of $\emptyset$ is overly sensitive, a small error in $\emptyset$ generating a large error in θ_t, resulting from the solution depending upon the "long-thin" triangle of ABD of Figure 3-1.

Since the AMR and PMR solutions both rely on this equation, from a computational accuracy and convenience standpoint, it would seem that an acceptable standard method should be based essentially on the NBS procedure. That is, the steps would be:

a. Compute the height to which integration should be performed.

$$h = r\left[\sqrt{\left(1+\frac{h_s}{r}\right)^2 - \left(\frac{R}{r}\right)^2 + 2\left(1+\frac{h_s}{r}\right)\frac{R}{r}\sin\theta_o} - 1\right]$$

b. For the upper end of each increment chosen such that $\frac{dn}{dh}$ is essentially constant over the altitude interval (significant levels on rawinsonde data are satisfactory for incrementation) compute the local elevation angle.

$$\theta_i = 2 \arcsin\left\{\frac{r+h_s}{2(r+\bar{h}_i)}\left[2\sin^2\frac{\theta_o}{2} + \frac{h_i-h_s}{r+h_s} - \frac{n_s-n_i}{n_i}\cos\theta_o\right]\right\}^{\frac{1}{2}}$$

c. Compute the mean elevation angle and index of refraction for each increment.

$$\bar{\theta}_i = \frac{1}{2}(\theta_i+\theta_{i-1}) \quad , \quad \bar{n}_i = \frac{1}{2}(n_i+n_{i-1})$$

d. Compute the total bending (τ) of the ray.

$$\tau = \sum_{i=1}^{j} (n_{i-1} - n_i) \frac{\cot \bar{\theta}_i}{\bar{n}_i}$$

e. Compute the first estimate of the refraction error.

$$\delta = \tau - \arctan \left[\frac{\frac{n_s - n_j}{n_j} + 1 - \cos\tau - \sin\tau \tan\theta_o}{\sin\tau - \cos\tau \tan\theta_o + \frac{n_s}{n} \tan\theta_j} \right]$$

f. Compute the first estimate of the true elevation angle.

$$\theta_t = \theta_o - \delta$$

g. Recompute height as in (a) above (using θ_t rather than θ_o), θ_i for this height as in (b), and $\bar{\theta}_i$, $\bar{n}_i$ as in (c).

h. Compute a better estimate of τ using the information from (g) in the last increment.

i. Compute the final estimate of δ and θ_t using (e) and (f) above.

j. Compute the angle at the center of the earth.

$$\phi = \tau + \theta_j - \theta_o$$

k. Compute the estimate of true range.

$$R_t = \frac{(r+h) \sin\phi}{\cos\theta_t}$$

Correction of the elevation angle for optical tracking devices can also be done in the above manner, utilizing the optical index of refraction.

Page	Line	Correction
89	--	Replace Figure 4-6 with the attached figure which is better drawn than the original and computed in a more accurate manner.
100	18	DELETE: "the Air Force and its Ranges and by the other"
100	19	ADD: "all" to read, ...by all the services...
100	23	DELETE: "also" to read,...should be invited...
100	28	ADD: "and undoubtedly best accomplished by themselves," to read,... especially among the National Ranges, and undoubtedly best accomplished by themselves, should...
102	5	ADD: "and" to read, ...as long as possible and they should...

CONTENTS

CONTENTS

FIGURES

AD HOC PANEL ON ELECTROMAGNETIC PROPAGATION

Panel Members

Mr. David K. Barton
Radio Corporation of America
Moorestown, New Jersey

Mr. John Berbert
Analysis and Evaluation Office, Goddard Space Flight Center
National Aeronautics and Space Administration

Mr. Charles F. Chubb
Engineering Department Head
Sperry Gyroscope Company, Great Neck

Dr. Warren A. Dryden
RCA Service Company
Patrick Air Force Base

Dr. A. B. Focke, Chairman
Chairman, Department of Physics
Harvey Mudd College, Claremont

Dr. J. J. Freeman
J. J. Freeman Associates
Silver Spring, Maryland

Dr. John B. Garrison*
Applied Physics Laboratory
John Hopkins University

Mr. Dean Howard
Naval Research Laboratory
Washington, D. C.

Mr. Harris B. Janes
National Bureau of Standards, Boulder
**while Dr. Thompson is abroad

Dr. Henry P. Kalmus
Chief Scientist
Diamond Fuse Laboratory

Mr. Preston Landry
Chairman, Electromagnetic Propagation Working Group - IRIG
Eglin Air Force Base

Dr. Robert B. Muchmore
Director, Physical Research Division
Space Technology Laboratories, Redondo Beach

Dr. Louis Neelands
Consulting Engineer
General Electric Company, Syracuse

Dr. Henry Plotkin
Tracking Systems Division, Goddard Space Flight Center
National Aeronautics and Space Administration

Mr. C. W. Querfeld
U. S. Army Signal Missile Support Agency
White Sands Missile Range

Mr. Joseph Salerno
M.I.T. Lincoln Laboratory
Lexington, Massachusetts

Dr. John B. Smyth
Smyth Research Associates
San Diego, California

Mr. Robertson Stevens
Section Chief, Communications Elemets Research
Jet Propulsion Laboratory, Pasadena

Dr. A. W. Straiton
Director, Electrical Engineering Research Laboratory
University of Texas

Dr. Moody C. Thompson**
Chief, Lower Atmosphere Physics Section
National Bureau of Standards, Boulder

Mr. E. W. Bullington, Secretary
Executive Secretary, Advisory Committee to AFSC
National Academy of Sciences

SUMMARY

Tropospheric bias errors are highly predictable using radiosonde or refractometer profiles; residual errors from 1% to 3% of the initial bias levels are commonly attained using procedures described in Section 3. Data to within one-half foot in range and 20 to 70 μradians in angle can be expected at elevation angles above five degrees.

Tropospheric fluctuation errors are not correctable using any known procedure, and will amount to a few tenths of a foot in range, and 10 to 50 μradians in angle (depending on the baseline or aperture used for measurement), under normal weather conditions.

The relationship between temporal and spatial correlation of tropospheric fluctuations has been investigated, based on data obtained by the National Bureau of Standards. The effect of short-period fluctuations is described by Figs. 2-7 and 2-8, and is consistent with a drift of tropospheric anomalies across a fixed measurement path at the speed of the prevailing wind.

In range instrumentation applications, where the beam is not fixed, the residual "bias" and long-term error components will change as the beam moves, and additional atmospheric rate errors will be generated, as shown in Fig. 4-6. These errors will be proportional to the tangential velocity of the missile, and will typically be five to fifty times the errors measured for a fixed beam.

The uncertainty in tropospheric path leads to errors equivalent to motion of the instrument on the ground. The motion of the "virtual source" typically amounts to several feet normal to the path and a few tenths of a foot along the path.

Ionospheric errors are essentially unpredictable, and will exceed the residual tropospheric errors when operating frequencies below 3000 mcps are used. Even in the 5000-6000 mcps band the ionospheric errors will contribute to overall atmospheric error during daytime operation.

Redundant measurements performed at two frequencies below 3000 mcps can be used to correct for ionospheric error in both range and angle.

The lowest atmospheric errors are found in trilateration systems using very long baselines. Total position and velocity errors for a typical satellite track (660 miles range, 100 miles altitude) through average weather, are as follows:

	RMS Position Error (feet)	RMS Velocity Error (ft/sec)
Range-angle tracker at 6000 mcps	310	16
Interferometer, 10,000 mcps (Mistram)	100	2.4
Trilateration system,		
2000 mcps	19	0.9
6000 mcps	2.5	0.15

The above errors may be increased or decreased by a factor of two or three for different weather conditions (and a 2000 mcps for different ionospheric conditions). The trilateration errors shown are dependent upon perfect survey of station location, as well as instrumental errors below one-half foot in range and 0.02 ft/sec in range-rate.

1. INTRODUCTION

The Ad Hoc Panel on Electromagnetic Propagation was convened as part of a continuing effort by the National Academy of Sciences-National Research Council on behalf of the Atlantic Missile Range as requested by Headquarters, Air Force Systems Command.

The Ad Hoc Panel on Basic Measurements discussed in its Report how well we can measure at the present time, such fundamental quantities as a length, time, and the velocity of light. The Report notes that there are fundamental limitations to tracking accuracy imposed by our inability to measure these basic quantities with more precision, but it points out that state of the instrumentation art has not yet approached these limitations. There are, however, other fundamental limitations to tracking accuracy which today are beginning to, if not already, restricting the capability of our instrumentation state-of-the-art. One of these major limitations is that imposed by atmospheric refraction. Consequently, the Ad Hoc Panel on Electromagnetic Propagation was formed to consider this problem.

This Panel met on 11 May 1962 in Washington, D. C. and heard discussions as to how tracking accuracy requirements were arrived at for one particular program, of the current tracking capabilities of the AMR, and of various research work which instrumentation and atmospheric physics people are conducting. Due to the quantity and divergence of the material presented, the Panel could not arrive at a consensus of opinion regarding a report. Consequently, Mr. David K. Barton was appointed Editor of the Panel's Report by the chairman. Mr. Barton drafted the Report of the Panel from material contributed by Dr. Robert S. Fraser, Dr. John B. Smyth, Mr. Preston Landry, and himself.

This Report of the Ad Hoc Panel on Electromagnetic Propagation has attempted to state the current extent of our knowledge concerning atmospheric refraction and its effect on tracking accuracy, which should be of as much benefit to the range users as to the range operators, and also has made recommendations which, if followed, should lead to increased accuracy both in the near and in the more distant future.

2. CLASSIFICATION AND DESCRIPTION OF ATMOSPHERIC ERRORS

2.1 Classification of Atmospheric Errors by Type.

There are many ways of describing propagation errors in precision tracking systems. The four classifications shown in Table I are suggested to cover the characteristics of most interest to the developers and users of missile and space range instrumentation:

Table I

a.	Source of Error:
	Tropospheric
	Ionospheric
b.	Measured Quantity
	Angle of arrival or phase difference
	Range delay or signal phase
c.	Spatial Correlation of Error:
	Across radar aperture (5 to 100 feet)
	Across short baseline (100 to 1000 feet)
	Across long baseline (1000 to 100,000 feet)
d.	Temporal Correlation of Error:
	Bias (fixed during one track)
	Fluctuation (periods of seconds or minutes)

For each combination of the above characteristics, the error should be known as a function of operating frequency, target altitude, elevation angle (or slant range) and state of the atmosphere. Except in rare instances, the instrumentation system may be assumed to be at sea level.

2.2 Effects of the Lower Atmosphere

The propagation errors caused by the lower atmosphere will be analyzed in this section. The lower atmosphere for the purposes of this discussion will be defined as the atmosphere below a height of 40 km. The object of the analysis is to find the accuracies that the position and motion of a target above the lower atmosphere can be measured by means of radio systems on the surface of the earth. The propagation effects can not be presented completely in this brief discussion. Hence, the location and motion of the target

will be restricted, in order to demonstrate simply the propagation effects encountered most frequently.

a. Refractive Index of Air

The refractive index of any substance is composed of a real and an imaginary part. The phase velocity of an electromagnetic wave depends on the real part. The attenuation of the electromagnetic energy depends on the imaginary part. The attenuation is important to radio tracking and guidance systems, if the radio signal becomes too weak for the system to operate on it. The attenuation by the atmospheric gas is negligible for most purposes at frequencies slightly below 22,000 mc/s, which is the lowest frequency of an absorption band of the atmospheric gas. Atmospheric particulate matter such as rain, snow, and clouds also attenuate electromagnetic energy passing through them. These latter effects are rarely important for many tracking and guidance systems. Consequently, this discussion of propagation errors will apply only to radio frequencies less than 20,000 mc/s, where atmospheric attenuation is not important for many tracking and guidance systems.

The real part of the index of refraction (n) of the atmospheric gas can be computed from the expression

$$(n - 1) \cdot 10^6 = N = \frac{77.6}{T} \left(P + \frac{4810p}{T}\right) , \qquad (2\text{-}1)$$

where T represents the temperature of the atmosphere in degrees Kelvin; P represents the total pressure of the atmosphere in millibars; p represents the partial water vapor pressure in millibars; and N, which is called the refractivity, is used frequently in radio propagation work instead of the index of refraction. The refractivity can be calculated from Eq.(2-1) with an accuracy of 0.5 per cent for the usual range of atmospheric variables and for radio frequencies less than 30,000 mc/s. Since only radio frequencies less than 20,000 mc/s will be considered in this report, the propagation effects to be discussed will be independent of radio frequency.

The dependence of the refractivity N on height is shown in Fig.2-1. Mean vertical profiles for summer, winter, and an elevated station (Ely) are shown. Also, the approximate extreme values are indicated. The values of N near sea level vary from about 270 to 405. The mean value of N near sea level

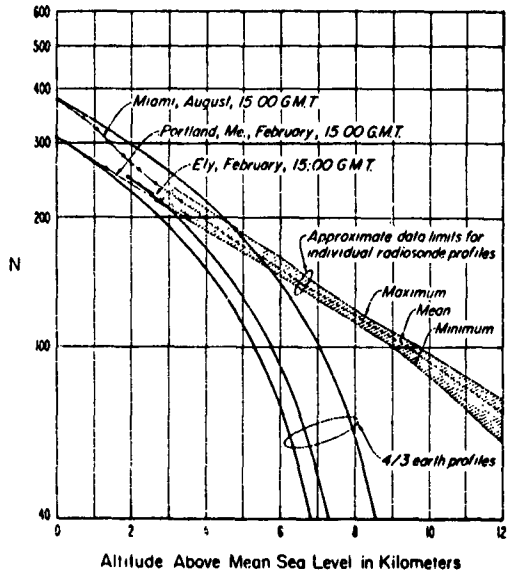

Figure 2-1. Means and extremes of radio-refractivity height structure, and a comparison with extreme 4/3 earth profiles (Bean and Thayer, 1959).

is 313. The comparatively large difference in N decrease with increasing height. The value of N is about one at a height of 40 km. Later, use will be made of the fact that the N-vertical profile can be approximated by an exponential function with sufficient accuracy to estimate many propagation errors.

b. Range and Angle Errors for a Mean Atmosphere

Because the index of refraction of the earth's lower atmosphere is greater than one, the apparent position of a target which is determined by a radio system differs from the position which the same system would measure if there were no atmosphere. The apparent position measured in the presence of an atmosphere minus the true position is the error in the position measurement. Important propagation effects are revealed when the position errors are calculated for a simple model of the earth's atmosphere, such as one that is spherically stratified. In other words, the refractivity N for such a model is constant on an arbitrary spherical surface which is concentric with the center of a spherical earth. Furthermore, N does not change with respect to time.

Range Errors

The range error measured by a radar is given by the expression

$$\Delta R_e = \int_o^h n(z) \csc \left[\theta(z)\right] dz - R_o, \qquad (2\text{-}2)$$

where the integral represents the distance measured by the radar and R_o represents the true distance; $\theta(z)$ is the elevation angle, or the angle between the curved radio ray and the spherical surface which the ray intersects at height z above the radar (z is measured normal to the spherical surfaces); and h is the distance between the two spherical surfaces that pass through the radar and the target. The integration above a height of 70 km. is negligible for most guidance and tracking purposes since the index of refraction is very small. (Ionospheric effects are not being considered). If the initial elevation angle at the radar is large enough, Eq.(2-1) can be written as

$$\Delta R_e \doteq \csc \theta_o \int_o^h N(z) \cdot 10^{-6} dz + \int_o^h \csc \left[\theta(z)\right] dz - R_o . \qquad (2\text{-}3)$$

The last two terms on the right of the above equation represents the difference between the length of the curved radio ray and the true distance. If the initial elevation angle is greater than 10° ($\theta_o > 10^{\circ}$), these two terms may be neglected in comparison with the first term on the right of Eq. (2-3). The latter term represents the apparent increase in distance to the target, because the phase velocity of the radio wave passing through the atmosphere is less than it is in free space. In order to estimate the magnitude of this term, assume that the refractivity N decreases exponentially with increasing height; that is,

$$N(z) = N_o e^{-z/H} , \qquad (2-4)$$

where N_o is the value of the refractivity at the radar; H is a scale height; and z is the height above the radar. When this value of N(z) is substituted into Eq. (2-3), the expression for the range error becomes

$$\Delta R_e \doteq N_o H \csc \theta_o \cdot 10^{-6} (1 - e^{-h/H}) . \qquad (2-5)$$

The range error increases as the path length through the atmosphere increases, or as the initial elevation angle (θ_o) decreases. To compute the range error for a particular case, use the following values of the parameters: the average value of the refractivity at sea level, $N_o = 313$; the average scale height, H = 7 km; the height of the target h = 30 km.; and the initial elevation angle $\theta_o = 20^{\circ}$. The range error for this case is $\Delta R_e = 6.4$m. Detailed computations of range errors for an exponential atmosphere are given by Bean and Thayer (1959). The range error ΔR_e computed by Bean and Thayer for the CRPL Exponential Reference Atmosphere with $N_s = 313$ is plotted in Fig. 2-2, as a function of slant range R_o and elevation angle θ_o.

Angular Errors

Next, the angular errors will be discussed. The errors which appear in interferometer measurements of angle will be derived before presenting the angular errors associated with a tracker. The following derivation of the interferometer errors is based on a report by Thayer and Bean (1962). The geometry for an interforometer system is shown in Figure 2-3. A_1 and A_2 indicate the two antennas which are

Figure 2-2

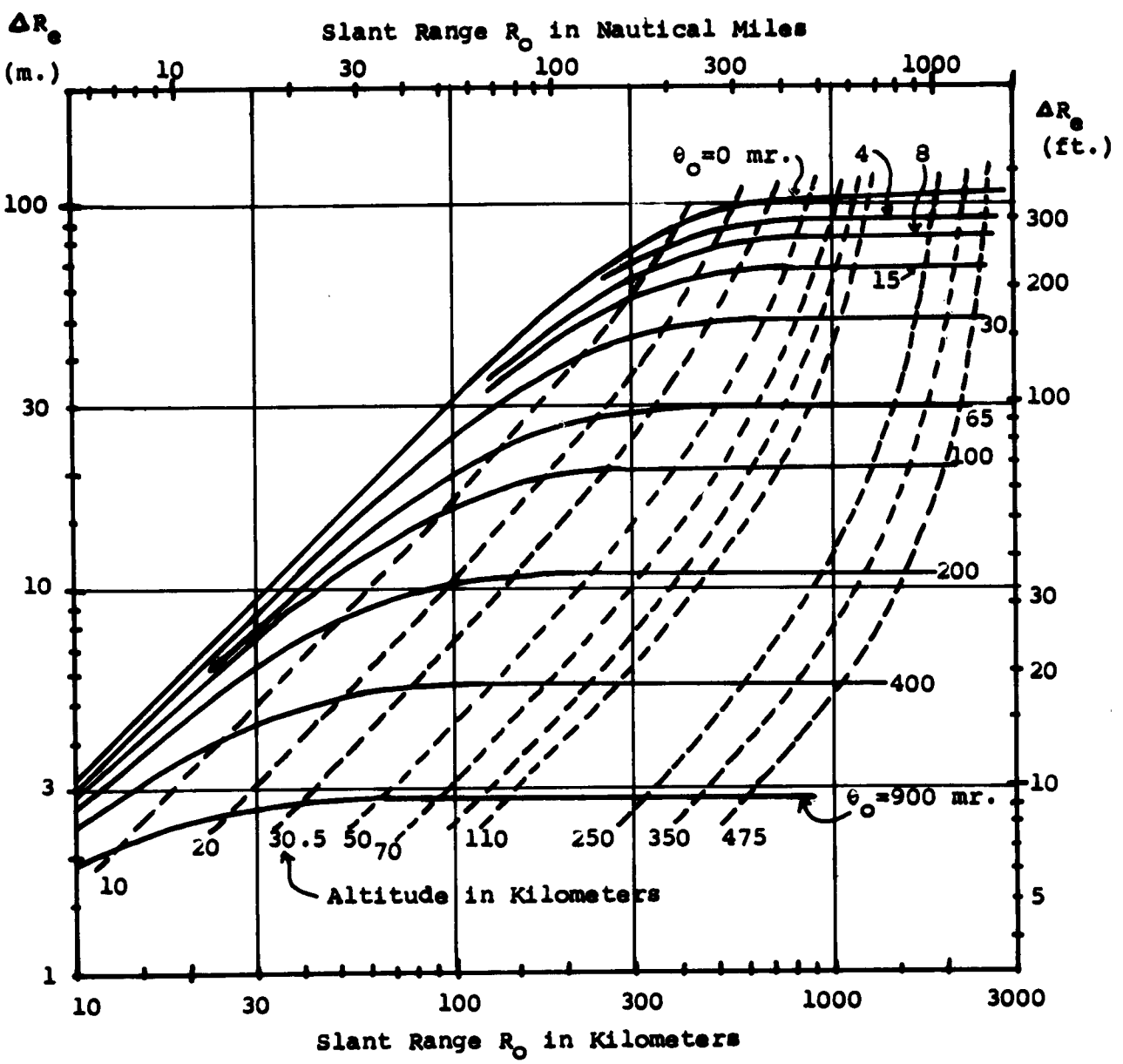

Range Bias vs. Range for CRPL Exponential Reference Atmosphere (N_o = 313)

Figure 2-2.

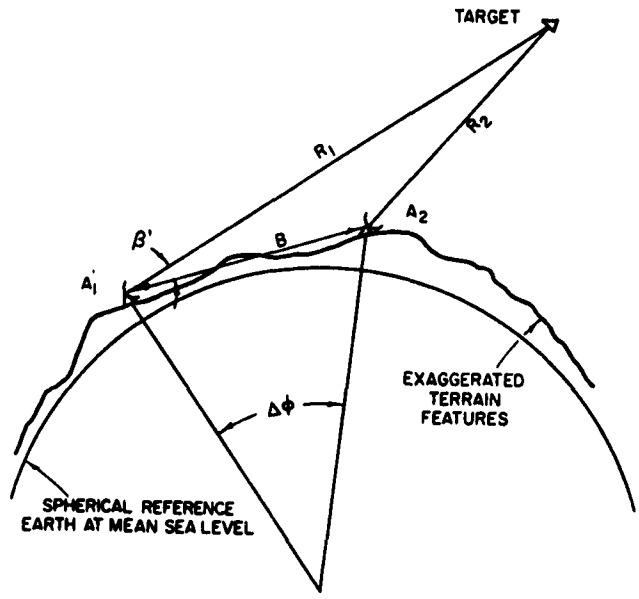

Figure 2-3. Geometry of an interferometer radio system.

separated by a distance B. R_1 and R_2 indicate the true distances between the target and the corresponding antennas. Note that β' refers to the angle between a radio ray from antenna 1 to the target and the baseline, and not the angle between the radio ray and the tangent plane. An exact solution for β' is

$$\beta' = \sin^{-1} \left\{ 1 - \left(\frac{\Delta S}{B}\right)^2 \left[1 + \frac{B^2 - (\Delta S)^2}{2R_1 \Delta S} \right]^2 \right\}^{\frac{1}{2}} ,$$

where

$$\Delta S = R_1 - R_2 \quad .$$

In order to show simply the refraction errors which depend on a spherically stratified atmosphere, the following assumptions are made:

a.) the range R_1 to the target is large compared to the baseline length B, say $R_1 > 100\ B$; and

b.) the value of β' is larger than 10° .

Then an expression for the error in the angle β' ($\Delta\beta'$) caused by a spherically stratified atmosphere is

$$\Delta\beta' \doteq \frac{\Delta R_{e1} - \Delta R_{e2}}{B \sin \beta'} \quad . \tag{2-7}$$

The same expression for the error $\Delta\beta'$ results from the derivation for a plane-parallel atmosphere. The numerator on the right of Eq. (2-7) represents the difference in range errors caused by the atmosphere; and the denominator on the right of Eq. (2-7) represents the effective baseline length, or the perpendicular distance between two rays from the distant target to antennas A_1 and A_2. If the expression for the range error (2-3) is substituted into (2-7), then the expression for the angular error can be approximated by

$$\Delta\beta' = \frac{\csc^3 \beta^*}{r_o} \int_o^h N(z) \cdot 10^{-6}\, dz, \quad \beta^* > 10^\circ, \tag{2-8}$$

where β^* is the angle that a radio ray at A_1 makes with the baseline; β^* is greater than 10°; r_o is the radius of the earth; and both antennas are at the same height. The refraction error for an interferometer is not zero, even when the atmosphere is spherically stratified. The error is nearly independent of the distance between the two antennas for the assumptions that have been made. The error is proportional to the cube of the cosec β^*; and the error depends on the vertical profile of the refractivity N. However, if N is assumed to decrease exponentially with increased height, then (2-4) can be substituted into (2-8) to obtain

$$\Delta\beta' \doteq \frac{\csc^3 \beta^*}{r_o} N_o H \cdot 10^{-6} \left(1 - e^{-h/H}\right) \quad . \qquad (2\text{-}9)$$

If the target is sufficiently high, the exponential is negligible, and the refraction error is directly proportional to the refractivity at the antennas.

The elevation angle error for a tracker has a different dependence on the initial elevation angle. If the refractivity (N) decreases exponentially with increasing height and if the initial elevation angle is not too small, then the tracker elevation angle error is given by the expression

$$\delta \doteq N_o \cdot 10^{-6} \operatorname{ctn} \theta_o \quad , \qquad (2\text{-}10)$$

where θ_o is the value of the elevation angle at the tracker. The tracker elevation angle error is also directly proportional to the refractivity at the tracker but decreases less rapidly with respect to decreasing elevation angle than does the interferometer elevation angle error. The angle error computed by Bean and Thayer for the CRPL Exponential Reference Atmosphere with $N_s = 313$ is plotted in Figure 2-4 as a function of slant range R_o and elevation angle θ_o.

Both the tracker and interferometer elevation angle refraction errors are shown for mean conditions in Figure 2-5. Both errors decrease with increasing elevation angle, but the interferometer errors decrease more rapidly than the tracker errors, except for large elevation angles. The

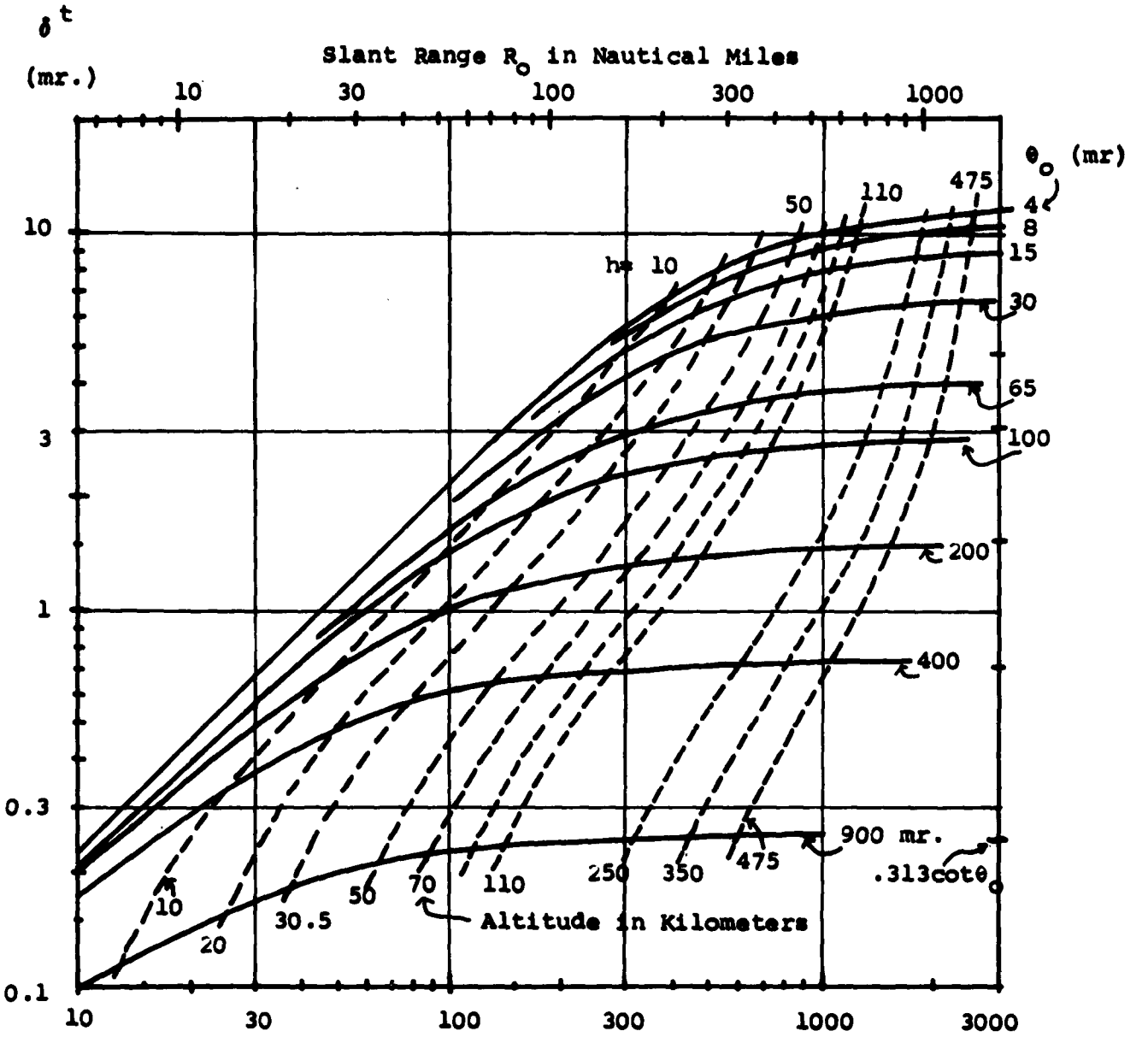

Figure 2-4 Slant Range R_o in Kilometers

Tracker Elevation Angle Error vs. Range for CRPL Exponential Reference Atmosphere (N_o = 313)

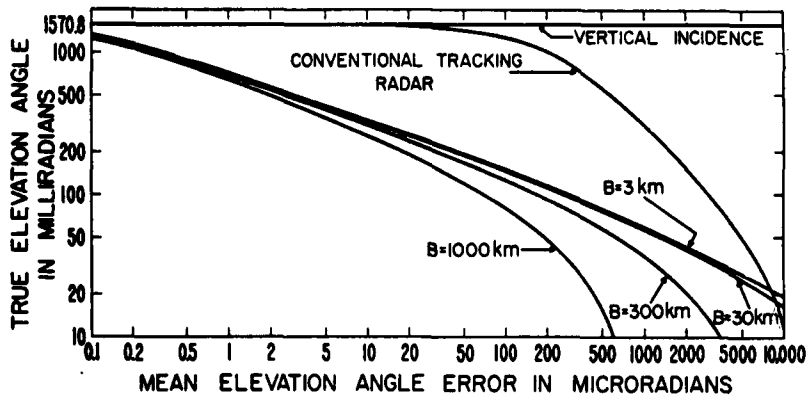

Figure 2-5. Mean tracker and interferometer refraction errors. The curve for B=3 km also represents the residual tracker error after correction according to Eq. 2-10.

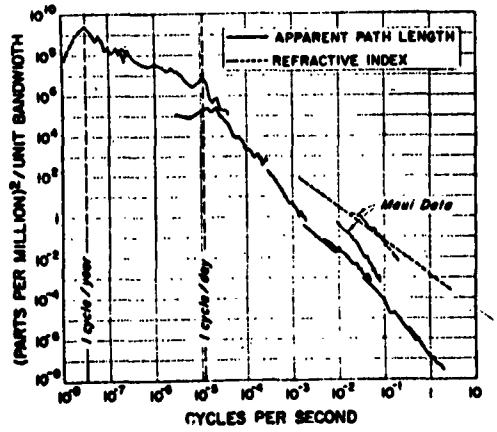

Figure 2-6. Spectra of refractivity and apparent range variations at Maui and Colorado (Thompson, Janes and Kirkpatrick (1960).

tracker error is greater than the interferometer error, except at small elevation angles where the effective baseline length of the interferometer becomes small. The interferometer errors are nearly independent of the distance between the antennas (B) for large elevation angles, but the errors are much smaller for the longer baselines at the small elevation angles.

The interferometer error, for the shorter baselines, is approximately equivalent to the tracker error corrected by Eq. (2-10) for surface refractivity. In such an interferometer, the term $N_o 10^{-6} \text{ctn } \theta_o$ is supplied by the added delay in the path R_1 to antenna A_1 after the wavefront has reached the antenna A_2. Any deviation from the conditions that apply in Eq. (2-10) will cause the interferometer data and the corrected tracker data to depart from the curves shown in Figure 2-5.

The interferometer azimuthal refraction errors are negligibly small for the condition that the two rays from the target to the two antennas are nearly parallel. In this case, both rays are refracted the same. The tracker azimuthal error is zero, since the refraction is proportional to the gradient of the index of refraction; the gradient is zero in the azimuthal direction for a spherically stratified atmosphere.

Rate Errors

The propagation rate bias errors of a guidance system operating in a spherically stratified atmosphere can be easily derived from the formulas for the position errors by taking derivatives with respect to time. The expression for the range rate error, as obtained from (2-5), is

$$\Delta \dot{R}_e \doteq - \text{ctn } \theta_o \, \dot{\theta}_o \quad \Delta R_e, \quad h \quad > 32 \text{ km.} \qquad (2\text{-}11)$$

The range rate errors are proportional to the rate of change of the elevation angle. For an example, let $\theta_o = 20^o$, $\dot{\theta}_o = 10^{-3}$ rad/sec, and $\Delta R_e = 6.4$ m; then the range rate error is $\Delta \dot{R}_e = - 0.02$ m/sec. The angular rate error for an interferometer is obtained by differentiating (2-9) with respect to time:

$$\Delta \dot{\beta}' = - 3 \text{ ctn } \beta^* \, \dot{\beta}^* \quad \Delta \beta', \quad h \quad > 32 \text{ km.} \qquad (12\text{-}12)$$

As an example, let β^* be the elevation angle and equal to 20°; let $\dot{\beta}^* = 10^{-3}$ rad/sec; then $\Delta\dot{\beta}' = 0.06$ μr/sec.

c. Geographical, Seasonal, and Diurnal Variations in Errors

Corrections can be made for the propagation errors that are caused by a spherically stratified atmosphere. As has been shown, the errors are nearly proportional to the surface value of the refractivity (N_o), if the target is far enough away and if the elevation angle at the antennas exceeds about 10°. The range and refraction corrections can be based on various averages of the surface refractivity, such as the annual, seasonal, or diurnal means, or on the value of the refractivity at the radio antennas a short time before the radio system is to be used for guidance or tracking. Then the standard deviation of the propagation errors are proportional to the standard deviation of the surface refractivity. A good compilation of climatic refractive data has been published by Bean, Horn, and Ozanich (1960). The standard deviation of the surface refractivity has been estimated approximately from that data and put in Table 2-2. The standard deviations for the range and elevation angle errors that appear in Table 1 have been computed from formulae (2-5) and (2-9), respectively, where the propagation errors and the refractivity in those formulae were replaced by the standard deviations of the corresponding quantities. The standard deviation of the refractivity which is measured one hour before

TABLE 2-2. Standard deviation of range and interferometer elevation angle errors. The elevation angle is assumed to be 20° and the height of the target exceeds 32 km. The temporal standard deviations of the refractivity apply to Miami.

Standard deviation	N_o measured one hour before guidance time	Diurnal (summer)	Seasonal	Annual	Geographical for the U.S. at sea level	
					summer	winter
N_o	5	10	15	20	30	20
ΔR_e	0.1m.	0.2m.	0.3m.	0.4m.	0.6m.	0.4m.
$\Delta\beta'$	0.1μr	0.3μr	0.4μr	0.6μr	0.8μr	0.6μr

the radio system is used to guide or track is based on the fact that the refractivity can be measured with an accuracy of 4 N-units and will change 3 N-units during one hour. The data in Table 2-2 show that as the period or geographical extent for which the error applies decreases, the error decreases.

Bean and his co-workers have developed empirical methods for making refraction and range corrections. The methods involved one to three parameters, the most important being the surface refractivity. These empirical corrections reduce the propagation errors caused by a spherically stratified atmosphere to a few per cent of the uncorrected errors.

d. Random Errors

The lower atmosphere is not quite spherically stratified, and its refractivity is constantly changing. Hence, the propagation errors are actually larger than have been given for a spherically stratified atmosphere. In general, the apparent position of a target fluctuates about its true position. The fluctuating position and rate errors depend on how the propagation errors pass through several filters that are either inherent to or designed in any guidance or tracking system.

Hence, it is useful to review how the propagation errors are filtered by a radio system. Such filters are discussed in an article by Wheelon (1959). Consider a propagation error, such as range error for example, to be a stochastic, stationary function of time and to have the spectral representation

$$x(t) = \int_{-\infty}^{\infty} e^{i\omega t}\, dS(\omega) \quad , \qquad (2\text{-}13)$$

where $\omega = 2\pi f$, f being the frequency of the radio wave, $E\,dS(\omega) = 0$, $E\,dS(\omega)\,dS^*(\omega) = s(\omega)\,d\omega$. E denotes the expectation operator and $s(\omega)$ the spectral density of the process. When $x(t)$ is the input to a linear, time-invariant, passive filter, which has the frequenty response function $l(\omega)$, the spectral density of the output is $|l(\omega)|^2\, s(\omega)$. The absolute square of the frequency response function for rate errors is ω^2, which implies that the rate errors are nearly independent of the low frequency errors. The finite size of the receiving antenna acts as a filter which does not pass errors caused

by atmospheric irregularities smaller than the cross section of the antenna aperature. Aperture filtering is not important for present guidance and tracking systems, since the propagation errors at frequencies above the aperature high frequency cutoff are generally negligible with respect to the low frequency errors which are passed. Linear filtering of the data for a time τ has the absolute square frequency response function of

$$\left(\frac{\sin \omega \tau/2}{\omega \tau/2}\right)^2 . \qquad (2\text{-}14)$$

This filter passes low frequency errors. Since the linear filter has a high-frequency cutoff at about the inverse of the smoothing time τ for some of the propagation errors, the variance of these errors decreases as the smoothing time increases. Some radio systems use much more sophisticated time filters than linear filters. Another filtering action depends on the procedure for applying corrections for propagation errors. For example, a tracker elevation angle refraction correction can be easily computed from (2-10). If T is the interval of time between the measurement of the refractivity N_o which is used in the correction formula and the use of the correction by the radio system, then the absolute square of the frequency response function is

$$4 \sin^2(\omega T/2) . \qquad (2\text{-}15)$$

If T = 0, the correction is not in error (assuming that the correction can be determined accurately). As T becomes large, the variance of the error approaches twice the variance which would result if no correction were applied. This filtering action has been indicated in section c about temporal and geographical variations of the refractivity. Besides the corrections for the low frequency propagation errors, which are sometimes considered as a bias correction, the filtering of the propagation errors in time is the most important filtering action for many systems. Hence, the effect of this filter (2-14) on measured errors will be discussed in the following discussion.

1. Maui Experiments

Valuable data on radio propagation errors have been collected from experiments made at Maui, Hawaii, by the

National Bureau of Standards. The experiments were designed to measure range and angle errors that occurred during periods of the order of minutes. The propagation path extended a distance of 25km. from near sea level to a summit 3 km. high. The elevation angle of the propagation paths was about 7°. The interferometer measured azimuthal errors, since the interferometer baseline was approximately level and perpendicular to a line from one antenna to the transmitter at the summit. The propagation path extended through only part of the lower atmosphere, but that path was chosen because it was believed that large propagation errors would occur there. The propagation errors observed at Maui have been consistent with propagation errors which have been measured while tracking moving targets above the lower atmosphere and at elevation angles greater than 15°. The speed at which such targets were moving is not given for security reasons. A summary of the propagation errors measured at Maui follows. The data are taken from a Space Technology Laboratory report (1958) and Norton et al (1961).

Range

Power spectra of apparent range and refractivity fluctuations are shown in Figure 2-6. The spectral values for frequencies higher than 10^{-3} sec^{-1} are the median values of many spectra. The parts per million indicated on the ordinate refers to either the change in path length from some arbitrary reference divided by the path length, or to the refractivity times 10^{-6}. The Colorado data shown apply to a horizontal path near Boulder, 15 km. long, and about 100 m. above the terrain. The spectral density of range errors increases with decreasing spectral frequency and converges to the spectral density of the refractivity fluctuations at a frequency of one cycle per day. (The spectra at the lowest frequency of the low frequency segments of the range and refractivity spectra may not be correct). The area under the Maui range spectrum is of the order of $1m.^2$, since the range changed less than 1.3m. at Maui during a five day period. This range error is less than the range error for a spherically stratified atmosphere.

Range Rate Errors

The range rate errors were computed as a simple average for a time interval t_o according to the formula

$$\dot{R}_{\text{ave } t_o} = \frac{R(t + t_o) - R(t)}{t_o} \quad . \qquad (2\text{-}17)$$

Table 2-3 contains RMS values of the above quantity for periods of time long compared to t_o .

Azimuthal Angular Errors

The azimuthal angular errors were computed from the expression

$$\Delta\beta = \frac{\Delta\phi_1 - \Delta\phi_2}{2\pi} \quad \frac{\lambda}{B \cos\beta} \; ,$$

where $\Delta\phi_1$ and $\Delta\phi_2$ are the phase errors recorded at two antennas separated by a distance B; $\cos\beta = 1$; and λ is the wavelength of the transmitted radio wave. RMS values of the above quantity were computed from instantaneous values of the phase errors; that is, no time smoothing was done; and the RMS values were computed for periods of data of 15 min. to 1 hour . The RMS errors are plotted as a function of the baseline length in Figure 2-7. (Please excuse the introduction of the English measure of length on the following figures. Sufficient time was not available to put the data in metric units and redraw the figures for this report.) The azimuthal errors decrease monotonically with increasing baseline length. Note that the results are essentially independent of λ , and may be described in terms of a "range-difference error" $\sigma_{\Delta r}$, divided by the baseline B. The maximum value of the error $\sigma_{\Delta r}$ approaches 0.1 ft as B approaches 10,000 ft.

Linear smoothing of the azimuthal errors for the longer baselines ($B \geq 1000$ ft.) is ineffective for a smoothing time t_o less than one minute. On the other hand, the phase difference power spectra curves for the short baseline (B = 2.2 ft.) suggests that smoothing for 20 sec. to 100 sec. could be very effective in reducing the azimuthal error.

Azimuthal Angular Rate Errors

The azimuthal angular rate error has been calculated from the azimuthal error $\Delta\beta$ according to the expression

$$\Delta\dot{\beta}_{t_o} = \frac{\Delta\beta(t + t_o) - \Delta\beta(t)}{t_o} \; ; \qquad (2\text{-}18)$$

cloud amount / t_o in sec.	Small	Average	Large
5	.015	.02	.055
20	.01	.015	.03
60	.003	.009	.02

TABLE 2-3 The range rate errors in centimeters per second versus smoothing time and cloud amounts

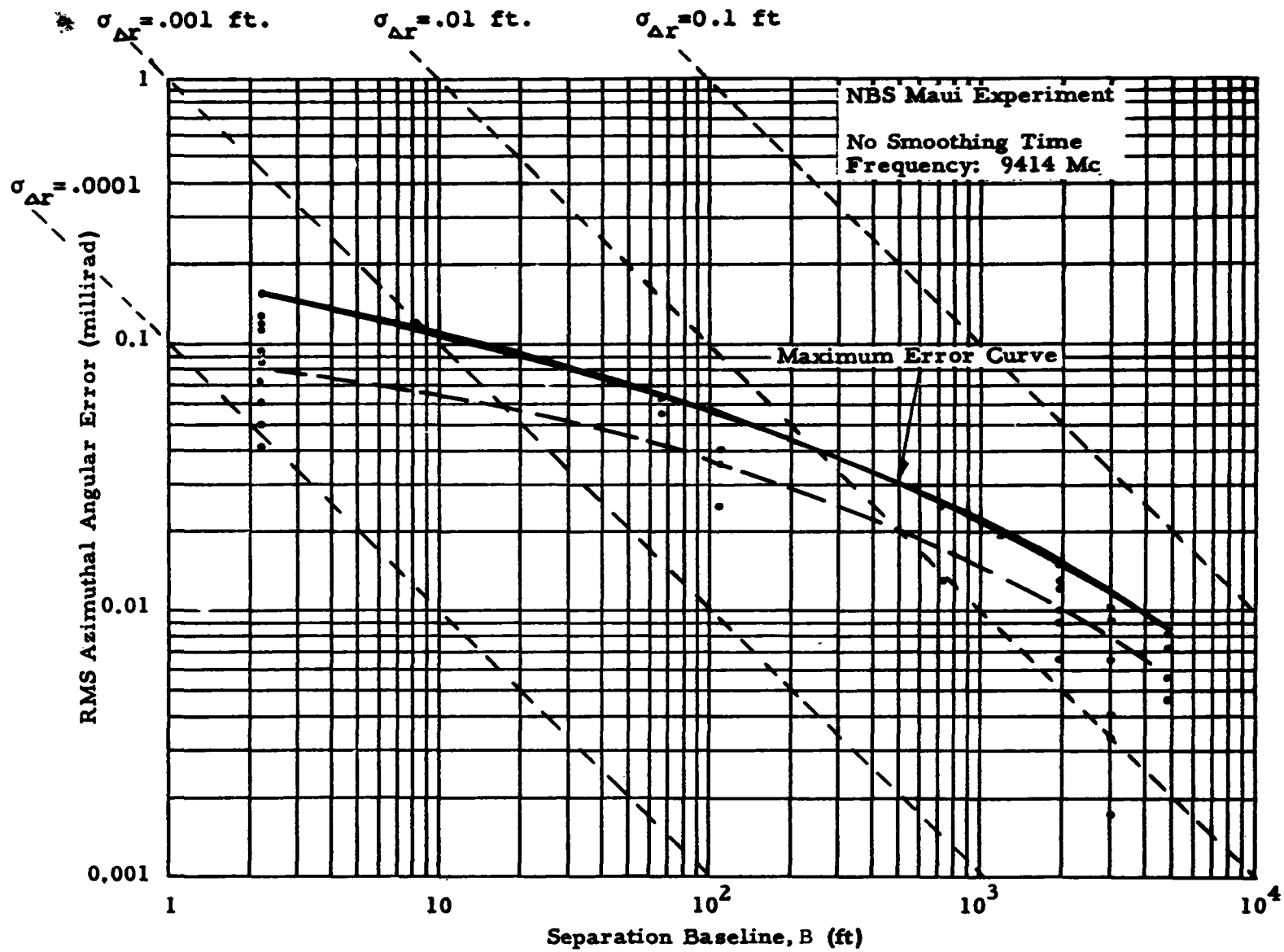

Figure 2-7. Measured Variation of Azimuthal Angular Position Error as a Function of Interferometer Baseline Length.

that is, the error is an average for the time interval t_o. The root mean square of this statistic is plotted on Figure 2-8 for a smoothing time t_o = 20 sec. The "range-rate difference error" $\sigma_{\Delta\dot{r}}$ is also indicated by reference to the diagonal dashed lines. The maximum value of $\sigma_{\Delta\dot{r}}$ is about 0.001 ft./sec for this data.

Table 2-4 is presented to show that the rate errors decrease as the smoothing time (t_o) increases.

TABLE 2-4. Median azimuthal angular rate errors in microradians per sec as a function of baseline length (B) and smoothing time (t_o).

B in feet / t_o in sec.	2.2	1914	4847
5	19	0.7	0.25
20	5.5	0.45	0.15
60	1.7	0.18	0.13

Elevation Errors

If the refractivity of the atmosphere is sufficiently isotropic, then the elevation angular position and rate errors can be deduced from the measured values of the azimuthal errors In this case, the elevation errors are determined from the azimuthal error data by using the effective baseline length instead of the distance between the antennas.

2. Cumulus Clouds

The Maui experiments did not measure the propagation errors caused by large, towering cumuli. R. M. Cunningham of the Air Force Cambridge Research Center has made an extensive study of the propagation errors caused by cumuli. He has measured the refractivity in and around clouds with an aircraft. With these data and cloud photographs he has constructed vertical cross sections of the refractivity. Then he has computed the range errors for various propagation

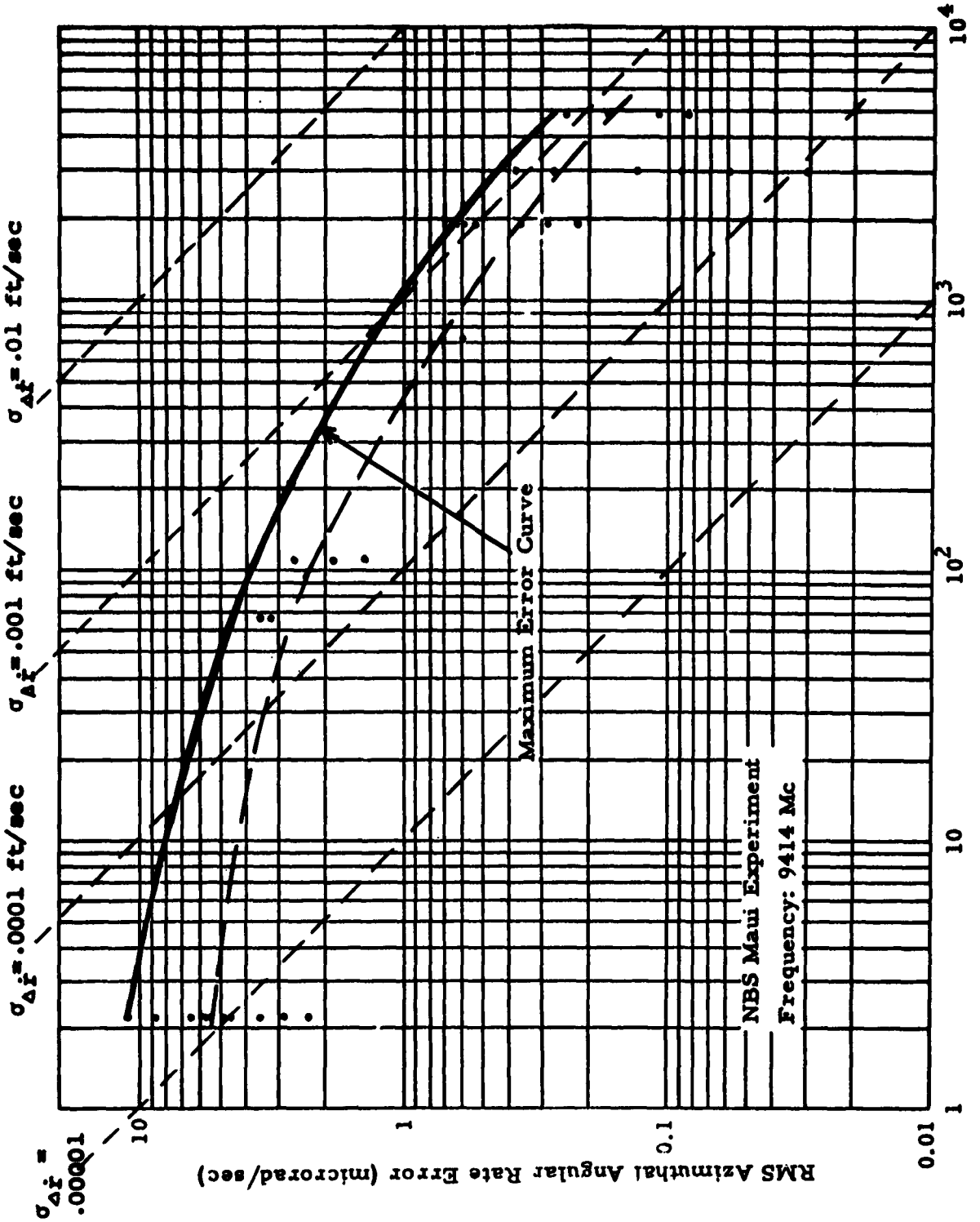

Figure 2-8. Measured Variation of Azimuthal Angular Rate Error as a Function of Interferometer Baseline Length, 20-Sec Smoothing.

pathes along the cross section.

The range errors which are caused only by cumulus clouds are shown on Figure 2-9. The cloud amounts referred to in the caption show the fraction of the earth's surface that would be shadowed by clouds if the sun were at the zenith. The range errors are largest when the clouds are largest. The range error decreases as the path length through the clouds decreases, or as the elevation angle increases (theory predicts the variation proportional to $\sqrt{\csc B}$, plotted in Fig. 2-9). The standard deviation of the range error measured at Maui during a period of 3½ days is also plotted and is about the same value as the error caused by clouds.

Cunningham computed rate errors from his cross sectional data under the assumption that the clouds and associated refractivity were "frozen" and moved with the mean air flow, which was only in the direction of the cross section. The range rate errors caused by cumulus clouds are shown in Table 2-5.

TABLE 2-5. The standard deviation of the range rate errors in cm per sec caused by cumulus clouds. The elevation angle of the propagation path is 7°.

cloud amount / t_o in sec	0.14	0.37	0.46	u in m/sec
33	0.015	0.035		9
43			0.015	7

As before, t_o refers to an effective smoothing time that the data were filtered linearly. The horizontal speed of the clouds in the direction of the cross section is given by u. The errors caused by cumuli have about the same values as the Maui errors, which were given in Table 2-3.

Cunningham computed the azimuthal angular errors for an interferometer from (2-7), where sin $\beta' = 1$. The standard deviation of the errors are plotted as a function of the distance between two interferometer antennas in Figure 2-10. The errors are not smoothed with respect to time. The errors

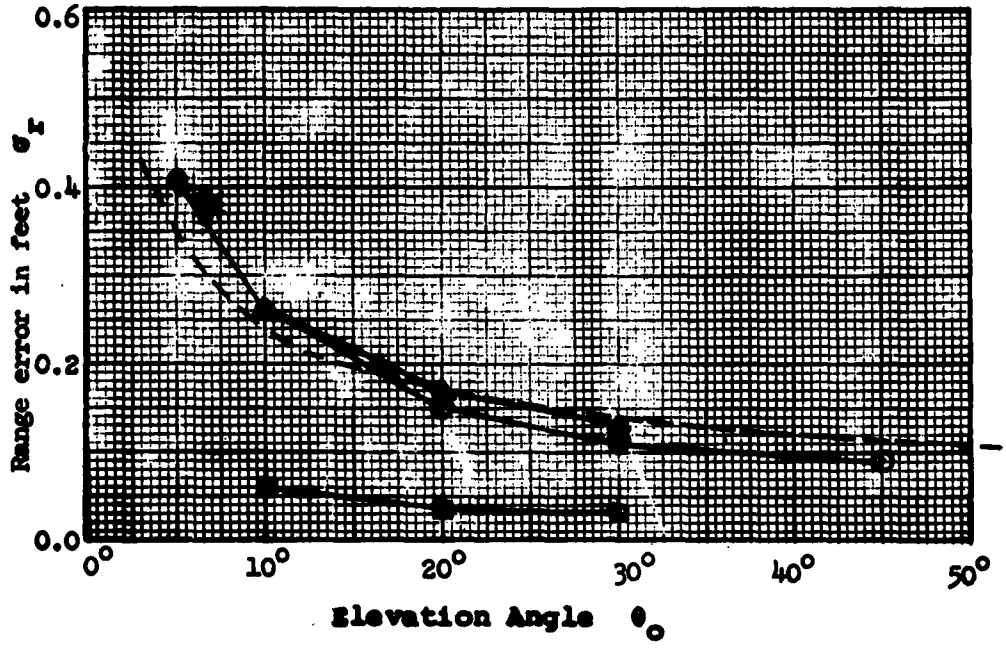

△ Florida, 1957; large cumuli; amount = 0.37

⊡ Florida, 1957; small cumuli; amount = 0.14

⊙ Florida, 1956; amount = 0.46

\# Maui

– – – – Theoretical curve, $\sigma_r = \sqrt{\csc \theta}$ /10 feet

Figure 2-9. RMS range errors which are caused by cumuli.

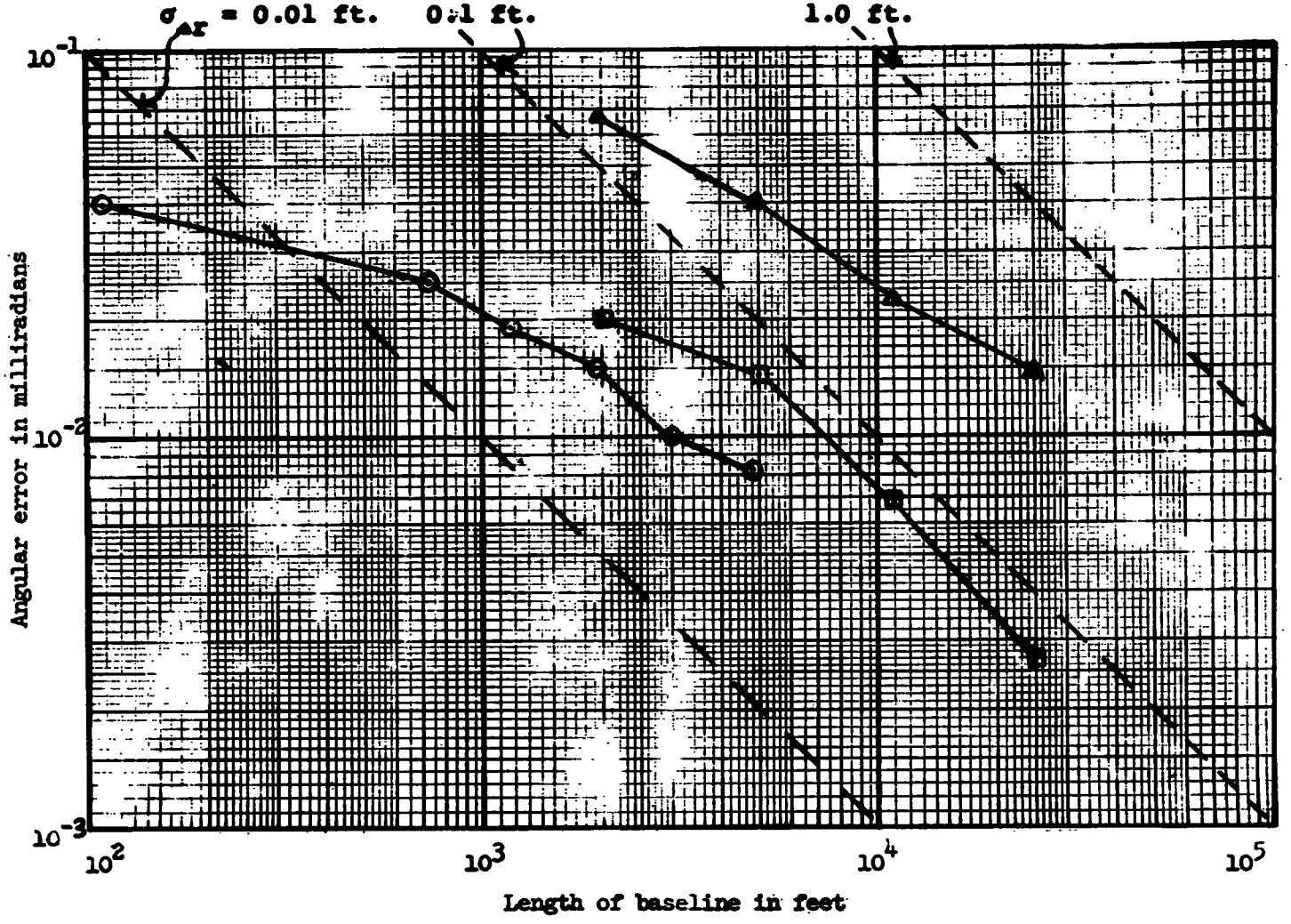

▲ Florida, 1957; Large cumuli, $\theta_o = 10^o$ Zero smoothing

⊡ Florida, 1957; Small cumuli, $\theta_o = 10^o$

⊙ Maui; maximum RMS error $\theta_o = 7^o$

Figure 2-10. RMS angular errors as a function of interferometer baseline length.

decrease with increasing baseline length and are seen to be larger than the maximum RMS Maui errors, approaching $\sigma_{\Delta r}$=0.5 foot for the longest baseline with large cumuli.

The azimuthal angular rate errors which are caused by cumuli are shown for a 2000 ft. baseline interferometer system in Figure 2-11. The errors show no clear dependence on elevation angle. The cumuli errors are larger than the average RMS Maui errors. Cunningham's computations also showed that the angular rate errors caused by cumuli were inversely proportional to the baseline length, when that length was between 2000 ft. and 25,000 ft.

Cunningham is presently computing the propagation errors from refractivity measurements made when no clouds were present over the Atlantic Missile Range. When no clouds were present, he has measured horizontal refractivity (N) changes as large as 60 N-units in a few meters. The changes appear to be confined to a layer of the order of 100 m thick at a height of about 1 km. to 2 km. above sea level.

During the previous discussions of fluctuating propagation errors, the range rate and angular rate errors have been given for the case that the radio system is tracking or guiding a stationary target. The rate errors also depend on the speed that the radio rays pass through the atmosphere while following a moving target. These errors are significant when the rays are cutting through the atmosphere at speeds above that of the prevailing wind (which was about 10 ft/sec for the data shown above). Further discussion of this appears in Section 4. of this report.

2.3 Effects of the Ionosphere

"Radio seeing" is a problem of considerable interest which affects many important applications. Just as in "optical seeing," the radio source near the horizon twinkles as a result of amplitude scintillation of the arriving waves, and in addition, the apparent direction of arrival jitters around. It is to be expected that the radio waves arriving from directions near the horizon will be drastically modified by the horizontally stratified atmosphere. There will, of course, be an overall gross bending or refraction of radio waves, depending on the angle at which they enter the earth's atmosphere. The purpose of this discussion is to evaluate

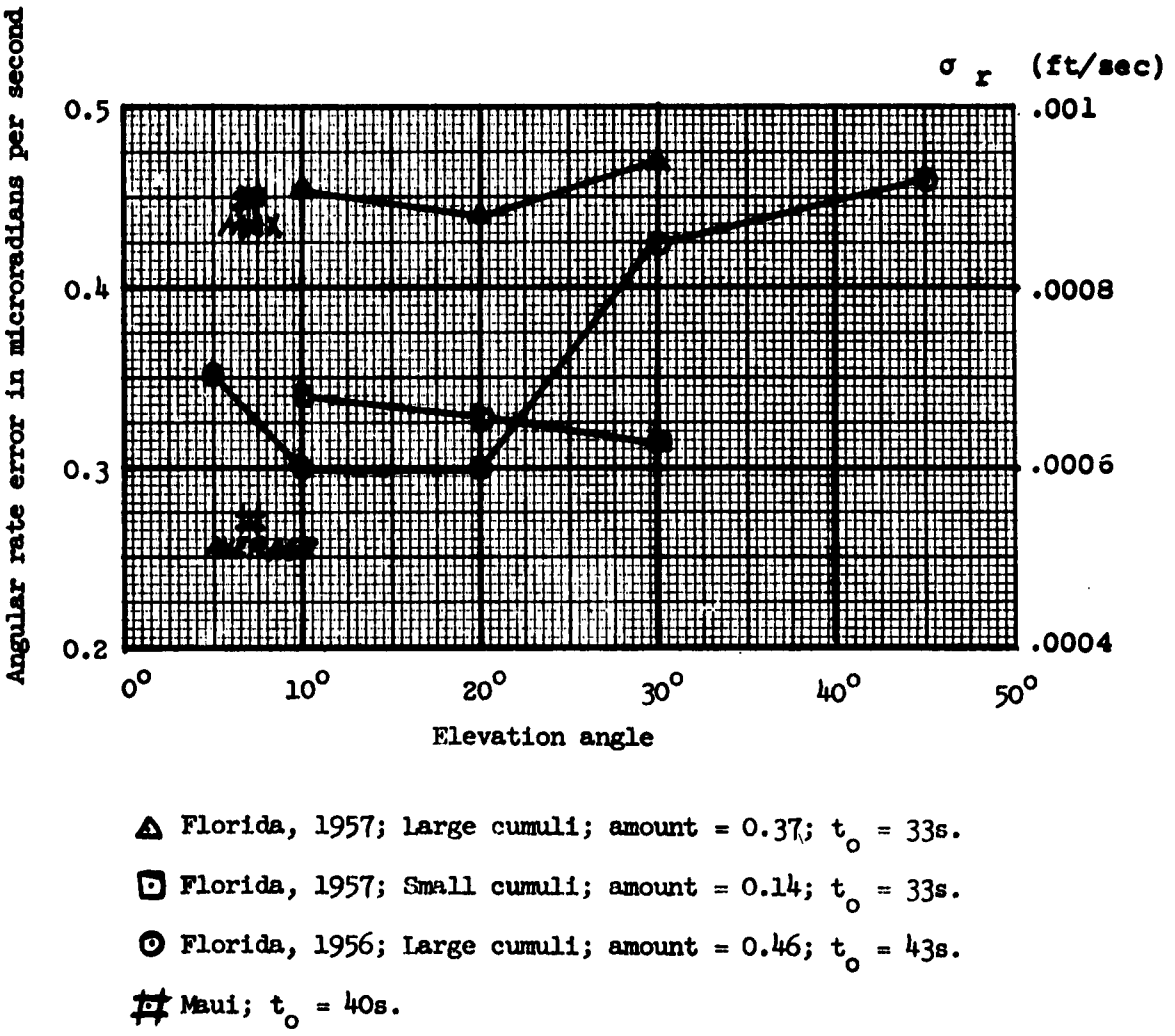

Figure 2-11. Azimuthal RMS angular rate errors as a function of elevation angle. 2000 ft. baseline interferometer system.

how the distortion of radio fields by the ionosphere affect radio frequency positioning systems, and to specify the limits on angle and range corrections possible for ionospheric refraction.

If the energy follows the radio ray, then the refraction effects of the troposphere and ionosphere are additive. In the troposphere the index of refraction is independent of radio frequency and the ray bending is a monotomically decreasing function of elevation angle. In the case of ionospheric bending, the magnitude of the refraction is frequency-dependent and it is a monotonically decreasing function of elevation angle only for sources at distances large compared to ionospheric heights. For vehicle heights between one hundred and four thousand miles, the refraction error initially increases with the elevation angle, attains a maximum value at elevation angles on the order of 100 to 200 milliradians, and then gradually decreases. At ionospheric heights, the elevation angle at which the ionospheric bending is maximum is roughly proportional to the square root of the layer height. In order to evaluate the range and angle errors to be expected, a model of the ionosphere must be selected.

a. Refractive Index of the Ionosphere

As a first approximation, it is assumed that the index of refraction in the ionosphere is spherically stratified with a radial gradient only. Weisbrod (1959) has developed a simple method for computing atmospheric refraction effects on radio waves, where the refraction index profile has been replaced by a finite number of linear segments whose thickness is small compared with the earth's radius. Since there is no limitation on the geometry of the calculations related to the shape of the refractive index profile, the method has a wide application to other refractive effects such as retardation, doppler error and Faraday rotation. The earth's magnetic field has a negligible effect on the phase velocity of very high frequency radio waves; on the other hand, the Faraday rotation may be appreciable.

The relationship between the index of refraction, the radio frequency and the electron density in the ionosphere is the following:

$$n = \left[1 - \frac{N_e e^2}{\epsilon_o m \omega^2}\right]^{\frac{1}{2}} , \qquad (2\text{-}19)$$

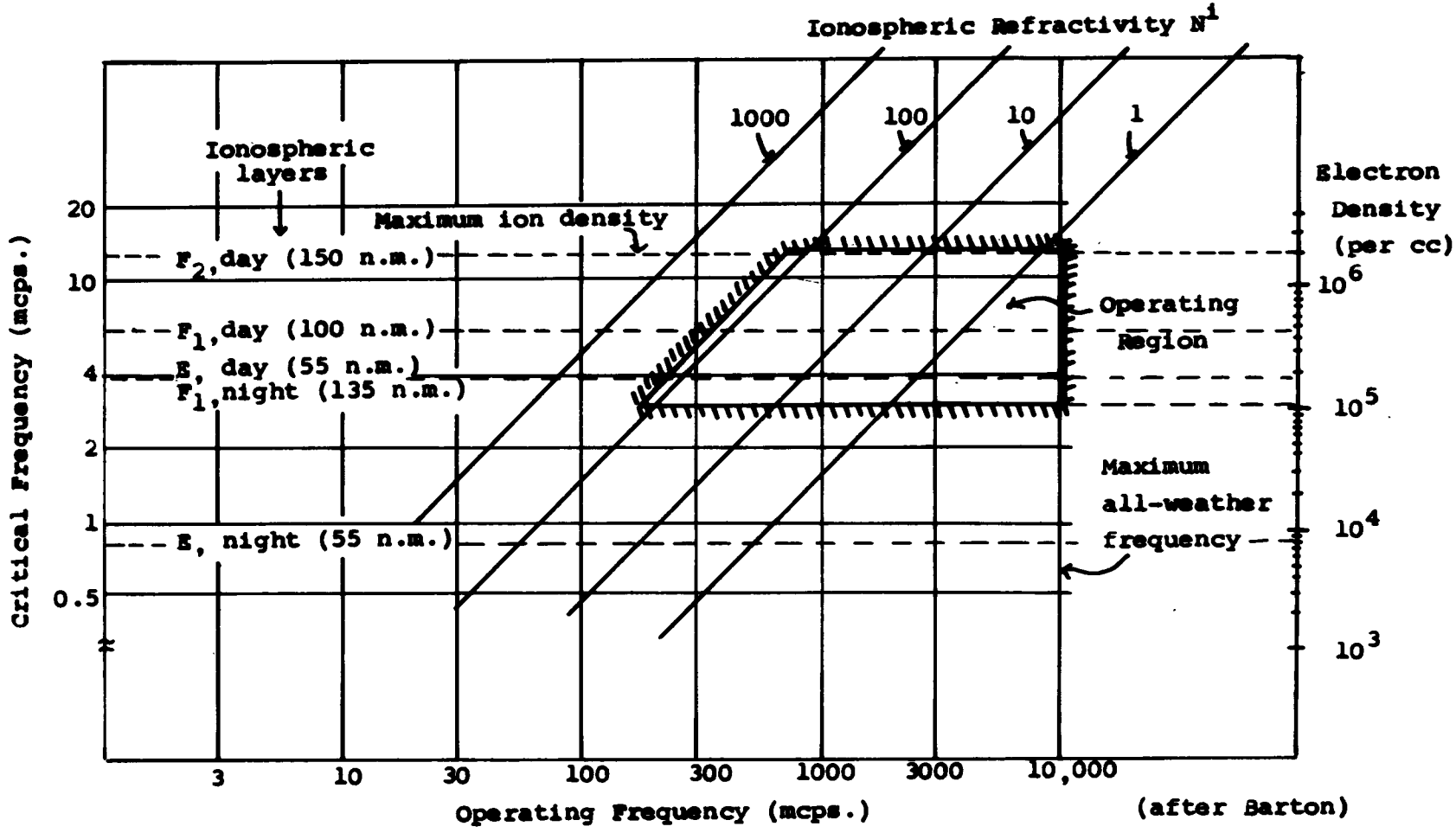

Figure 2-12. Ionospheric Refractivity vs. Operating and Critical Frequencies and Electron Density

$$n \cong 1 - \frac{1}{2} \frac{N_e e^2}{\epsilon_o m \omega^2} \quad , \qquad (2\text{-}20)$$

where:

N_e = electrons per cubic meter,
e = electronic charge (1.60×10^{-19} coulomb),
m = electronic mass (9.08×10^{-31} kilogram),
ω = 2π times the frequency,
ϵ_o = permittivity of free space (8.854×10^{-12} farad/meter).

The electron density variation with elevation is not the same all over the earth; it varies with latitude, season, time of day, sunspot cycle, and sporatic conditions. A great deal of information is available on the electron density profiles below the height of maximum density; these data are computed from ionospheric vertical soundings taken at a network of stations. Jones (1962) has attempted to represent the diurnal and geographic variations of these data by numerical methods. He discussed the various problems associated with the basic data and the analysis. To gain information about the electron profile above the F maximum requires a different kind of measurement. Currently, rocket and backscatter data are available; in the near future a satellite carrying a "top-side" sounder will yield ionogram data above the F maximum.

An electron density profile obtained from rocket measurement above Wallops Island, Virginia at a latitude of 38° made during the daytime up to an altitude of 600 kilometers is shown in Figure 2-13 (taken from Jackson (1961)). Bowles (1962) has reported results of observations of incoherent scatter obtained at the Lima Radar Observatory, located at minus twelve degrees latitude. Two electron density profiles taken at this station are shown in Figure 2-14. These results indicate a tendency of the decay of electron density with height of the top-side of the F region to be exponential. The slope of the exponential decay appears to vary from one day to the next and from one time of day to the next by a factor of two. Electron density profiles available above the F layer maximum indicate that a hyperbolic secant is a better fit than the Chapman distribution, which is parabolic. Therefore, the model for electron density selected consists of a parabolic variation below the height of maximum electron density matched

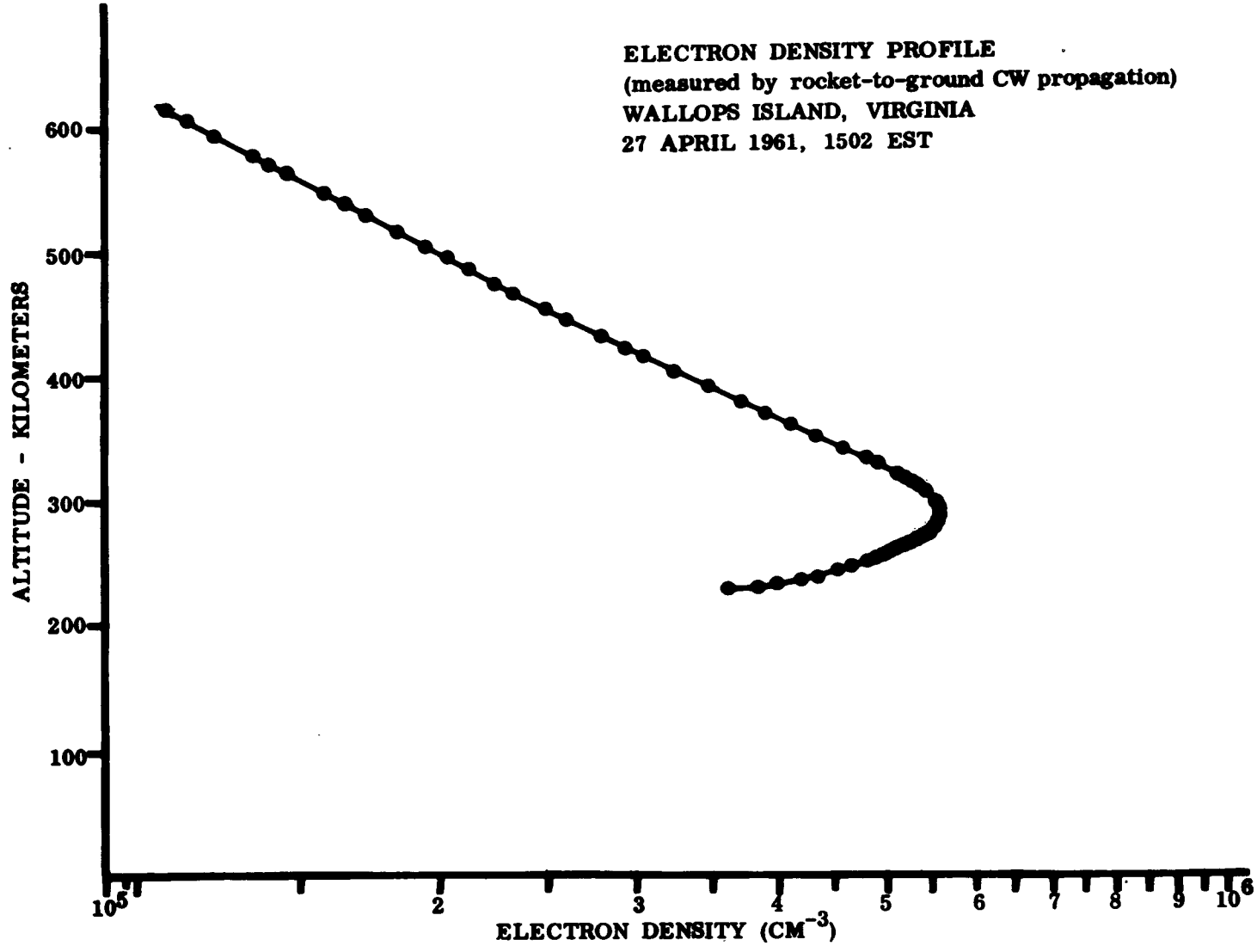

Figure 2-13. Typical measured electron density profile.

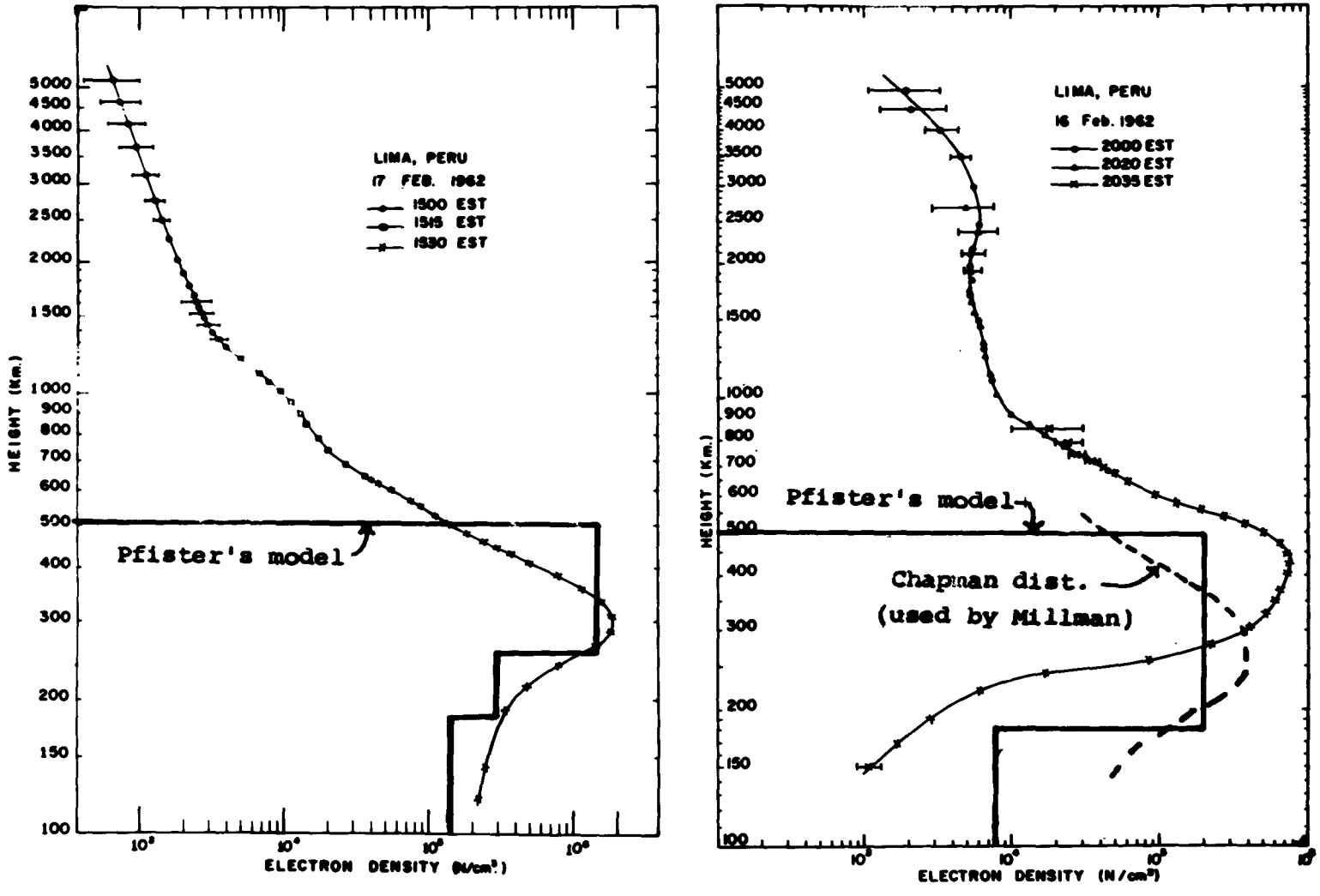

Figure 2-14. Comparison of ionospheric models with measured profiles for day and night conditions.

to a hyperbolic secant profile above the maximum.

An early study of ionospheric effects on tracking (Pfister and Keneshea, 1956) used simplified models of day and night profiles, indicated by the rectangular plots on Fig. 2-14. The results of this study, which indicate the order of magnitude of ionospheric range and angle errors, are shown in summary form in Figs. 2-15 and 2-16. It should be emphasized, and will be shown below, that these errors are subject to large variations on a day-by-day basis, in addition to the diurnal, seasonal and sunspot-cycle trends.

Ionospheric Model

For the purpose of computation of refractive effects from ionosonde data, it is necessary to postulate a model of the ionosphere which would approximate the observed data. The normally available data contain information from which one can obtain the height of the base of the layer, h_o, the height of the maximum electron density, h_m, and the critical frequency of the layer, f_c. It is therefore desirable to choose a model which has three degrees of freedom and is also in accord with available experimental data regarding the electron density profiles.

The shape of the ionospheric electron density profile below the maximum can be fairly well approximated by a parabolic distribution. The shape of the profile above the region of the maximum density is less well known. From data obtained from rocket soundings of electron density, it is believed that the electron density above the peak of the F region does not fall off as rapidly as it might have been expected from the Chapman distribution. Also, the Faraday rotation experiments indicate that the total electron content above the maximum density is about three times as large as below it. Using these facts the following model may be postulated.

$$N_e/N_o = 1 - (1 - \sigma)^2 \quad , \quad 0 \leq \sigma \leq 1 \qquad (2\text{-}21)$$

$$= \operatorname{sech} 1/4\pi\,(\sigma - 1) \quad , \quad \sigma \geq 1$$

where:

N_e = electron density per cubic meter,
N_o = maximum density,
$\sigma = (h - h_o)/y_m$,

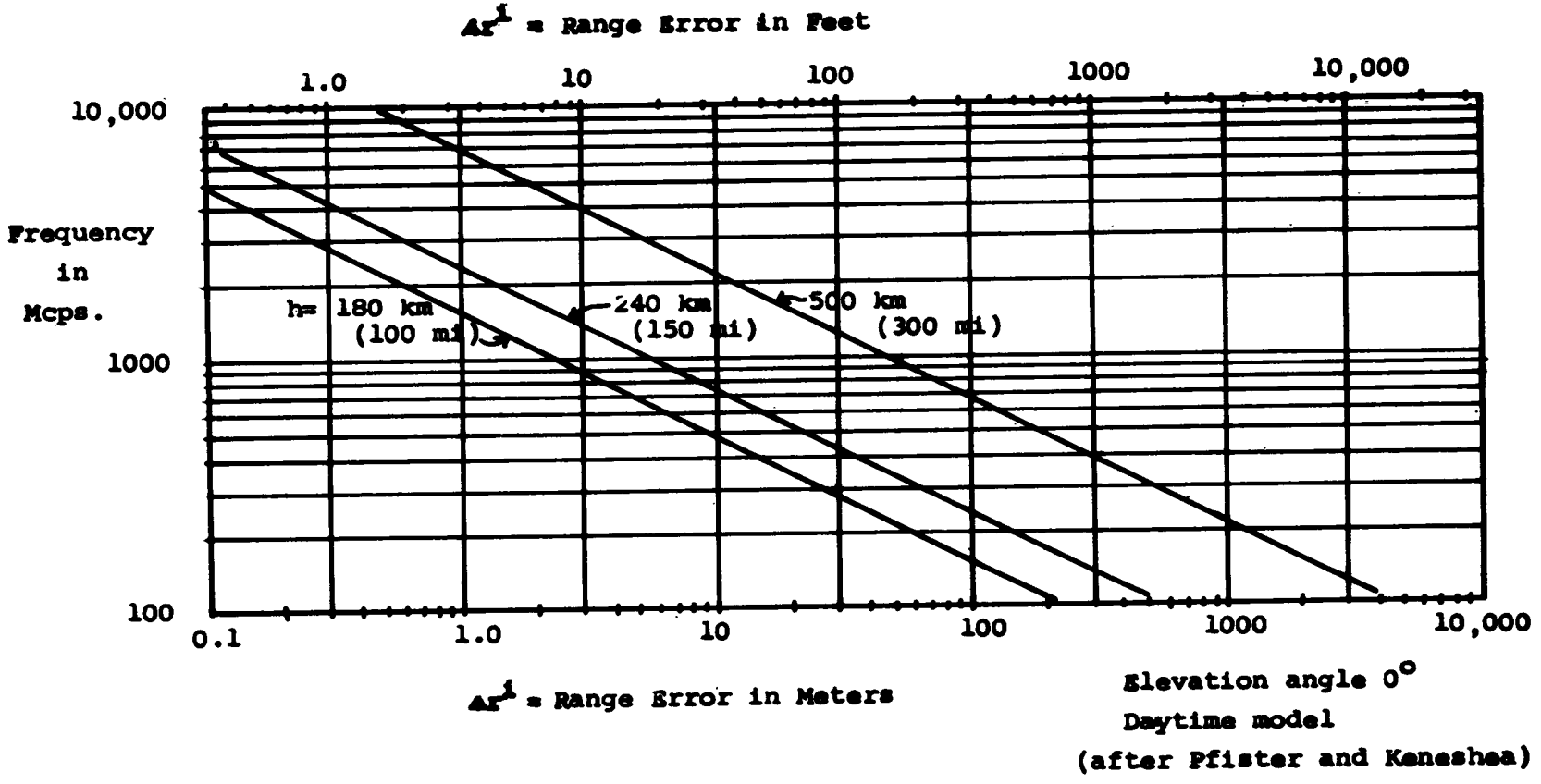

Figure 2-15. Ionospheric range error vs. Frequency

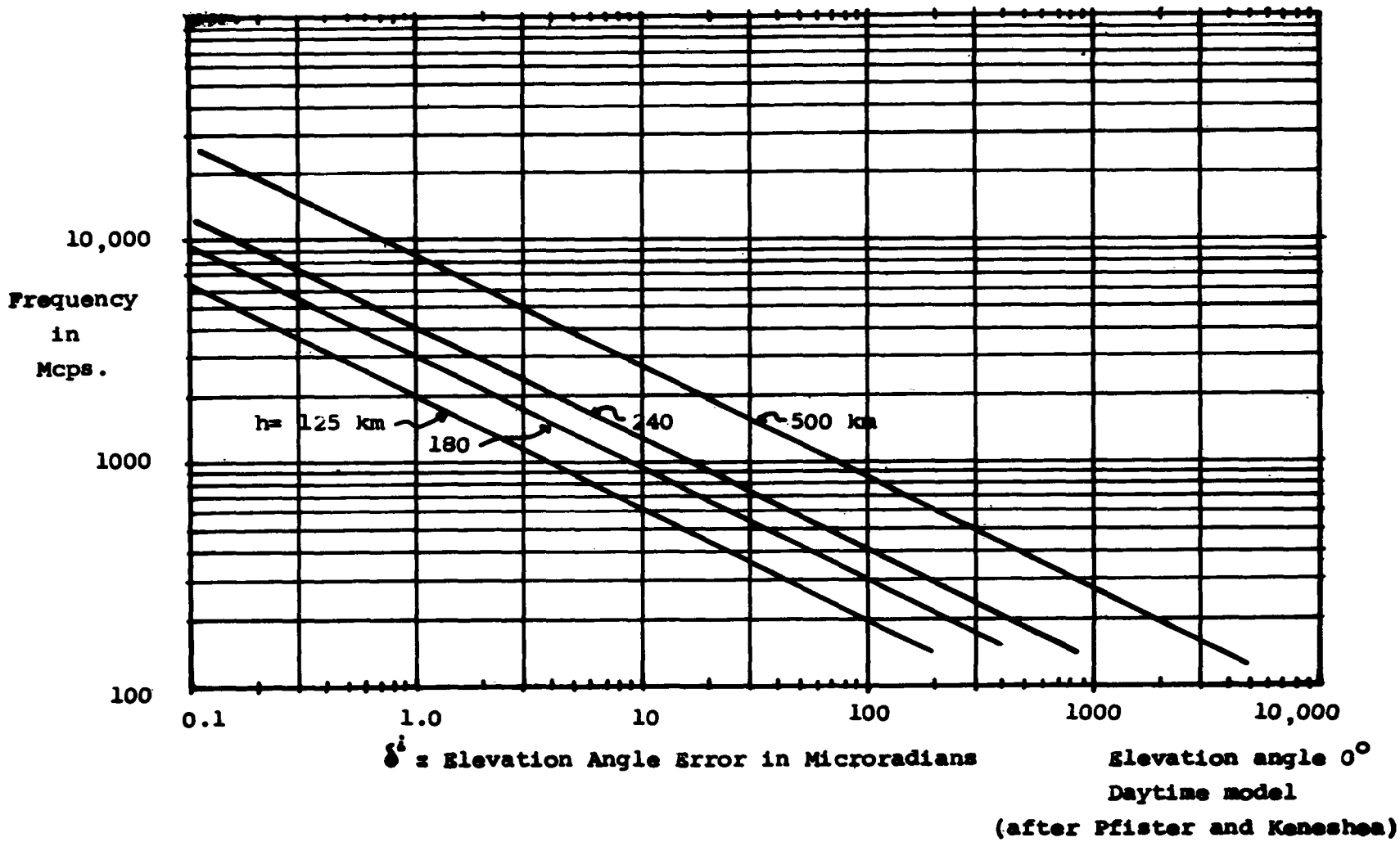

Figure 2-16. Ionospheric angle error vs. Frequency

y_m = half thickness of the parabolic layer
$= h_m - h_o$,
h = height above the ground,
h_o = height of the base of the layer,
h_m = height of the maximum electron density.

This model has the following desirable characteristics:

1. The model has three degrees of freedom, (h_o, y_m, and N_o) which can be obtained from ionogramic data. These parameters uniquely specify the entire distribution.
2. The distribution is parabolic below the maximum density, nearly twice as thick parabolic immediately above the maximum and exponential at great heights.
3. The electron content of the distribution above the maximum is three times that below it.
4. The entire electron density profile and its derivative are continuous everywhere.

Figure 3-17 is a plot of the ionospheric model. The heights of the base, the maximum density and the point of interest define σ, and the ionospheric N^i unit is obtained from

$$N^i = 1/2 \ (N_e/N_o) \ (f_c/f)^2 \times 10^6 \ , \qquad (2\text{-}22)$$

where:

f_c = critical frequency of the layer
$= 8.97 \ N_o^{1/2} \times 10^{-6}$ megacycles per second,
f = signal frequency in megacycles per second.

The h_o, h_m, and f_c parameters refer to the F layer.

Using this model, the refractive effects of the D and E layer are not singled out. The reason for this is that they are quite small in comparison with those due to the F layer and are approximately accounted for by allowing the electron density at the bottom edge of the F layer to be zero. Furthermore, the shape of the electron density profile above the maximum is not too well known and since this region, as far as the refractive effects of the ionosphere are concerned, is probably much more important than the D and E layers, it was felt that the introduction of a more complicated ionospheric model is not justifiable. However, if and when accurate ionospheric data from rocket soundings are available

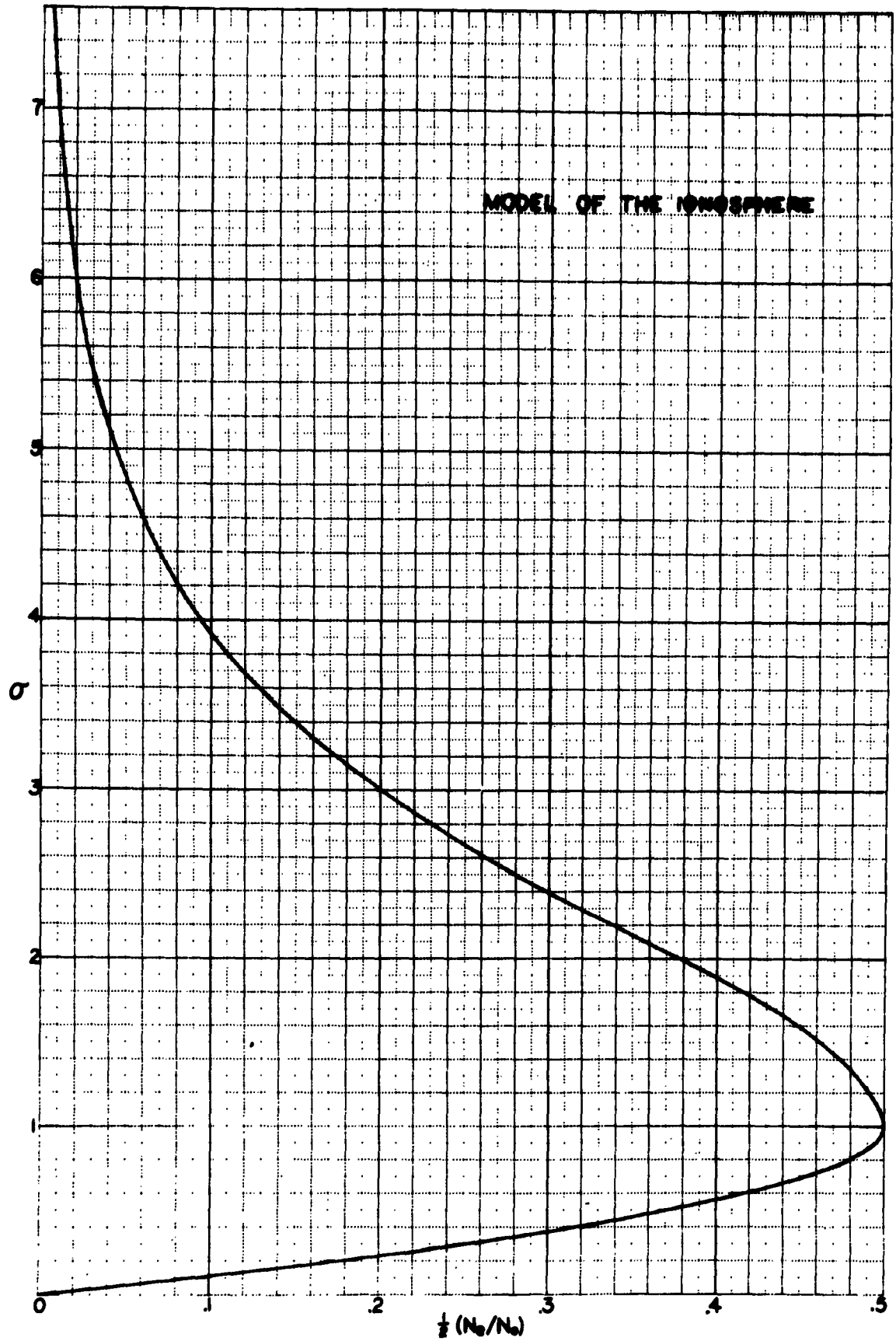

Figure 2-17. Three-parameter model of ionosphere.

with comparable regularity to present radio soundings, it is possible that the use of more intricate models should be undertaken.

b. Computation of Ray Bending Due to the Ionosphere

Computational methods have been developed which afford simple means of calculating ionospheric bending from electron density profile data. These are described by Weisbrod (1959). In essence these methods are based on the following:

1. Index of refraction profiles are computed from electron density profile data, where the index of refraction, "n", as a function of transmission frequency, "f", and electron density, "N_e", is given by equation 2-19 and may be approximated by

$$n \approx 1 - \frac{40.3N_e}{f^2} \quad , \tag{2-23}$$

for frequencies well above the critical frequency. If "N" units are employed in the calculations where $n = 1+N \times 10^{-6}$, then

$$N = -4.03 \left(\frac{N_e}{f^2}\right) \times 10^{-5} \quad . \tag{2-24}$$

In these calculations, the magnetic field of the earth is neglected, since, at frequencies above 100 mc, the effect of the terrestrial field on refractive bending is negligible.

2. To afford practical means of computation, index of refraction profiles are approximated by straight line segments.

3. Account is taken of the spherical stratification of the ionosphere. Thus the angles of importance in application of Snell's law are those angles between the ray tangent and layer tangent at a given point. See Figure 2-18.

Principle formulae in the resulting calculations for bending are

$$\gamma_{jk} = \frac{2(h_j - h_k) \times 10^3}{\tan \beta_j + \tan \beta_k} = \frac{N_j - N_k}{500\,[\tan \beta_j + \tan \beta_k]} \quad , \tag{2-25}$$

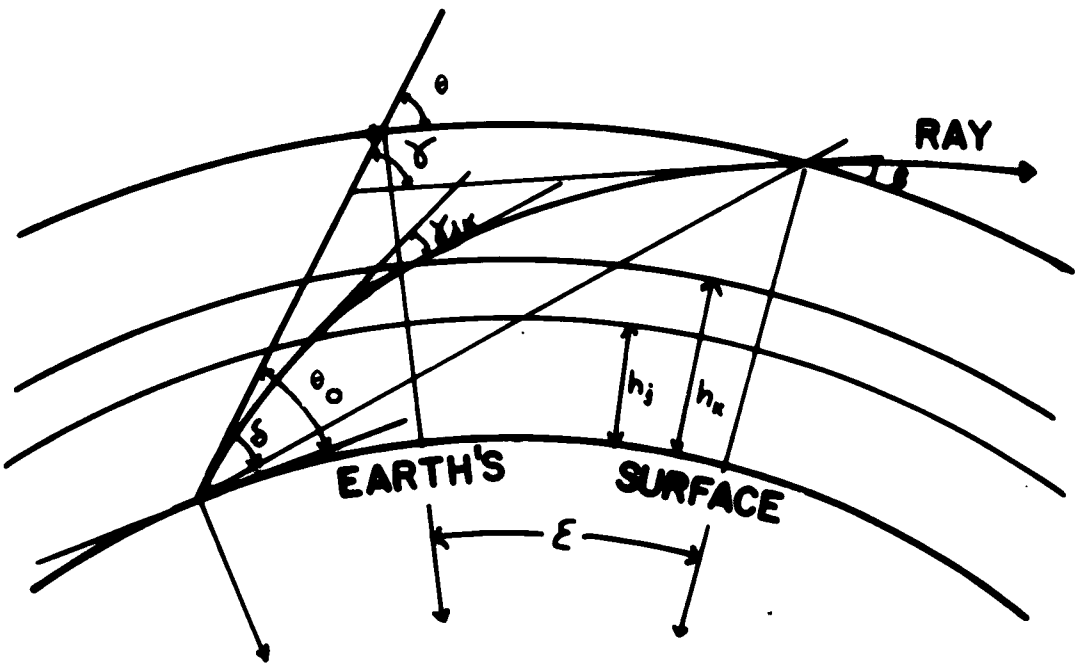

Figure 2-18. Geometry of refraction.

where γ_{jk} is the incremental bending in milliradians through altitude change from h_j to h_k (k referring to upper boundary), and the β's are the ray inclinations at the layer boundaries. The value of β at each layer boundary is determined from Snell's law,

$$n\rho \cos\beta = h_o a \cos \theta_o \quad , \tag{2-26}$$

where a is the earth's radius, and $\rho = a + h$, the latter symbol denoting the height of the layer boundary. Total bending through the ionosphere is then given by

$$\gamma_{total} = \sum_{k=0}^{m} \frac{N_k - N_{k+1}}{500 \left[\tan \beta_{k+1} + \tan \beta_k \right]} \tag{2-27}$$

For ionospheric bending, the minimum value of β even for a tangentially departing ray ($\theta_o = 0$) is about 200 milliradians. Under these conditions the difference between the ray inclination angles of the refracted and the unrefracted rays is very small such that very little error is introduced if equation (6) is written as,

$$\gamma = \sum_{k=0}^{m} \frac{N_k - N_{k+1}}{500 \left[\tan \theta_{k+1} + \tan \theta_k \right]} \quad , \tag{2-28}$$

where the θ's denote ray inclination angles at the boundaries of the layer neglecting curvature of the ray within the layer.

Computation of Error Angle

As will be noted from Figure 2-18, the apparent shift in position of the target is not described by the ray bending γ, but by the angle δ. Moreover, since δ is the practical angle of interest at this point in the discussion, it is necessary to consider the troposphere effects together with those produced by the ionosphere.

In order to determine the value of δ from calculated values for γ, it is useful to express the refractive bending in terms of the angle subtended at the earth's center between the refracted and the unrefracted rays. This angle, ϵ, is given by

$$\epsilon = \delta - (\theta - \beta)$$
$$= \delta - (N_o - N) \cot \theta \quad , \tag{2-29}$$

where:

$\epsilon = \epsilon^t + \epsilon^i$,

$\delta = \delta^t + \delta^i$,

N_o = surface value of the refractivity,

N = value of the refractivity at the target height.

At infinite distances cot θ approaches zero and ϵ and δ become equal to each other. For computational reasons it is usually convenient to split equation (2-27) into the tropospheric and ionospheric components.

$$\epsilon^t = \delta^t - N_o \cot \theta \tag{2-30}$$

$$\epsilon^i = \delta^i + N^i \cot \theta \tag{2-31}$$

The quantity of the greatest practical interest is the elevation angle error δ, which can conveniently be expressed in terms of

$$\delta = \frac{\epsilon \tan \theta + \epsilon^2/2}{\epsilon + \tan \theta - \tan \theta_o} \quad . \tag{2-32}$$

It should be noted that the tropospheric and the ionospheric contributions to δ are not strictly additive. However, in nearly all practical cases $\epsilon/2$ is much less than tan θ and ϵ is much less than tan θ - tan θ_o, so that only a negligible error is introduced if δ is considered to be directly proportional to ϵ. This approximation is extremely convenient since it permits a separate treatment of the tropospheric and the ionospheric δ's.

Range Errors and Faraday Rotation

The range errors can be evaluated by a method analogous to that used for computing γ:

$$\Delta r^i = \sum_{k=0}^{m} \frac{(N_k + N_{k+1})\ (h_{k+1} - h_k)}{1000\ (\sin \theta_{k+1} + \sin \theta_k)} \tag{2-33}$$

where:

h = height in kilometers,

and Δr^i = range error in meters.

The accuracy of equation (2-33) is adequate for most practical purposes. For layer laminations of less than 100 km, and a tangentially departing ray, the values of Δr^i are within 5% of the exact values. For thinner laminations, (which is normally the case) or higher angles of elevation, the agreement is even better.

Equation (2-33) also offers a convenient method for computing the Faraday rotation. It turns out that the number of rotations of the plane of polarization is very nearly proportional to Δr^i. For the case of a thin layer the relationship between the Faraday rotation and Δr^i is

$$\Delta \Omega = \frac{2 \cos \phi}{\lambda_g} \Delta r^i \quad , \qquad (2\text{-}34)$$

where:

Ω = the number of rotations of the plane of polarization for a double passage through the layer,

ϕ = the angle between the wave normal and the magnetic field,

λ_g = gyro wavelength.

Both ϕ and λ_g are functions of a position. However, the rate of change of these quantities is sufficiently slow so that F region values of these parameters may be treated as constants applicable to the entire path.

c. Statistics of Ionospheric Errors

To illustrate the magnitude and variation of the errors in elevation angle and range which may be ascribed to the ionosphere, the results of calculations are given in Figures 2-19 through 2-22 for 100 mc for three different locations: Iverness or Leuchars, Scotland; Thule, Greenland; and Fairbanks, Alaska. Since ionospheric parameters are subject to wide fluctuations, it is necessary to select representative situations and group them in some logical

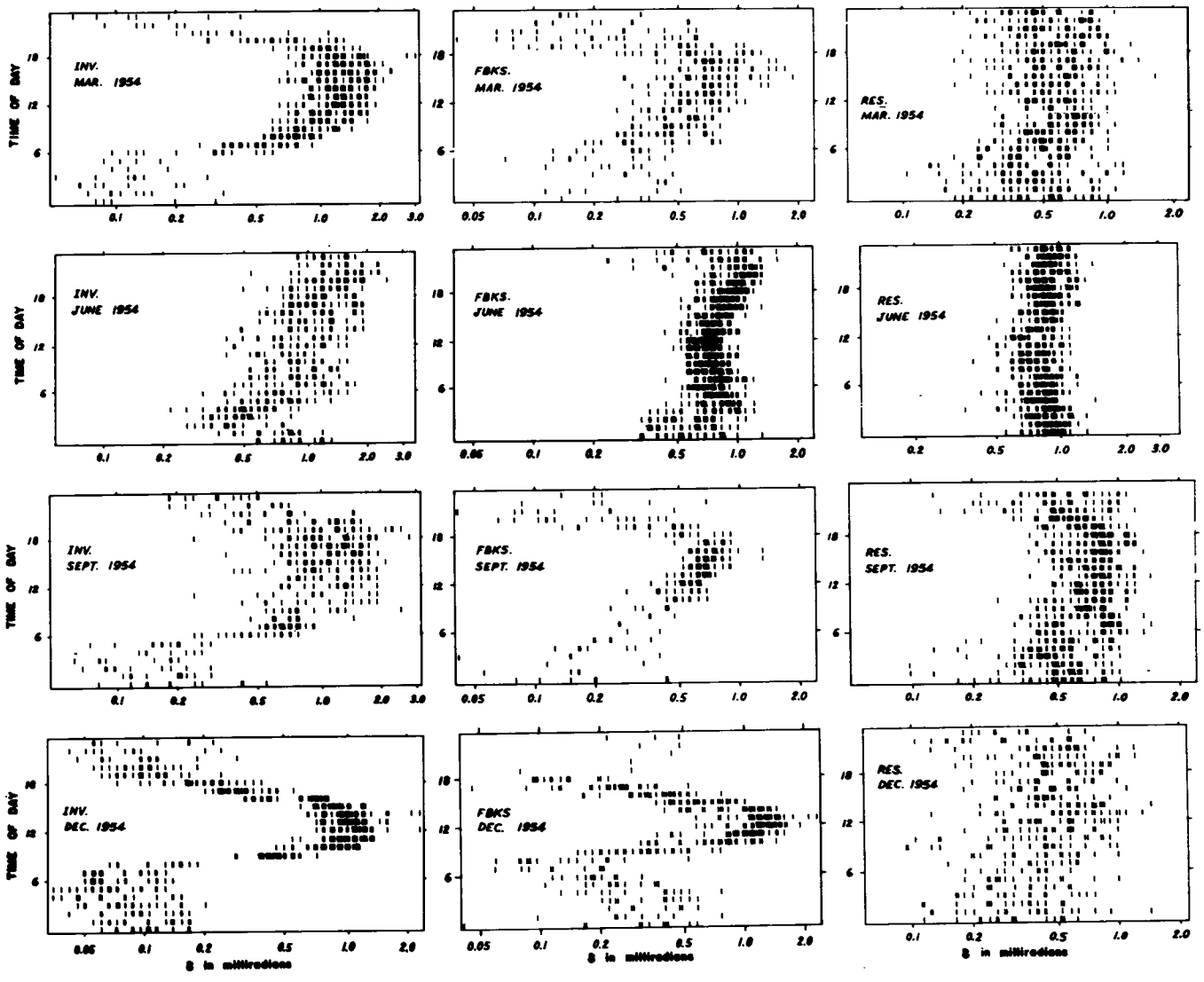

Figure 2-19. Distribution of ionospheric angle error
(f=100 mcps, θ_o=0, h=1000 n.mi.)
Low sunspot activity.

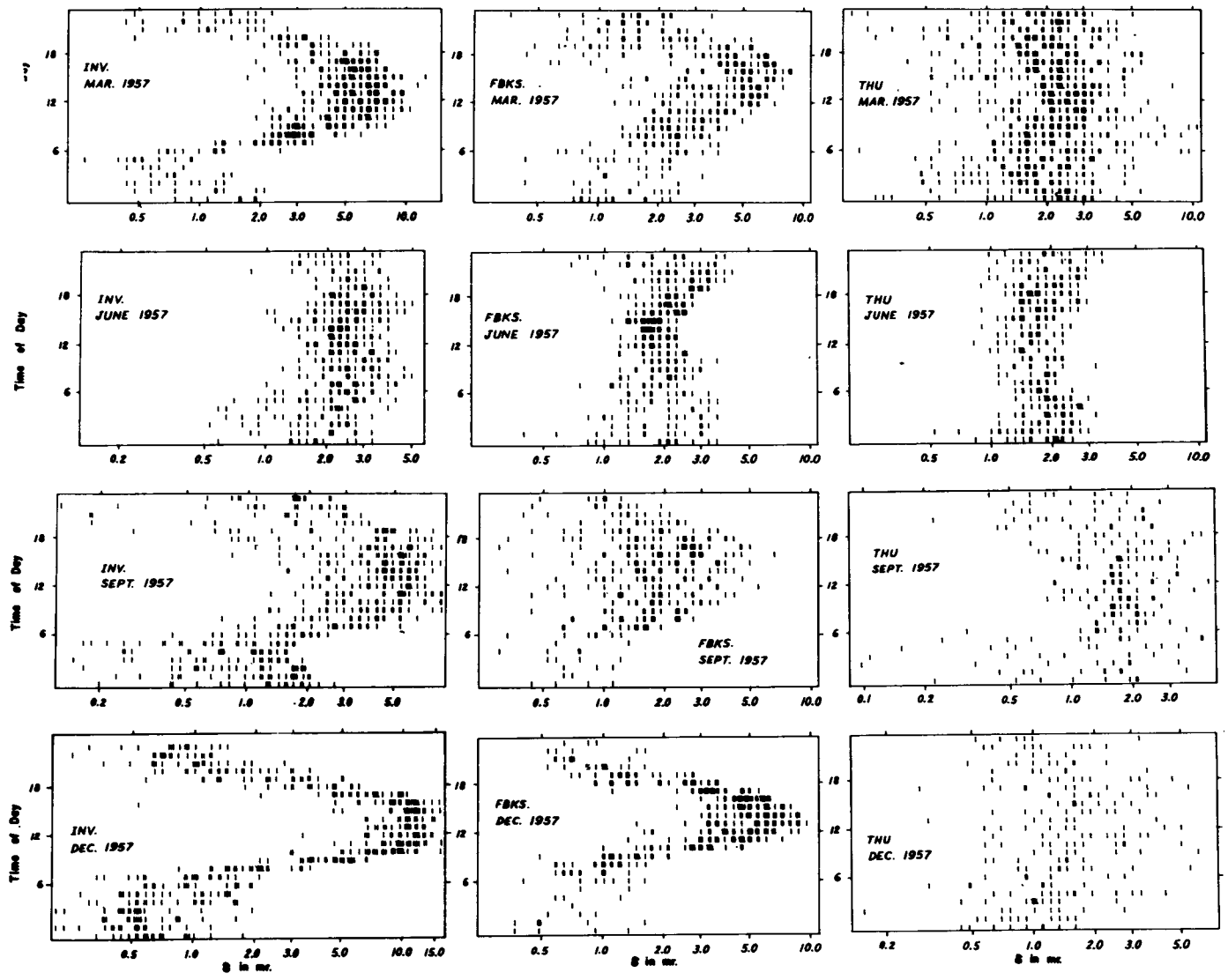

Figure 2-20. Distribution of ionospheric angle error .
(f=100 mcps, θ_o=0, h=1000 n.mi.)
High sunspot activity.

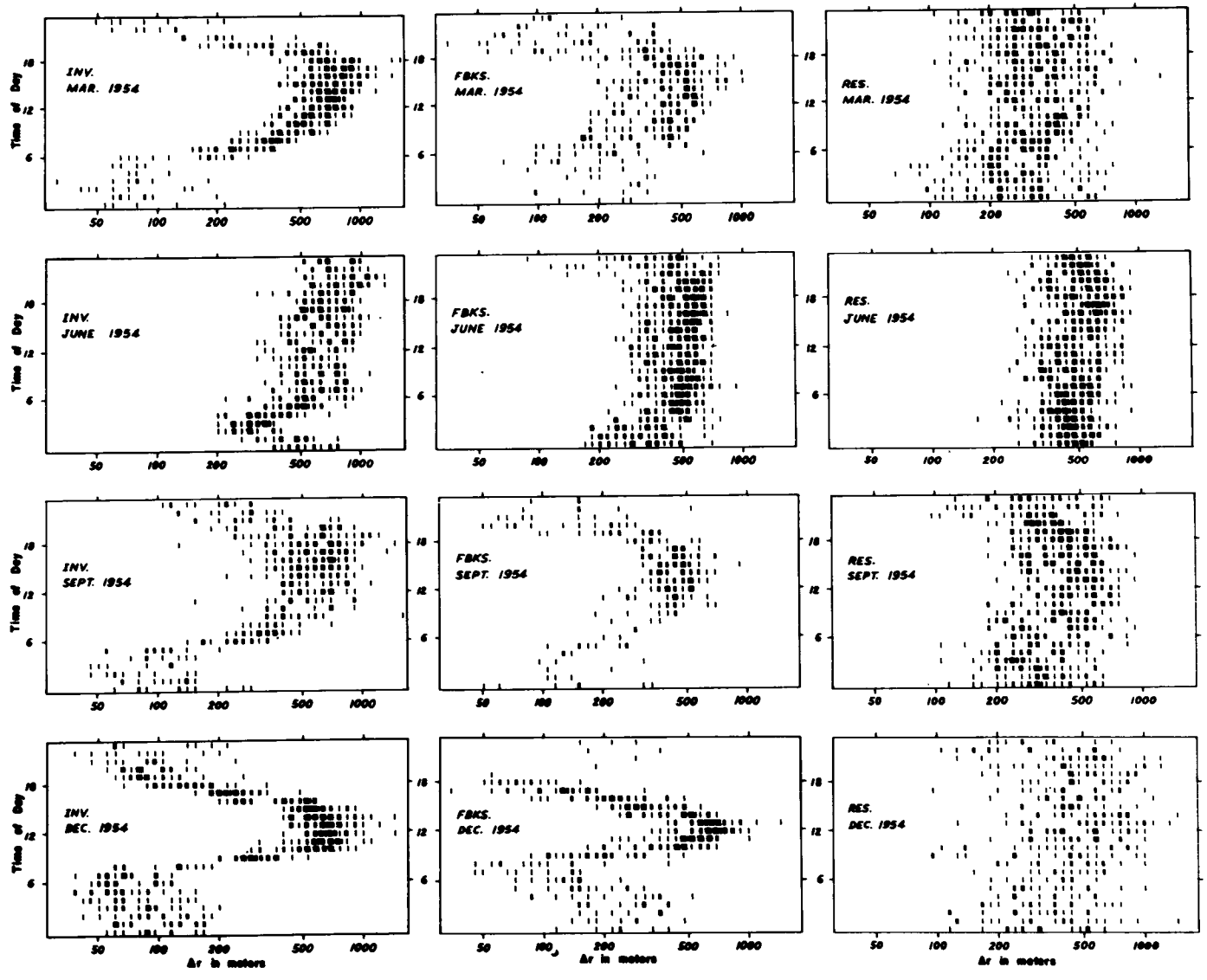

Figure 2-21. Distribution of ionospheric range error Δr^1.
(f=100 mcps, θ_o=0, h=1000 n.mi.)
Low sunspot activity.

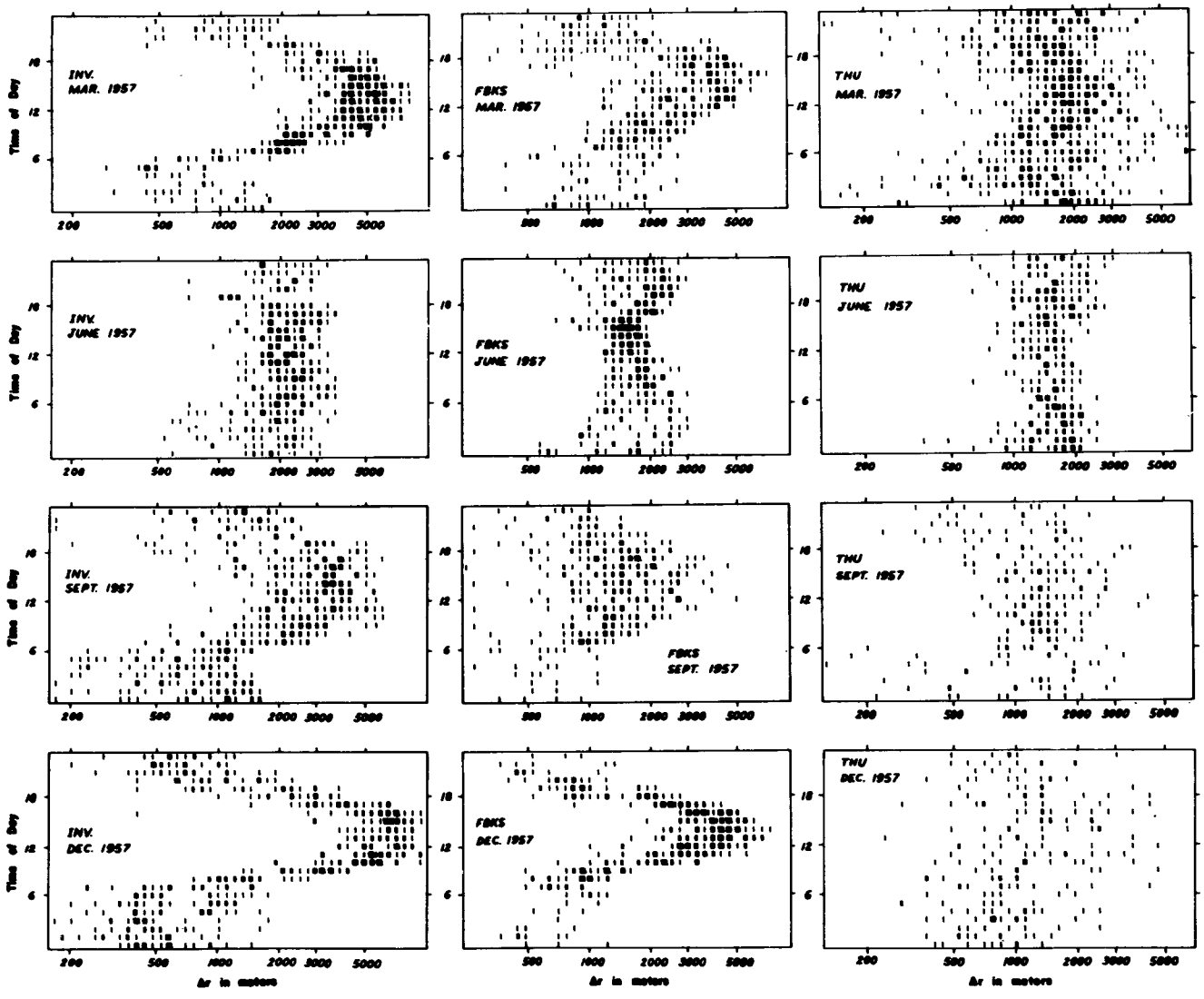

Figure 2-22. Distribution of ionospheric range error r^i.
(f=100 mcps, θ_o=0, h=1000 n.mi.)
High sunspot activity.

fashion. The three most important parameters are the sunspot cycle, the seasonal, and the diurnal variations. Thus, data is shown for March, June, September, and December of 1954 and 1957. Individual points are for particular days of the month. Average diurnal variations may therefore be inferred from maximum point density distribution. The years of 1954 and 1957 represent, respectively, low and high sunspot activity. Since there is no 1954 ionospheric data for Thule, the data for Resolute Bay, Canada were used in the calculations for that year since the location of Thule and Resolute Bay lie in reasonable comparable geographic and geomagnetic latitudes and thus ionospheric data from the two locations are similar. Since the data in Figures 2-19 through 2-22 were calculated for 100 mc, to employ these results for higher transmission frequencies, advantage may be taken of the inverse square dependence of ionospheric index of refraction on frequency. Thus, error angles for 200 mc could be determined from these data by scaling down each value for error angle by a factor of four.

Figures 2-23 and 2-24 show the change in error angle and range error with sighting elevation angle, θ_o. These data were computed for a critical frequency of one megacycle. Thus, the values for δ^i and Δr^i in Figures 2-19 through 2-22 which are given for $\theta_o = 0$, may be determined for other sighting elevation angles. It is interesting to note the increase of δ^i with θ_o to a maximum near 100-200 milliradians.

The following interesting generalizations may be drawn from the data in Figures 2-19 through 2-22:

1. When there is a diurnal variation it is strongest in December and weakest in June.
2. The shape of the diurnal variation is the same throughout the sunspot cycle, but the values of the errors are approximately five times as great during the sunspot maximum as during the sunspot minimum.
3. The diurnal variation is greatest at the station farthest from the geomagnetic pole and almost non-existent near the pole.
4. The relative spread of values at any one hour is greater during the night time hours than during the daylight hours and is larger near the pole than away from the pole.
5. The diurnal variation may exceed an order of magnitude.

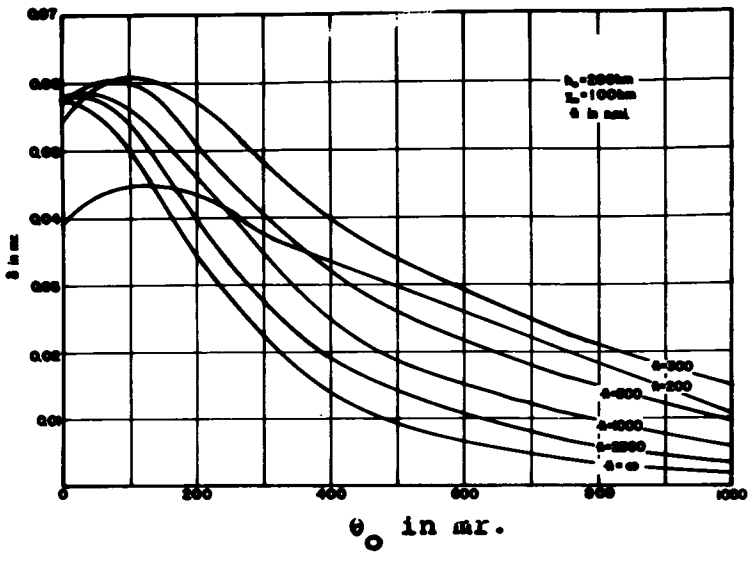

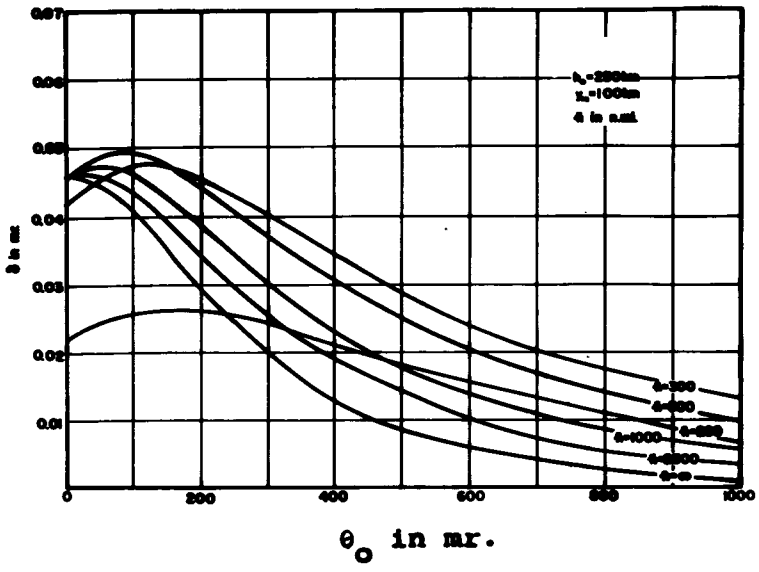

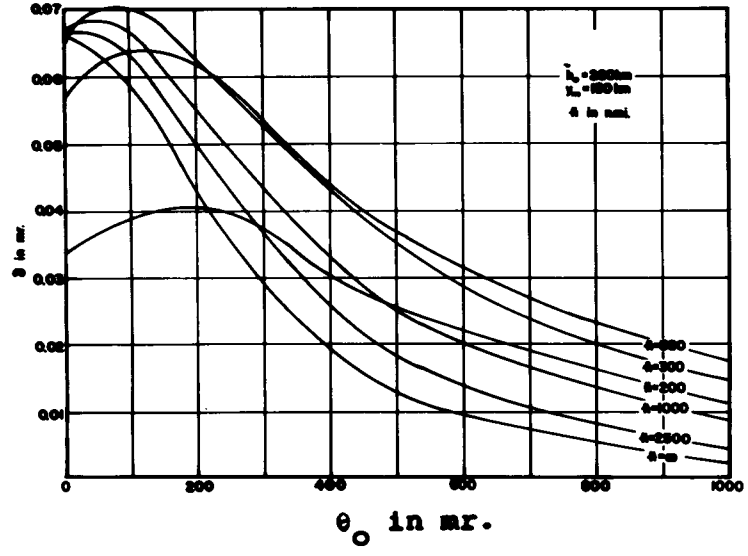

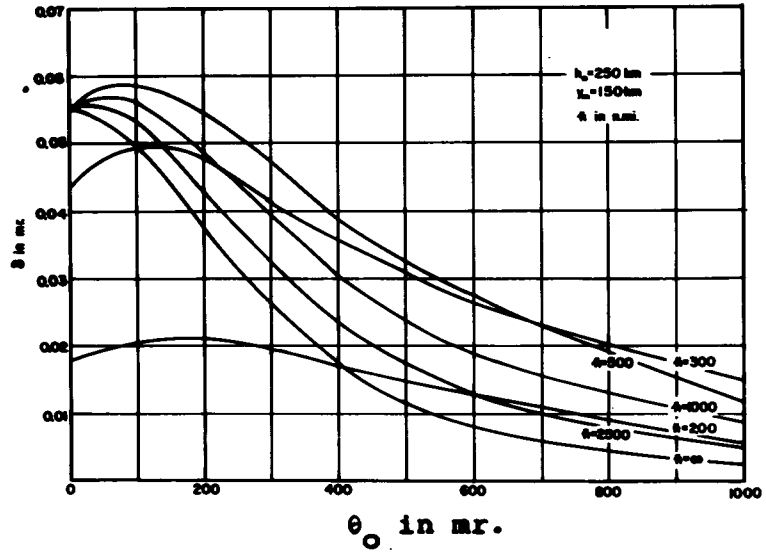

Figure 2-23. Variation of angle error with elevation.
(f=100 mcps, f_c=1.0 mcps.)

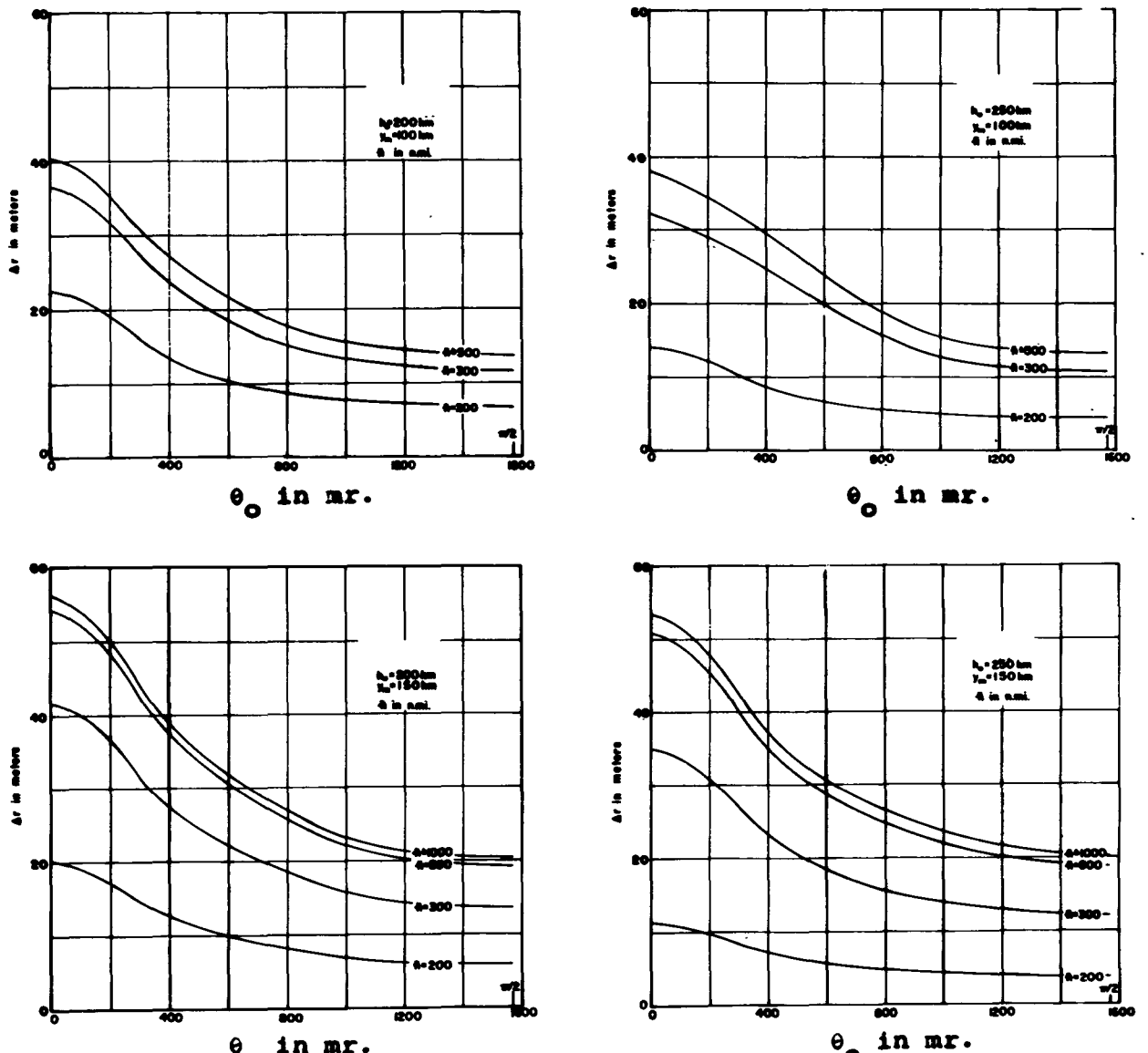

Figure 2-24. Variation of range error with elevation.
(f=100 mcps, f_c=1.0 mcps.)

Of the three factors which affect the magnitude of δ^i and Δr^i, the critical frequency of the layer appears to be the most dominant. It is for this reason that the diurnal shapes of δ^i and Δr^i are quite similar. The second factor which influences the magnitude of the error is h_o. The lower the layer the more oblique is the angle of entrance into the layer and consequently the greater the error. The third factor, y_m, has a greater effect on Δr^i than δ^i.

In general the critical frequency has a more pronounced diurnal variation in winter than in summer, is greater at Inverness than at Thule, and is generally higher during the peak of the sunspot cycle than at its minimum. However, the effects of h_o on δ^i and Δr^i cannot be neglected. In December, h_o decreases during the day and increases at night approximately in phase with f_c. The combination of effects greatly accentuates the diurnal variation in δ^i and Δr^i. In June, h_o is approximately constant, but the variation which does occur is in such a direction as to partially cancel out the smaller effects of f_c, resulting in almost no diurnal variation of δ^i. The variations in y_m have a similar effect on Δr^i.

In addition to the errors discussed above, short-term fluctuations in electron density will cause variation in range measurements over periods of ten seconds to a few minutes. Figure 2-25 is an estimate of such fluctuations, based on data from Pfister and Keneshea (1956) and Colin (1960).

The smooth gross structure of the N profile causes errors which can be corrected if one knows the shape of the N profile, but the inhomogeneities cause an indeterminancy in the actual vehicle location which cannot be resolved. A discussion of observed elevation angle errors using a sea interferometer technique is given in Appendix A.

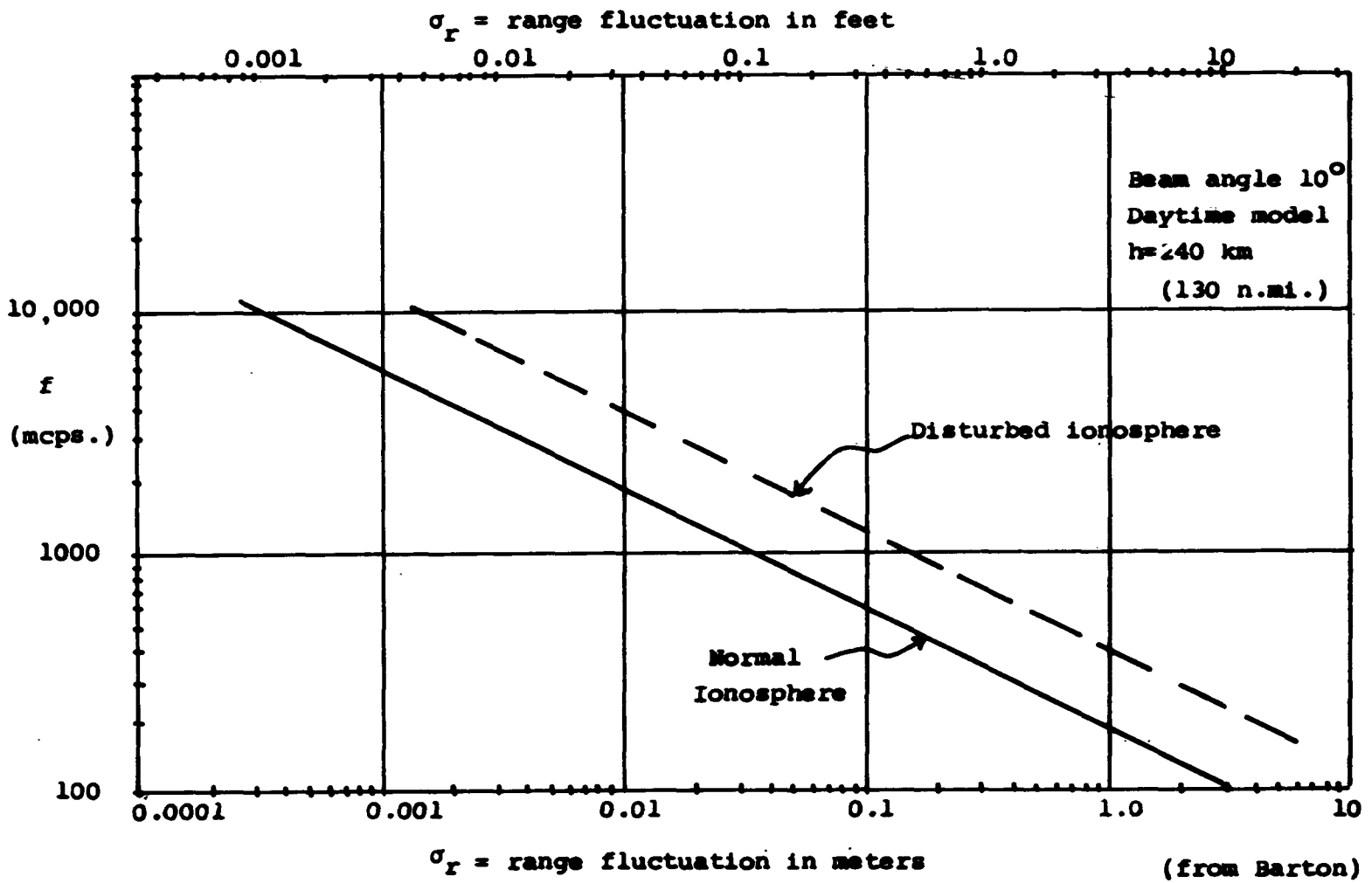

Figure 2-25. Ionospheric range fluctuation vs. Frequency

2.4 References

Bean, B. R., J. D. Horn, and A. M. Ozanich, Climatic Charts and Data of the Radio Refractive Index for the United States and the World., N.B.S. Monograph 22., 1960.

Bean, B. R., and G. D. Thayer, CRPL Exponential Reference Atmosphere, N.B.S., Monograph 4., 1959.

Bowles, Kenneth L., Lima Radar Observatory, N.B.S. Report 7201, 30 April 1961 (Supplement).

Jackson, J. E., and S. J. Bauer, Rocket Measurements of a Daytime Electron Density Profile up to 620 Kilometers, J.G.R., 66, 3055-3057, 1961.

Jones, W. B., and Roger M. Gallet, The Representation of Diurnal and Geographic Variations of Ionospheric Data by Numerical Methods, N.B.S. Report 7230, February 28, 1962, N.B.S. J. Research 66D, (in press).

Norton, K. A., J. W. Herbstreit, H. B. Janes, K. O. Hornberg, C. F. Peterson, A. F. Barghausen, W. E. Johnson, P. I. Wells, M. C. Thompson, M. J. Wetter, and A. W. Kirkpatrick, An Experimental Study of Phase Variations in Line-of-Sight Microwave Transmissions, N.B.S., Monograph 33, 1961.

Pfister, W., and T. J. Keneshea, Ionospheric Effects on Positioning of Vehicles at High Altitudes, A.F. Surveys in Geophysics, No. 83, March 1956 (AD 98777; AFCRC TN-56-203).

Space Technology Laboratories, Inc., Tropospheric Scintillations, STL Report GM-TM-0165-00308, 1958.

Thayer, G. D., and B. R. Bean, An Analysis of Atmospheric Refraction Errors of Phase Measuring Radio Tracking Systems Part I, N.B.S., Boulder, 1962.

Thompson, M. C., H. B. Janes, and R. W. Kirkpatrick, An Analysis of Time Variations in Tropospheric Refractive Index and Apparent Radio Path Length, J.G.R., 65, 1960.

Weisbrod, Steven and L. J. Anderson, Simple Methods for Computing Tropospheric and Ionospheric Refraction Effects on Radio Waves, Proc. I.R.E., 47, 1770-1777, 1959 .

Wheelon, A. D., Radio Wave Scattering by Tropospheric Irregularities, N.B.S. J. Research 63D, 205-233, 1959.

3. ATMOSPHERIC SOUNDING FOR CORRECTION OF TRACKING DATA

3.1 Methods of Measuring & Estimating Tropospheric Profiles

The index of refraction profile may be obtained indirectly through use of radiosonde or dropsonde instruments. Although there are a number of classes of these instruments, their function is similar. Carried aloft on free balloons, or jettisoned by parachute from aircraft or rockets, the device samples the absolute values of dry-bulb temperature, relative humidity, and in some instances, atmospheric pressure of the air through which they move in generally oblique directions as a result of lateral displacement by winds. The measurements are transmitted as a modulation of an r-f carrier signal. A switching device alternately switches circuits to the transmitter, thereby providing a sequence of samples of the parameters being measured, one at a time. It is thus necessary to interpolate over the interruptions in these data by arbitrarily assuming that the intervening variations are smooth. The data are normally recorded on a strip-chart (ground based or in an aircraft) as a deflecting trace. Deflections must be measured and properly interpreted to reconstruct the original parameters. There may be an associated radar tracking the sonde to give space position. At many installations electronic computers are utilized in determining from the chart readings the electrical and optical index of refraction, as well as many other atmospheric parameters.

In the newer radiosonde packages (AN/GMD 2), the temperature element is a resistance type thermister (ML-419/AMT-4). The humidity element (ML-476/AMT) is carbon coated. This humidity element is a vast improvement over the old type ML-418/AMT which was lithium chloride coated. The carbon element has virtually eliminated the lag in the response to humidity changes that was characteristic of the lithium chloride element.

Because of the alternate observations of the parameters, and some lag in the sensors, and since ducting layers may be only a few hundred feet in thickness, the radiosonde may fail to detect the existence of such conditions, or may simply integrate over the whole range of values between the bottom and top of a duct, so that an indication of the true gradients throughout the layer cannot be achieved.

Once a determination is made of the necessary quantities, the index of refraction, n, or more conveniently refractivity, N, can be determined from the equation

$$N = (n-1)\ 10^6 = \frac{77.6}{T}\left(P + \frac{4810p}{T}\right) \qquad (3\text{-}1)$$

where T is absolute temperature in degrees Kelvin, P is atmospheric pressure in millibars, and p is vapor pressure. The constants are reasonably correct as determined by various empirical studies. These particular constants are a re-expression of those recommended by Smith and Weintraub to yield an over-all standard error of $\pm$.5% in N, assuming P, T, and p to be error free.

Much more reliable refraction data can be obtained through the use of any one of several types of apparatus known as microwave refractometers, which measure directly the refractivity of the atmosphere. Since the velocity of propagation of radio waves is a direct function of the radio refractive index, the resonant frequency of cavity resonators and tuned resonant frequency devices in general, are also a direct function of the radio refractive index of the material within the resonant cavity or the dielectric material in the capacitor determining the frequency of resonance. Refractometers using this principle can be classed into two broad categories: those that are capable of determining only the relative change in refractivity from one point to another in space, and those that determine the absolute value of N at any such point. The refractometer can ascertain within plus-or-minus a few N-units the small scale variations of refractivity over the path that it follows. The lag of a refractometer is dictated by the speed of its carrier, and the time required to flush the sample air from the instrument. These usually combine to permit accurate sensing of layers as thin as 100 feet.

AFSC is currently attempting to develop an operational expendable refractometer, which will make economically feasible the routine acquisition of highly accurate refraction data.

In instances when it is not possible to sample the atmosphere, approximations of various sorts may be used to estimate what the N-structure is but with considerable loss in the probable reliability of the profile and of any corrections of space positioning data based on the generated N-structure. Some of the approximations include use of a standard atmosphere, a local average atmosphere, or one of the above adjusted for seasonal and diurnal average variation. Use of a suitable mathematical model which is a function of surface refractivity (which is readily determined from surface observations) is perhaps the best approximation procedure to use.

3.2 Ray Tracing Prodecures for Correction of Tracking Data

Once a table of index of refraction versus altitude is obtained, one might think it possible to obtain an exact propagation correction for an observed elevation angle and range. However, there are several difficulties. Refractivity profiles cannot be obtained for all places and times of interest. Assumptions are therefore normally made that the atmosphere is non-moving, spherically stratified, and the strata are homogeneous, any or all of which may not be true. Thus, any error in the index of refraction profile resulting from measurement or from the above assumptions will be propagated through the calculations, resulting in errors in the computed corrections.

The equations used to perform the calculations leading to corrections for propagation effects are normally based on "ray-tracing" theory which assumes a ray of energy, rather than a "wave front" travels between the target and the receiver. Restrictions of ray-tracing include:

(1) The refractive index should not change appreciably in a wave length.

(2) The fractional change in the spacing between neighboring rays (initially parallel) must be small in a wave length.

Conditions (1) and (2) will be violated if the gradient of refractive index, dn/dh, is very large. "Trapping" can occur whenever a layer of refractive index exists with a vertical decrease of N greater than 157 N-units per kilometer. A layer of this type is a "duct" and the mode of propagation through such a layer is similar to that of a wave guide (Booker and Walkinshaw, 1946). Condition (1) should be satisfied if

$$\frac{(dn/dh) \text{ per km}}{N} < .002\ f_{kc} \qquad (3\text{-}2)$$

where refractivity, N, is defined as

$$N=(n-1)\ 10^6$$

and f_{kc} is the carrier frequency in kilocycles (Bean and Thayer, 1959).

In addition to the ray theory assumptions, some error is introduced into the developed equations through the spherical earth assumption, and even more by a flat earth assumption when such is used.

The correction equations necessarily include definite integrals which cannot be integrated explicitly. It is therefore necessary either to make further simplifying -- and error producing -- assumptions which modify the equations in such a way that they can be explicitly integrated, or to choose a numerical integration technique to perform the integrations. All numerical integration techniques are approximations, and there are many techniques, each with possible variations to choose from. Which technique is "best" for a given integral is not easy to determine. It is thus apparent that errors will be introduced because of the nature of the required computations.

Once a basic technique is chosen, there remain still other possibilities of error. Many mathematical formulas are such that for certain critical spreads of values, to prevent loss of accuracy extended precision (retaining a larger number of significant figures in the computation than is available in a computer "word") is required in the computations, and at times the formulas may completely fail. It is thus sometimes desirable if possible to re-express the equations being used -- either in critical areas or over the entire range -- in a mathematically equivalent form less susceptible to computational error.

Even with these limitations of ray-tracing theory and numerical integration techniques, experience has proven they are still capable of providing much more accurate refraction corrections than are methods based upon approximate curves or assumed standard conditions which do not accurately reflect the actual weather conditions or properly utilize the geometrical considerations.

Understanding that any technique is not error free, it is desirable to select one which will produce a minimum

error. Several good techniques will be described, essentially those used by NBS, PMR, AMR, and APGC. No comparison of results of the various methods against an adequate standard has been made, hence, there may be a definite order of relative merit.

The NBS development of correction equations is given first.

Snell's law for a spherical earth, forming the basis of ray tracing theory, may be expressed in the forms

$$n_o\ (r+h_o)\ \text{Cos}\ \theta_o = n_i(r+h_i)\ \text{Cos}\ \theta_i = \text{Const} \qquad (3\text{-}3a)$$

$$n_i r_i\ \text{Cos}\ \theta_i = n_{i+1}\ r_{i+1}\ \text{Cos}\ \theta_{i+1} = \text{Const} \qquad (3\text{-}3b)$$

where $r_i = r+h_i$

r = local radius of the spherical earth

h_i = height above the spherical earth

In (3-3b) let

$$n_{i+1} = n_i + \Delta n,\ r_{i+1} = r_i + \Delta r,\ \theta_{i+1} = \theta_i + \Delta\theta$$

where Δn, Δr, $\Delta\theta$ are small increments. Choosing these increments sufficiently small, they may be considered as infinitesimals. Then substituting in (3-3b) we have

$$n_i r_i \text{Cos}\ \theta_i = n_{i+1}\ r_{i+1}\ \text{Cos}\ \theta_{i+1} \equiv \qquad (3\text{-}4)$$

$$(n_i+dn)\ (r_i+dr)\ \text{Cos}\ (\theta_i+d\theta)$$

Expanding, discarding products of differentials, and setting

$$\sin d\theta = d\theta,\ \cos d\theta = 1$$

gives

$$n_i r_i\ \text{Cos}\ \theta_i = n_i r_i\ \text{Cos}\ \theta_i - n_i r_i\ \sin\theta_i\ d\theta + n_i\ \text{Cos}\ \theta_i dr + r_i \text{Cos}\ \theta_i dn \qquad (3\text{-}5)$$

Subtracting $n_i r_i$ Cos θ_i from both sides, dividing by Cos θ_i, and solving the resultant equation for tan θ dθ gives

$$\tan \theta_i \, d\theta = \frac{n_i \, dr + r_i \, dn}{n_i r_i} = \frac{dr}{r_i} + \frac{dn}{r_i} \qquad (3\text{-}6)$$

or

$$d\theta = \frac{dn}{n} \text{ Cot } \theta + \frac{dr}{r} \text{ Cot } \theta \qquad (3\text{-}7)$$

From the infinitesimal portion of the ray path pictured in Fig. (3-2), it can be seen that

$$\text{Cot } \theta_i = \frac{x}{dr} \quad , \quad X = r_i \, d\theta \, , \quad \text{Cot } \theta_i = \frac{r_i \, d\phi}{dr}$$

Thus,

$$\frac{dr}{r} \text{ Cot } \theta = \frac{dr}{r} \frac{r d\phi}{dr} = d\phi \qquad (3\text{-}8)$$

and (3-7) becomes

$$d\theta = \frac{dn}{n} \text{ Cot } \theta + d\phi \qquad (3\text{-}9)$$

From Fig. (3-1),

$$(\theta_o + 90) + \phi + (90 - \theta) + (180 - \tau) = 360$$

or

$$\theta_o + \phi - \tau = \theta \qquad (3\text{-}10)$$

Differentiating,

$$d\theta = d\phi - d\tau$$

Comparing this with (3-9), it is seen that

$$d\tau = \frac{-dn}{n} \text{ Cot } \theta$$

or

$$\tau = -\int_{n_o}^{n_i} \frac{dn}{n} \text{ Cot } \theta \qquad (3\text{-}11)$$

GEOMETRY OF THE REFRACTION OF RADIO WAVES

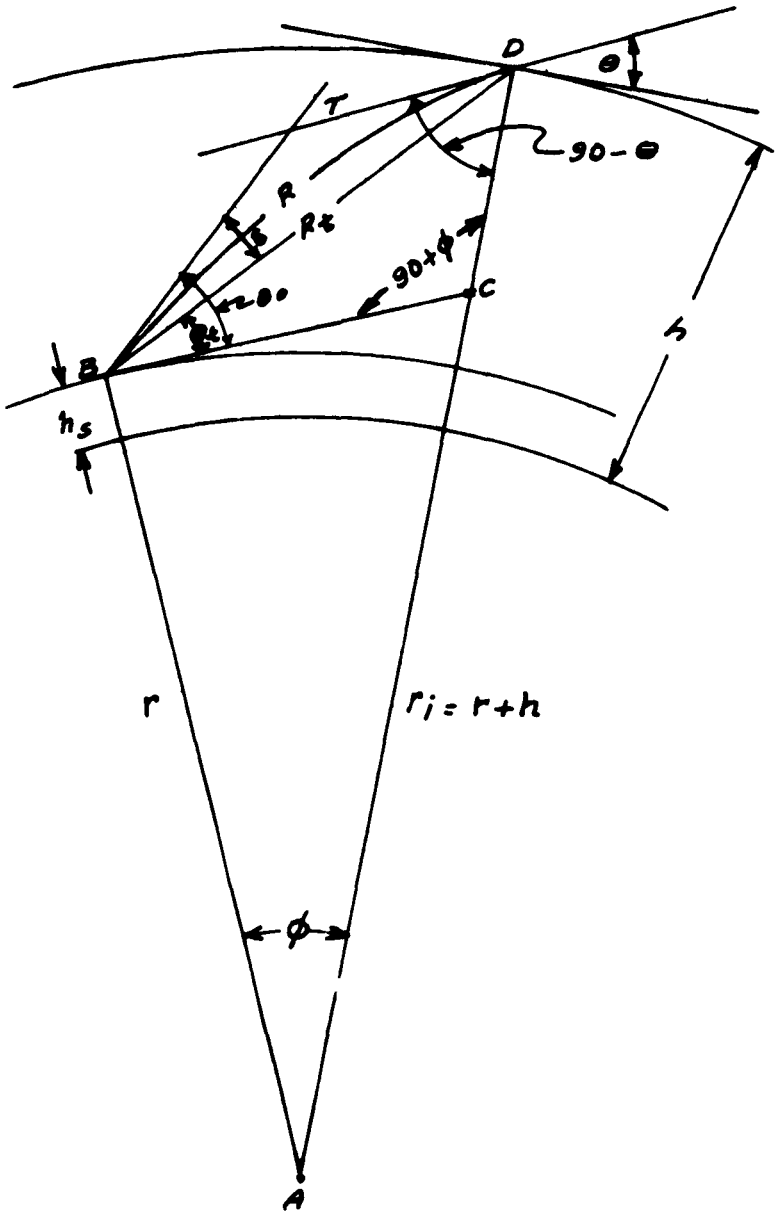

Figure 3-1

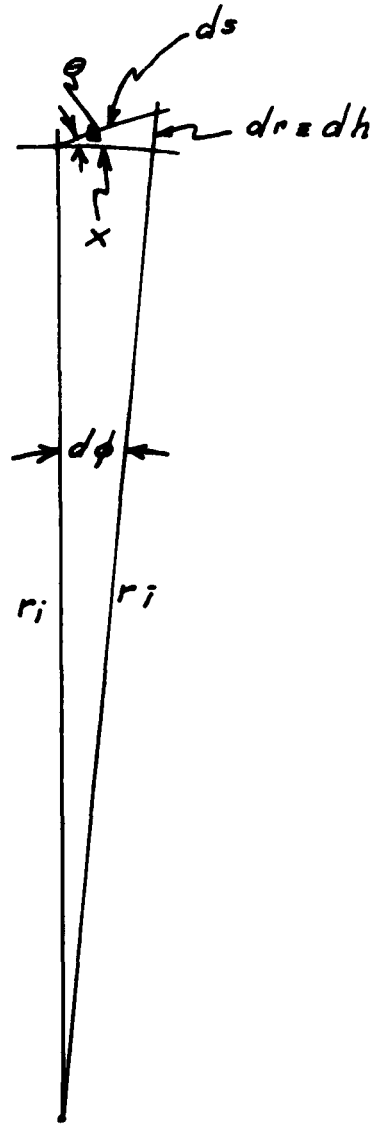

Figure 3-2

In the numerical evaluation of integral for τ, the height increments may be chosen such that the change in n is never large, so that a linear gradient of n may be assumed between sample points, with negligible error. For the case of a linear n gradient between h_1 and h_2, the integral can be solved in essentially closed form by assuming that over a small increment $\frac{1}{\bar{n}}$ and Cot θ, can be considered to be constants expressible as $\frac{1}{\bar{n}_i}$ and Cot $\bar{\theta}$, and this can be factored out of the integral. Incorporating this concept, equation (3-11) can be restated as

$$\tau = - \sum_{i=1}^{j} \frac{\text{Cot } \bar{\theta}_i}{\bar{n}_i} \int_{n_{i-1}}^{n_i} dn = - \sum_{i=1}^{j} \frac{\text{Cot } \bar{\theta}_i}{\bar{n}_i} (n_i - n_{i-1}) \tag{3-12}$$

where

$$\bar{\theta}_i = \frac{\theta_i + \theta_{i-1}}{2} , \quad \bar{n} = \frac{n_i + n_{i-1}}{2}$$

and θ_i is obtained through a re-expression of Snell's Law in a half-angle sine form to permit retention of significance.

$$\theta = 2 \text{ arc sin} \left(\frac{r+h_s}{2(r+h)} \left[2 \sin^2 \frac{\theta_o}{2} + \frac{h-h_s}{r+h_s} - \frac{n_s - n}{n} \text{ Cos } \theta_o \right] \right)^{\frac{1}{2}} \tag{3-13}$$

Once τ and θ for the observation of interest are established, the elevation angle error, δ , may be obtained from

$$\delta = \tau - \text{arc tan} \frac{\frac{n_s - n}{n} + 1 - \text{Cos}\tau - \sin\tau \tan \theta_o}{\sin\tau - \text{Cos}\tau \tan \theta_o + \frac{n_s}{n} \tan \theta} \tag{3-14}$$

The true elevation angle is then

$$\theta_t = \theta_o + \delta \tag{3-15}$$

the angle at the center of the earth is

$$\phi = \tau + \theta - \theta_o , \tag{3-16}$$

and the true range (from geometry of Fig. (3-1)) is

$$R_t = \frac{(r+h)\ \sin\ \phi}{\text{Cos}\ \theta_t} \qquad (3\text{-}17)$$

Since the NBS work is all theoretical the height to which integration is performed is provided the computer program as a constant. For the correction of tracking radar data, the height to which integration is to be performed can be determined as the height above a spherical earth indicated by the observed elevation angle and range.

$$h = r\left[\left(1+\left(\frac{R}{r}\right)^2 + 2\ \left(\frac{R}{r}\right)\ \sin\ \theta_o\right)^{\frac{1}{2}} - 1\right] \qquad (3\text{-}18)$$

To increase accuracy of the correction the solution can be performed as indicated above, then a better approximation of height of the target can be obtained from (3-18) using the value obtained for θ_t in place of θ_o. Using this height, the last increment of the numerical integration and subsequent computation should be repeated.

The mathematical equation formulation used by APGC is patterned after that used by NBS, except for the evaluation of the integral for τ (Eq. (3-11)) which is done through usage of a ten point Gauss-Legendre method of mechanical quadrature. This method yields exact results for the function if it can be expressed as a polynomial of degree nineteen or less.

The AMR mathematical development is slightly different. Using the equation (3-3a) expression for Snell's law, dividing both sides by r, and solving for Cos θ gives

$$\text{Cos}\ \theta = \frac{n_o\ (1+\frac{h_o}{r})\ \text{Cos}\ \theta_o}{n\ (1+\frac{h}{r})} \cong \frac{k}{n(1+\frac{h}{r})} \qquad (3\text{-}19)$$

letting k denote the constant numerator of the fraction.

Substituting this expression for Cos θ into (3-8), one gets

$$d\phi = \frac{\text{Cos } \theta \; dh}{(r+h)\sqrt{1-\text{Cos}^2\,\theta}} = \frac{k\,dh}{(r+h)\,n\,(1+\frac{h}{r})\sqrt{\frac{n^2\,(1+\frac{h}{r})^2 - k^2}{n^2\,(1+\frac{h}{r})^2}}}$$

$$= \frac{k\,dh}{(r+h)\sqrt{n^2\,(1+\frac{h}{r})^2 - k^2}} = \frac{k\,dh}{r\,(1+\frac{h}{r})\sqrt{n^2\,(1+\frac{h}{r})^2 - k}} \qquad (3\text{-}20)$$

where dh ≡ dr of equation (3-8). Integrating,

$$\phi = \frac{k}{r}\int_{h_o}^{h_t} \frac{dh}{(1+\frac{h}{r})\sqrt{n^2\,(1+\frac{h}{r})^2 - k^2}} \qquad (3\text{-}21)$$

AMR evaluates ϕ using a five point Gauss-Legendre numerical integration technique, which should yield exact results if the function under the integral can properly be expressed as a polynomial of degree nine or less.

From Fig. (3-1), the law of sines applied to triangle ABD gives

$$\frac{\sin \phi}{R_t} = \frac{\sin\,(90 + \theta_t)}{r+h} = \frac{\text{Cos } \theta_t}{r+h} \qquad (3\text{-}22)$$

From the definition of Cot ϕ, the length of side $\overline{AC}$ is

$$\overline{AC} = \frac{r}{\text{Cos } \phi}$$

and thus the length of side $\overline{CD}$ is

$$\overline{CD} = (r+h) - \frac{r}{\text{Cos } \phi}$$

Now in triangle BCD, the law of sines gives

$$\frac{\sin \theta_t}{(r+h) - \frac{r}{\cos \phi}} = \frac{\sin (90 + \phi)}{R_t} \equiv \frac{\cos \phi}{R_t}$$

or

$$R_t = \frac{(r+h) \cos \phi - r}{\sin \theta_t} \tag{3-23}$$

Substituting this into (3-22) and solving for Cot θ_t

$$\cot \theta_t = \frac{(r+h) \sin \phi}{(r+h) \cos \phi - r} = \frac{\sin \phi}{\cos \phi - \frac{1}{(1+\frac{h}{r})}} \tag{3-24}$$

The true elevation angle is computed using equation (3-24). The same comment applies here as stated immediately after Eq. (3-18), that one "iteration" will improve accuracy. The true range is calculated as indicated in Eq. (3-17).

The PMR development follows that of AMR through Eq. (3-21). At this juncture a substitution is made:

$$\sin \theta = \sqrt{1 - \cos^2 \theta} = \frac{\sqrt{n^2 (1+\frac{h}{r})^2 - k^2}}{n (1+\frac{h}{r})} \tag{3-25}$$

and (3-21) becomes

$$\phi = \frac{1}{k_r} \int_{h_o}^{h_t} \frac{\cos \theta}{\sin \theta} \, n \, dh \tag{3-26}$$

The index of refraction profile if plotted can be broken into a number of segments of essentially constant gradient. This can be expressed as

$$n_i = n_{i-1} + a_i (h_i - h_{i-1}) \tag{3-27}$$

where

$$a_i = \frac{n_i - n_{i-1}}{h_i - h_{i-1}}$$

is the slope of the segment. Differentiating (3-27)

$$\frac{d\, n_i}{d\, h_i} = a_i$$

Now, differentiating Eq. (3-19) with respect to h, we have

$$-\sin\theta \frac{d\theta}{dh} = \frac{-k}{n} \cdot \frac{1}{r} (1+\frac{h}{r})^{-2} - \frac{k}{n^2(1+\frac{h}{r})} \frac{dn}{dh}$$

or

$$\frac{k \sin\theta}{\cos^2\theta} d\theta = \left[a (1+\frac{h}{r}) + \frac{n}{r}\right] dh$$

where

$$a = \frac{dn}{dh}$$

which can be rearranged in the form

$$n\, dh = \frac{n}{(a(r+h)+n)} \frac{r\, k \sin\theta}{(\cos^2\theta)} d\theta \qquad (3\text{-}28)$$

Substituting this into equation (3-26),

$$\phi = \int_0^{\theta} \frac{n}{a(r+h)+n} d\theta \qquad (3\text{-}29)$$

Over appropriate intervals, where $\frac{dn}{dh}$ is approximately constant, the coefficient

$$D = \frac{n}{a(r+h)+n}$$

is approximately constant. There will be a small, approximately linear variation of this coefficient over the altitude

interval chosen. The mean value of the coefficient is very nearly the average of the coefficients at the beginning and ending of this altitude interval. Thus,

$$\bar{D}_i \cong \frac{\bar{n}_i}{a_i(r+\bar{h}_i)+\bar{n}_i} = \frac{\frac{1}{2}(n_i + n_i)}{\frac{n_i-n_{i-1}}{h_i-h_{i-1}}\left[r+\frac{1}{2}(h_i+h_{i-1})\right]+\frac{1}{2}(n_i+n_{i-1})}$$

$$= \frac{(n_i + n_{i-1})(h_i - h_{i-1})}{(n_i - n_{i-1})\left[2r + (h_i + h_{i-1})\right] + (n_i+n_{i-1})(h_i-h_{i-1})} \qquad (3\text{-}30)$$

and equation (3-29) becomes

$$\phi = \sum_{i=1}^{j} \int_{\theta_{i-1}}^{\theta_i} \bar{D}_i \, d\theta = \sum_{i=1}^{j} \bar{D}_i \, (\theta_i - \theta_{i-1}) \qquad (3\text{-}31)$$

and θ_i is evaluated from equation (3-19). The height to which integration is performed may be determined through usage of equation (3-18), and the true elevation angle from equation (3-24), and the true range from equation (3-17).

From a computational accuracy and convenience standpoint, it would seem that an acceptable standard method based on portions of all of the above methods could utilize equations (3-18), (3-13), (3-30), (3-31), (3-24) and (3-17). That is, the steps would be:

a. Compute the height to which integration should be performed.

$$h = r\left[\sqrt{1+\left(\frac{R}{r}\right)^2 + 2\left(\frac{R}{r}\right)\sin\theta_o} \; -1\right]$$

b. For the upper end of each increment chosen such that $\frac{dn}{dh}$ is essentially constant over the altitude interval, compute the local elevation angle.

$$\theta = 2 \text{ arc sin } \left(\frac{r+h_s}{2(r+h)} \left[2 \sin^2 \frac{\theta_o}{2} + \frac{h-h_s}{r+h_s} - \frac{n_s-n}{n} \text{Cos } \theta_o \right] \right)^{\frac{1}{2}}$$

c. Compute the "integration constant" for this interval

$$\bar{D}_i = \frac{(n_i + n_{i-1})(h_i - h_{i-1})}{(n_i - n_{i-1}) \left[2r + (h_i + h_{i-1}) \right] + (n_i + n_i - 1)(h_i - h_{i-1})}$$

d. Compute the angle at the center of the spherical earth determined by the radar site and the item being tracked retaining also the values of the two components defined as A and B.

$$\phi = \sum_{i=1}^{j-1} \bar{D}_i \, (\theta_i - \theta_{i-1}) + \bar{D}_j (\theta_j - \theta_{j-1}) \equiv A + B$$

e. Compute the first estimate of true elevation angle.

$$\theta_t = \text{Arc Cot } \frac{\sin \phi}{\text{Cos } \phi - \frac{1}{(1+\frac{h}{r})}}$$

f. Recompute height from (a) using θ_t in place of θ_o.

g. Recompute θ_j, $\bar{D}_j$ from b and c, and compute a new ϕ using the original component A and a newly computed component B.

h. Compute the final estimate of true elevation using e.

i. Compute the true range. $R_t = \frac{(r+h)\sin \phi}{\text{Cos } \theta_t}$

Correction of the elevation angle for optical tracking devices can also be done in the above manner, utilizing the optical index of refraction.

3.3 Estimated Accuracy of Corrected Measurements.

The accuracy of atmospheric refractivity measurements has been discussed by McGavin (1962) who states:

"Meteorological sensing is limited mainly by the inaccuracy in measuring humidity which under ideal conditions appears to limit the accuracy to ± 1.0 N. Gradient measurements utilizing radiosondes reflect an accuracy no better than ± 3 N units. Radio frequency refractometers are capable of accuracies as much as an order of magnitude better than that achieved by meteorological sensors. Lightweight refractometers have been devised for balloon-borne and dropsonde measurements reflecting accuracies inferior to the conventional refractometer but superior to the radiosonde."

Since the surface refractivity is in the order of 330 N units, the range corrections resulting from use of complete profiles with the above accuracies will be in error by 0.3% to 1%. Angle corrections, which depend upon gradients of refractive index and are more sensitive to variations in the profile, will have a larger percentage error, usually between 2% and 4% of the initial value of error. The accuracy of the angle correction will be better for long-range targets than for those which lie within the troposphere, since the elevation error approaches the total bending τ in the long-range case.

Bean and Cahoon (1957) showed by ray-tracing calculations that the residual error in τ could be reduced to within 50 uradians RMS at elevation angles above 3° using surface refractive index only. This corresponds to an error of 1% of the initial value at 3°. Radio measurements described by Iliff and Holt (1962) demonstrated that good accuracy could be achieved in prediction of total bending from surface refractive index. Their results showed residual errors of 150 uradians at 2° elevation, or 2.5% of the initial error of 6000 u rad. Experience at the test ranges, reported to the Panel, confirms the feasibility of correcting tracker data to about 50 uradians. Both AMR and APGC reported residual bias errors in the order of 100 uradians for AN/FPS-16 radar data, and a large portion of this figure must be attributed to the radar itself.

The present state of the art in correction of range and elevation data, using combined radiosonde and refractometer data to derive accurate surface refractivity and profiles, is estimated to provide the accuracy of correction shown in Table 3-1.

TABLE 3-1.

Optimum Accuracy of Range and Angle Corrections

		$\theta_o = 5^o$	$\theta_o = 20^o$
Long-Range Case (R 300 n. mi.)			
Initial range bias R_e	(ft)	75	22
Residual range bias σ_{rb}	(ft)	0.75	0.2
% residual error		1	1
Initial angle bias	(urad)	3500	900
Residual angle bias $\sigma_{\theta b}$	(urad)	70	20
% residual error		2	2
Short-Range Case (R = 50 n. mi.)			
Initial range bias R_e	(ft)	22	7
Residual range bias σ_{rb}	(ft)	0.5	0.15
% residual error		2	2
Initial angle bias	(urad)	2000	700
Residual angle bias $\sigma_{\theta b}$	(urad)	60	20
% residual error		3	3

(Values shown should be doubled for disturbed meteorological conditions such as heavy cloud cover, fronts, and inversions; also for lack of reliable and frequent soundings covering the entire tropospheric path used in measurement).

4. EFFECT OF THE ATMOSPHERE ON ACCURACY OF INSTRUMENTATION SYSTEMS

4.1 Relationship between Position and Velocity Errors.

Since the atmosphere introduces errors in measurement of target position, it will also cause errors in target velocity and higher derivatives of position. In order to evaluate the atmospheric effects on velocity error, it has been found convenient to divide the problem into two parts. The first, which was discussed in Section 2. of this report, is the effect of temporal fluctuations in the atmospheric paths between the measuring instruments and a fixed point in space. The rate of these fluctuations is governed by wind speed and the presence of turbulence within the atmosphere through which the measurement is made. This "direct" component of velocity error is independent of the target velocity.

A second term, which may be described as "indirect", is due to the motion of the measurement paths through the atmosphere as they follow a moving target, and is dependent upon the target velocity rather than on the velocity of the atmosphere relative to the earth. The two effects may be combined in a single term, but since most of the measured data contains only the "direct" component it must be modified before being applied to high-velocity target tracking. The problem here is similar to that of relating bias (or systematic) errors of target position to velocity errors. Brown (1958) pointed out a relationship that had been overlooked by many in the instrumentation field:

> "It is to be emphasized that, contrary to popular opinion, the determination of extremely precise velocities requires a correspondingly high degree of absolute precision of observations of the tracking system. This arises from the fact that tracking systems measure space coordinates indirectly only. Consequently small, constant biases in the basic observations are transformed into small, but slowly varying biases in the space coordinates. This produces an effect equivalent to a warpage or a distortion in the scale of the space coordinate system. If an accuracy of, say, 1 part in 100,000 is desired

for velocity, the distances between trajectory points must be unbiased to 1 part in 100,000. Hence the need for high absolute accuracies."

The effect of the "indirect" errors for the moving target is most pronounced in systems using range and range-rate data, because in these systems the atmospheric limits have been most closely approached. It was stated in Section 3. of this report that the angle corrections were more sensitive to variations in the refractivity profile because they depend upon the gradients of this profile, measured in both vertical and horizontal planes. In the moving-target case, the range and radial velocity errors will also depend upon these gradients, since the measurement ray will move through hundreds or thousands of feet in the troposphere during the period of measurement.

In calculating the effect of motion of the beam, we may use either of two methods, which yield identical results. Starting from the range error spectrum of Fig. 2-6, which applied to a fixed path, we may derive expressions for both position and velocity errors over the path:

$$\sigma_r^2 = \int_{f_1}^{fmax} W(f)\ df \qquad (4\text{-}1)$$

$$\sigma_v^2 = (2\pi)^2 \int_{f_1}^{fmax} f^2\ W(f)\ df \qquad (4\text{-}2)$$

Here, the spectral density of the range error is represented by $W(f)$, in units of length ^{2}/cps, and the errors are those observed over a period $t_1=1/(2f_1)$. Integration of the spectra shown in Fig. 2-6 indicates that the position error is quite sensitive to the lower limit of the integral, corresponding to the period of the observation. The value of σ_r varies from about 0.1 foot over 15 to 30 minutes, to almost ten feet over a period of a year, for paths at 6^o to 7^o elevation extending through the entire atmosphere. On the other hand, the velocity

error is almost independent of the period, and also of the smoothing time (up to several seconds). Most of the velocity error appears in the spectral region from 0.003 to 0.01 cps, which contributes about 0.001 ft/sec to the total error for the fixed path.

To modify the spectrum of Fig. 2-6 for the moving path, we must consider the velocities and spatial distributions of the atmospheric variations causing the error. The wind velocities encountered during the Maui tests averaged about ten ft/sec across the path, and Fig. 4-1 shows good agreement between the spectral data and that representing the spatial correlation of error, derived from Fig. 2-7. If the spectrum were solely the result of motion of the air mass across the path, a frequency of 0.01 cps would correspond to a distance of 1000 feet at ten ft/sec.

When the target being tracked has a tangential velocity component (normal to the measurement path), the relative velocity of the troposphere with respect to the measurement path is increased by an amount which varies with distance from the instrument. Using, as an effective velocity, the beam velocity at an altitude equal to one-half the scale height, or at 12,000 feet, the relative velocity v_b due to beam motion will be (Fig. 4-2):

$$v_b = \frac{1}{2} R_s \omega = \frac{1}{2} \frac{R_s}{R} v_t \qquad (4\text{-}3)$$

Here, R_s is the range to the point where the beam reaches the scale height, R is the total range to the target, and v_t is the tangential velocity of the target. For example, in a satellite track, with R=660 miles (4×10^6 ft), elevation $\theta_o = 6^o$, and v_t=10,000 ft/sec, we would have:

R_s= 210,000 feet, ω =2.5 mr/sec, v_b=260 ft/sec

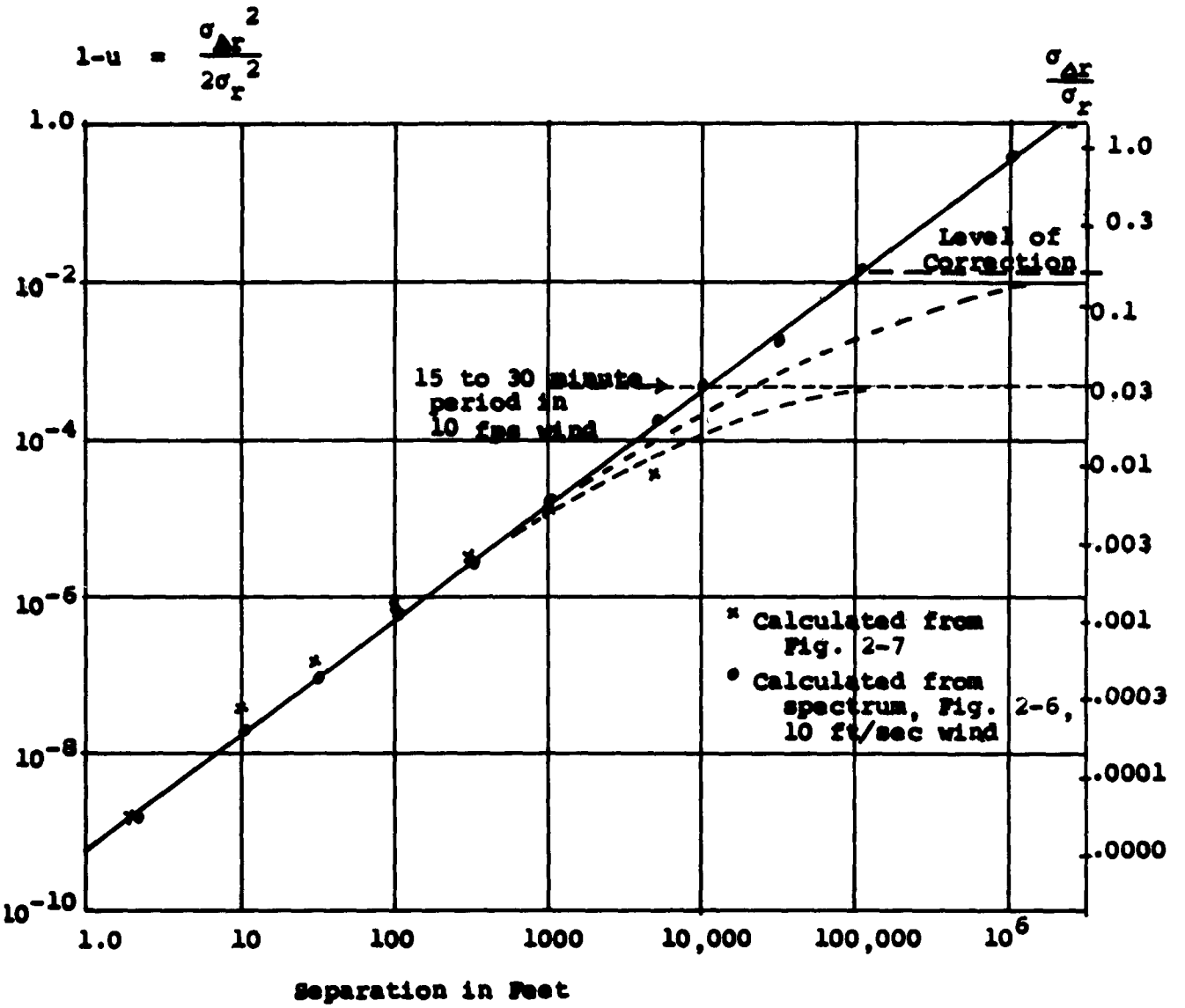

Figure 4-1. Spatial Correlation calculated from Phase-difference data and from single-path spectra.

Correlation coefficient for two paths $u = \frac{\sigma_{r_1 r_2}}{\sigma_{r_1}\sigma_{r_2}}$

Range-difference error $\sigma_{\Delta r} = \sigma_r\sqrt{2(1-u)}$

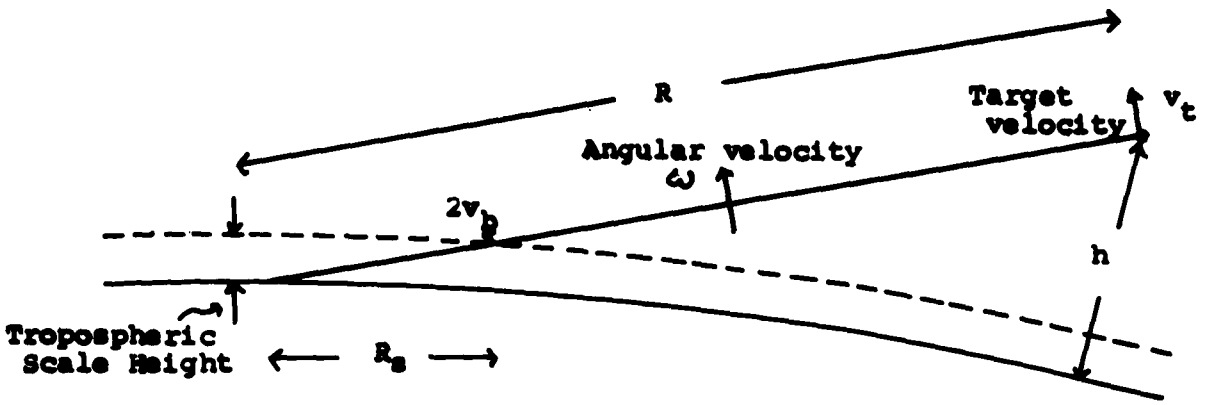

a. Beam motion in vertical plane.

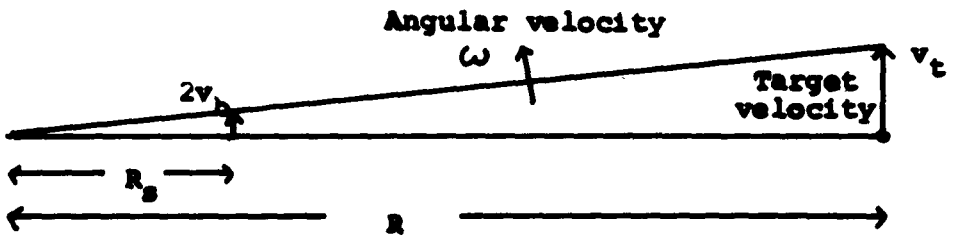

b. Beam motion in horizontal plane.

Figure 4-2. Motion of Measurement Beam for Moving Target

In this case the spectral distribution plotted in Fig. 2-6 will be shifted upwards in frequency by a factor of 26, and the velocity error σ_v will be increased by the same factor, to about 0.026 ft/sec. The predominant spectral components will now be from 0.08 to 0.25 cps, and some reduction in error will be possible using smoothing times of a few seconds.

The second way of describing the "indirect" component of velocity error is to consider the geometry of the measurement path, and the exact direction of the path as it passes the target. The radial velocity observed at the instrument (by Doppler or differentiated range measurements) represents the projection of the target velocity vector on the measurement ray path at the target. In traversing the atmosphere, the ray is bent through an angle $\Delta\alpha$ relative to the assumed path, which has been estimated using the best available tropospheric profiles.

It was shown by Millman (1958) that the effect of ray bending on Doppler velocity measurement was more important than the direct error due to the uncertain propagation velocity at the target or along the path. He expressed this component of velocity error as the product of the target's tangential velocity times the ray error angle at the target:

$$\Delta v = v_t \sin \Delta\alpha_t \cong v_t \Delta\alpha_t \qquad (4\text{-}4)$$

The ray error angle $\Delta\alpha_t$ describes the difference in angle of arrival at the target of the measurement ray relative to the angle estimated by the measuring device. If no correction is applied for refraction effects, the error would be largest in the elevation plane, and would be equal to the difference between the total amount of ray bending (designated γ in Fig. 2-18 or τ in Fig. 3-1) and the elevation angle error at the instrument (δ).

When corrections are applied in the measuring system, a major part of the tropospheric portion of $\Delta\alpha_t$ can be eliminated by computation in the system. As shown in Fig. 4-3, there will remain a small residual error due to fluctuation and bias error

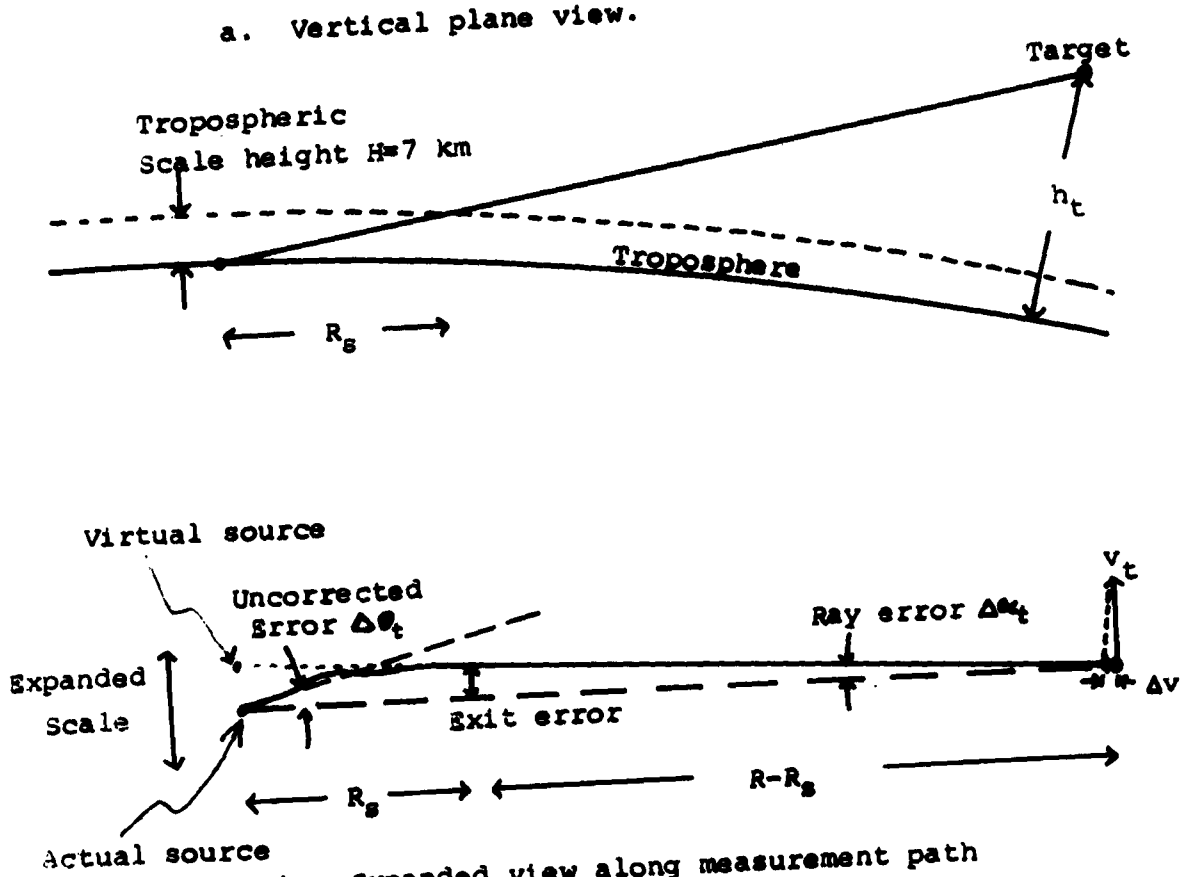

Figure 4-3. Geometry of Velocity Error Cross-Coupling

in both elevation and azimuth at the instrument. In the presence of a tangential component of target velocity, this ray error will produce an error in apparent radial velocity given by Δv. It should be pointed out that the need for correction applies both to those systems which use the angular data given by the antenna and to those which attempt to ignore these angles by interferometric and trilateration solutions for target position, as long as radial velocity measurements are used.

For the troposphere, the uncorrected part of the ray error angle may be estimated using the geometrical relationships of Fig. 4-3b. Considering a tropospheric scale height H=7 km (23,000 feet), the beam will extend for a range $R_s=H/\sin\theta_o$ below this height, and the angle $\Delta\alpha_t$ will be related to the elevation error δ by:

$$\Delta\alpha_t \cong \delta \times \frac{R_s}{R_s+R} \qquad (R>R_s, \text{ flat earth}) \quad (4\text{-}5)$$

Similarly, if the residual elevation error after correction (or the unpredictable azimuth error) is σ_{θ_t}, the unpredictable component of $\Delta\alpha_t$ will be:

$$\sigma_{\alpha_t} \cong \sigma_{\theta_t} \times \frac{R_s}{R_s+R} \qquad (4\text{-}6)$$

For example, let us assume that the target is at an altitude of 160 miles (10^6 ft) with a range of 660 miles (4×10^6ft), corresponding to an elevation angle $\theta_o=6^o$. The tropospheric path length R_s will be about 1/20 of the total path, and the ray error will be 1/20 of the uncorrected elevation or azimuth error. Placing σ_{θ_t} at about 50 μradians, this would leave a ray error residue σ_{α_t} of about 2.5 μradians. For a missile with a tangential velocity of 10,000 feet per second, the radial velocity measured by even the most precise Doppler system would be in error by .025 ft/sec. (the same as found by the first method). Fortunately, this error will be reduced at higher altitudes by the factor $R_s/(R+R_s)$, but the

possible increase in the tangential velocity component to values near 30,000 feet per second will lead to probable values of several hundredths of a foot per second in most radial measurements on objects in orbit. These errors will consist of both bias and fluctuating components, as mentioned above, and will be largely uncorrelated over distances of several thousand feet. This factor will place a severe limit on the attainable accuracy of long-baseline interferometer systems when operating against targets with substantial tangential velocity components. Although not too serious in some guidance applications, where the missile at fuel cut-off is moving along a near-radial course, it will cause problems in most other tracking missions.

The ionospheric component of ray error may be calculated in similar fashion, except that the bending occurs at a point much nearer the target, and correction is virtually impossible. Thus, the ray error will be approximately:

$$\Delta\alpha_i = N^i/\tan\theta_i \qquad (4\text{-}7)$$

Here, θ_i is the ionospheric elevation angle, having a minimum value of about 9^o for rays which leave the earth at an elevation angle of zero. A plot of Δ_{α_i} vs. frequency for a target altitude of 300 km is shown in Fig. 4-4. Two ground elevation angles are shown, and the top scale indicates radial velocity error in feet per second for a tangential component of 10,000 feet per second. When a lower limit of 3000 mcps. is observed for range-rate measureing systems, the velocity error will be between 0.1 and 0.2 feet per second for v_t=10,000 feet per second, rising to a maximum of three times this value for orbital objects crossing the beam at 30,000 feet per second. Operation below 3000 mcps. is permissible only at night, when high tangential velocities are not expected, or when the range-rate accuracy need not be better than about one foot per second. Under extreme ionospheric conditions, it may be necessary to use frequencies well above 3000 mcps. in order to reduce this component of error to tolerable levels.

The effect of the atmosphere on the operation of any instrumentation system can be visualized as a drift in the

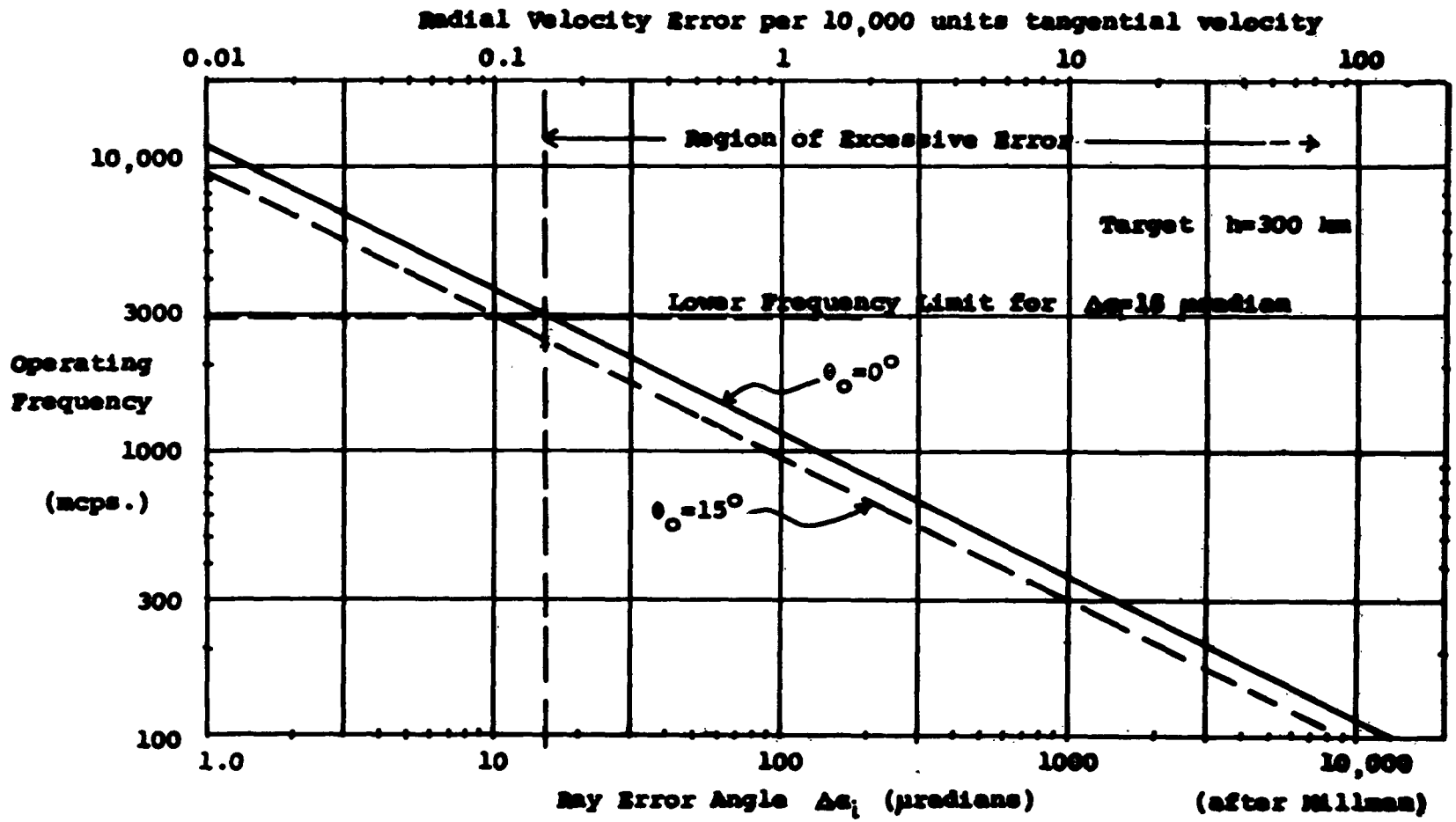

Figure 4-4. Ray Error Angle vs. Operating Frequency

position of the measuring instrument. After correction for measured tropospheric profiles, the "virtual source" (see Fig. 4-3) will be found to drift over a small ellipsoid, as shown in Fig. 4-5a. The extent of the uncorrected fluctuations in a period of fifteen to thirty minutes is about 0.1 foot along the path and perhaps ten feet normal to the path. When two instruments are used in an interferometer system, the drifts will be partially correlated, as shown by Fig. 4-1 and 4-5b. The long-period terms can be reduced by obtaining tropospheric refractivity profiles at hourly (or shorter) intervals and at several locations around the instrumentation complex. However, the location of the virtual sources to absolute accuracies of one foot or better appears very questionable, as this is equivalent to correction of angle-tracker data to within 5.0 μradians. Ionospheric errors will remain important at all frequencies below 5000 or 6000 mcps, when radial velocity data approaching 0.1 ft/sec is required.

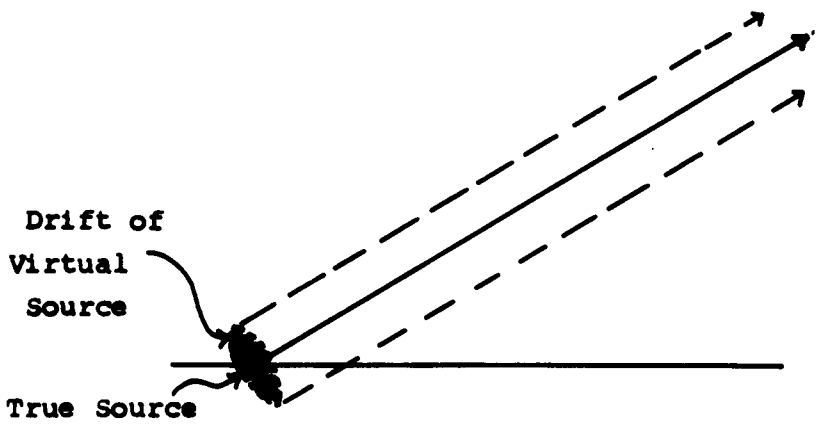

a. Drift in Location of Virtual Source of Measurement Ray

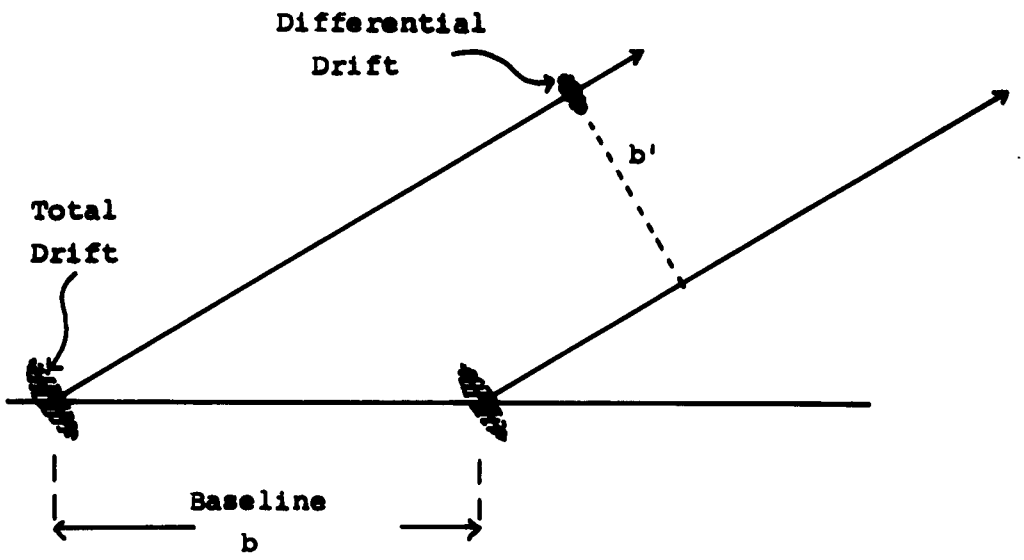

b. Correlated and Uncorrelated Portions of Drift for Interferometer

Figure 4-5. Atmospheric Error in Terms of Drift in Location of Instruments

4.2 Sensitivity of Present and Proposed Systems to Atmospheric Errors.

In evaluating atmospheric errors, we may consider separately the three major types of precision instrumentation system. These are the trackers (e.g. pulsed radar), the interferometers (e.g. Azusa or Mistram), and the trilateration systems (e.g. Glotrack, the Goddard "Range, Range-Rate System", or the radar trilateration system). The errors to be evaluated for each system are shown in Table 4-1. Using the data presented in Section 2. for the tropospheric and ionospheric errors, and the correction methods described in Section 3 for the troposphere, it is possible to estimate the atmospheric components of error in both position and velocity of targets for each type of system. This will be done below for the case of high-altitude targets such as satellites, and the principal sources of atmospheric error will be identified.

First, however, there are some general statements which may be made regarding the errors introduced in the various systems.

a). The error in range measurement, due to the atmosphere, is independent of the type of system and dependent upon frequency and atmospheric path length. Residual errors in the order of one foot are to be expected for systems operating between 5000 and 10,000 mcps.

b). Trackers and short-baseline interferometers ($b<1000$ ft) will face limits of angular accuracy near 0.05 milliradians, due both to fluctuations in the troposphere and to residual bias errors. Operating frequencies above 1000 mcps. are necessary to approach this limit.

c). Systems using longer baselines will make possible the achievement of better accuracies. The angular accuracy of an interferometer is limited by the ratio of the range-difference error $\sigma_{\Delta r}$ to the effective baseline b', measured normal to the direction of the target. Fluctuating components of $\sigma_{\Delta r}$ show a gradual increase from about 0.001 foot

for b=10 feet to about 0.1 foot for $b>10^4$ feet (see Fig. 2-7).

d). Beyond the baseline length $b=10^4$ feet, the short-term fluctuating component of $\sigma_{\Delta r}$ remains near 0.1 foot, and system precision improves directly with baseline length. The trilateration systems represent a limiting case; where the range-difference error is equal to $\sqrt{2}$ times the individual range error. Residual bias (long-term) errors are to be expected in both interferometer and trilateration systems, approaching $\sigma_{\Delta r}=1$ foot for large station separations. The residual bias for separations in the order of 10^4 feet has not been established, but presumably lies between the values of the fluctuating component (0.1 foot) and the bias for large separations (1 foot). All the cited errors are typical of cloudy weather, for paths at 7 to 10 degrees elevation angle.

e). The fluctuating component of range-rate difference (see Fig. 2-8) approaches 0.001 foot per second for $b=10^4$, assuming 20-second smoothing and a fixed target. The low value of this error in rate is due to the long periods involved in the tropospheric anomalies. For the systems using long baselines or trilateration, a much larger error can be expected to result from the effect of ray motion in following a moving target, discussed in Section 4.1. Typical values for this component will be given for particular target conditions in the next section.

TABLE 4-1

Identification of Propagation Error Components
for Instrumentation Systems

1. Trackers (e.g. Radar)

   Range error σ_r

   Angle error σ_θ

2. Interferometers (e.g. Azusa, Mistram)

   Range error σ_r

   Range-difference error $\sigma_{\Delta r}$ or

   Equivalent angle error $\sigma_\theta = \sigma_{\Delta r}/(b \sin \beta)$ or

   Direction cosine error $\sigma_c = \sigma_{\Delta r}/b$

3. Long-Baseline Trilateration (e.g. Glotrack, Goddard Range, Range-Rate System, or Radar Trilateration)

   Range error σ_r

   Target position error $\sigma_p = \sigma_r \times \text{GDOP} \times \sqrt{2}$ or

   Equivalent angle error (at long range)
   $\sigma_\theta = \sqrt{2}\, \sigma_r/(b \sin \beta)$

All error components consist of bias and fluctuating parts. Evaluation of first derivatives is usually necessary.

a. Tracker Error Analysis

The procedure for analysis of errors in the tracker systems (e. g. radar) is straightforward. For a given target range and altitude, the elevation angle θ_o and the tropospheric path length R_s are first determined. The initial values of tropospheric range and angle bias may be estimated from Figs. 2-2 and 2-4. Assuming that a correction procedure as described in Section 3. is to be applied to the data, the residual bias errors may be estimated at one-half to one percent of the initial range bias ΔR_e and two to four percent of the angle bias δ. Fluctuating components may be estimated from Fig. 2-9, using an effective aperture width of the antenna in place of the separation baseline, and finding the range fluctuation for the single-path case as:

$$\sigma_{rf} = \underset{b \to \infty}{\text{Limit}} \frac{\sigma_{\Delta r}}{\sqrt{2}}$$

The tropospheric rate errors are somewhat more difficult to evaluate. Smoothed values of range rate fluctuation may be read from the limiting value of $\sigma_{\dot{\Delta r}}$ in Fig. 2-8. To these must be added the errors due to motion of the ray in the atmosphere, including both bias and fluctuating components. When smoothed, the fluctuating effects will tend towards zero velocity error, but the bias portion will change very slowly as the target passes through a wide interval in elevation or azimuth angle and will not be smoothed out. The constant part of this error can be considered as a rotation of the apparent coordinate system with respect to the true coordinate system in which the data is expressed, the rotation having a value equal to the average residual bias in the tracker elevation angle. The angular rate errors may be read directly from Fig. 2-8, using the effective aperture. Unsmoothed values will be considerably higher than those shown in this figure (see Table 2-4), and the amplitude and spectral spread of the rate errors will be increased by motion of the beam through the atmosphere in tracking a moving target.

Ionospheric errors for the tracker are found in the same way as the tropospheric errors, except that initial bias values are used without allowance for correction

(see Figs. 2-15 and 2-16). Fluctuating and ray bending components are found from Figs. 2-25 and 4-2. In general, the bending angle $\Delta\alpha_i$ will contribute the major part of the effective range-rate bias error.

Total RMS position and velocity errors for the tracker are found by summing (in an rms fashion) the several components of range and angle errors, multiplying the angle errors by target range, and summing the three final components corresponding to range, azimuth and elevation coordinates. (See Table 4-2).

b. Interferometer Error Analysis.

The procedure used in analysis of interferometer errors is somewhat more complex than for the tracker. In the first place, two different values of baseline are used, one for azimuth and one for elevation (assuming elevation angles below 90°). For distant targets, the average elevation angle β at which rays arrive at the two stations may be used to find an effective baseline b' for elevation measurement:

$$b' = b \sin \beta$$

In most cases, tracking will be carried out at elevation angles between five and twenty degrees, with the effective elevation baseline shrinking to one-third to one-twelfth the azimuth baseline. As a result, the azimuth error will contribute very little to the final RMS target position and velocity error compared to the elevation errors. Using the effective elevation baseline, Figs. 2-7 and 2-8 will yield fluctuating components of position and smoothed velocity for the target with low tangential velocity.

An angle bias error must be found, either by assuming corrected values of the initial bias shown in Fig. 2-5 or by estimating the residual bias in the range-difference measurement. An upper limit for interferometer angle bias will be the value of residual bias assumed for the tracker. This corresponds to correction of the interferometer curve of Fig. 2-5 to leave a residue of about 20% of the initial error. A lower limit would be to assume a residual bias error in range-difference equal to the fluctuating component.

The former method will be more accurate for the short-baseline systems, while the latter will be assumed here for the long-baseline systems.

The evaluation of velocity errors is made more complex by the interaction between error spectra and smoothing time for the system. Instantaneous rate errors will be governed primarily by the product of the ray-bending error σ_α (see Eq. 4-6) and the tangential velocity. When smoothing is employed, the errors will be reduced, as shown in Fig. 4-6. Calculations were made from the spectrum of Fig. 2-6 (v_b=10 ft/sec) and from a similar spectrum shifted upwards in frequency by a factor of twenty-five (v_b=250 ft/sec). The spectral density was adjusted to obtain the same total range error, but the shift in the spectral location of the errors was found to cause much larger velocity errors, as would be expected. Two curves are shown for the high-velocity target case, one with the 20-second smoothing used in Fig. 2-8, and one with a 2-second smoothing time, as often used in range instrumentation. The latter curve shows the expected increase of approximately 25:1 over the curve for low velocity. It should be noted that the curve for 2-second smoothing levels out sharply below b=320 feet when large apertures are used, due to the smoothing effect of the aperture on the received ray. When a thirty-foot aperture is used, the error is 35 urad/sec. The curves plotted in Fig. 4-6 are for maximum errors, and values about 70% as great will be used for the "average weather" case to be discussed.

c. Trilateration Error Analysis

The analysis of errors in the trilateration system is quite simple, since all range errors may be assumed equal and uncorrelated. An equivalent angle error will be found according to Table 4-1, assuming a GDOP factor of three for the system. This is equivalent to assuming that the measurement rays intersect at an angle near 20° or 160°, as would be the case if a satellite were being tracked from two stations separated by about 1000 miles, with the satellite midway between at low altitude. The analysis of velocity errors will be based on the ray bending theory, with no

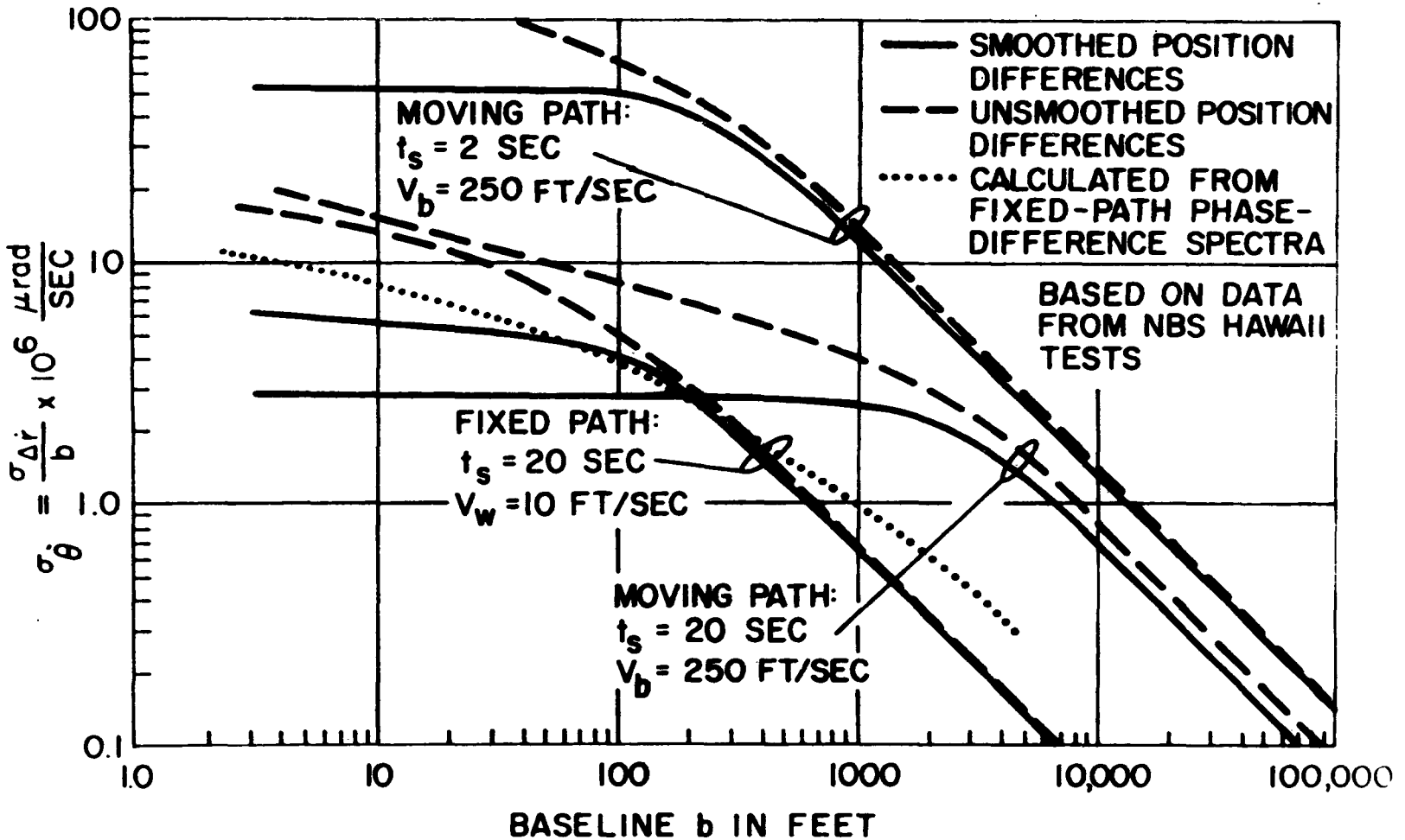

Figure 4-6. Effect of Beam Velocity on Interferometer Rate Error

allowance for smoothing. As shown in Fig. 4-6, the effect of smoothing is relatively slight for very long baselines, since the significant errors have very long periods.

4.3 Results for High-Altitude Targets.

The foregoing data and analysis will be applied to the case of a satellite in orbit, at an altitude of 160 nautical miles (10^6 feet), to illustrate the problems imposed by the atmosphere on precision tracking systems. Three different configurations will be assumed, with two operating frequencies compared. The results are summarized in Tables 4-2 through 4-4. In each case, the target parameters are as follows:

Target altitude:	h = 160 n.mi. = 10^6 ft
Target range:	R = 660 n.mi. = 4×10^6 ft
Tangential velocity:	V_t = 10,000 ft/sec
Angular rate of beam motion:	ω = 2.5 mr/sec
Effective tropospheric beam velocity:	V_b = 250 ft/sec
Beam elevation angle:	$\theta_o = 6^o$ = 105 mr

The errors will be given for "average" weather conditions, corresponding to the median curves of Figs. 2-7 and 2-8, or to presence of small amounts of cumulus clouds. The errors for heavy cloud coverage will be about twice the values shown, while for clear sky they will be about one-half as great. Similarly, the ionosphere will be assumed to follow the characteristics of the daytime model (Fig. 2-14), without extreme sunspot conditions or other "disturbed" characteristics. Where the ionospheric errors are important, the variation in level may be taken as about three to one, both above and below the values given, depending upon time of day and sunspot cycle.

The velocity errors for the tracker and interferometer systems have been found from Figs. 2-7, 2-8 and 4-6, taking into account the measured spectra of tropospheric errors. For the trilateration system, the predominant error has been calculated from the uncertainty of the ray-bending component. Total error has been found as the rms sum of all bias and fluctuating components, and has been expressed in terms of range, angle, target position and target velocity. In each case, the components due to angular measurement (or equivalent) are seen to govern the system accuracy, and of these, the elevation component is of greatest importance. The results are not consistent with some of the published figures for interferometer systems, but are believed to represent the most accurate values for this tracking problem. The primary

cause of the difference lies in the fact that the satellite may have appreciable tangential velocity, causing the measurement beams to move through the atmosphere at rates which greatly magnify the frequencies in the atmospheric error spectrum. If similar calculations were made for targets which had little or no tangential velocity (as, for instance, missiles traveling directly away from the instrumentation site) the errors would be appreciably lower in magnitude.

Table 4-2. Typical Atmospheric Errors

Tracking Radar on Satellite Tracking Mission

A. Tropospheric Components (average weather)

Range bias ΔR_e (Fig. 2-2):	60 ft
Angle Bias δ (Fig. 2-4):	2500 μrad
Residual range bias σ_{rb} (Table 3-1):	0.3 ft
Residual angle bias $\sigma_{\theta b}$ (Table 3-1):	50 μrad
Range fluctuation σ_{rf} (Fig. 2-9):	0.1 ft
Angle fluctuation $\sigma_{\theta f}$ (Fig. 2-7):	60 μrad
Range rate bias $\sigma_{\dot{r}b}=v_t \sigma_{\theta b}$:	0.5 ft/sec
Range rate fluctuation $\sigma_{\dot{r}f}=v_t \sigma_{\theta f}$:	0.6 ft/sec
Angle rate fluctuation $\sigma_{\dot{\theta}}$ (Fig. 4-6):	4 μrad/sec

B. Ionospheric Components (normal ionosphere)

Operating frequency	2000	6000 mcps
Range bias Δr^i (Fig. 2-15):	10	1.1 ft
Range fluctuation σ_{r_i} (Fig. 2-25):	0.05	.006 ft
Angle bias δ^i (Fig. 2-16):	8	0.9 μrad
Ray error $\Delta\alpha_i$ (Fig. 4-4):	30	3.3 μrad
Range rate error $\sigma_{\dot{r}_i}=v_t\Delta\alpha_i$	0.6	.066 ft/sec

C. Total Error

Operating frequency	2000	6000 mcps
Range error σ_r	10	1.2 ft
Angle error σ_θ	78	78 μrad
RMS target position σ_p	310	310 ft
RMS target velocity σ_v	16	16 ft/sec

Significant error components:

Residual tropospheric range and angle bias
Ionospheric range bias (2000 mcps only)

Table 4-3. Typical Atmospheric Errors

Interferometer System (Mistram) on Satellite Track

A. Tropospheric Components (average weather)

Range bias ΔR_e (Fig. 2-2):	60 ft
Angle bias $\Delta\beta'$ (Fig. 2-5):	180 μrad
Range-difference bias (El. b'=1000 ft)	0.18 ft
Residual range bias σ_{rb} (Table 3-1):	0.3 ft
Range fluctuation σ_{rf} (Fig. 2-9):	0.1 ft

	Elevation	Azimuth
Effective baseline b' (position data):	1000	10,000 ft
Residual range-difference bias $\sigma_{\Delta rb}$:	.02	.06 ft
Residual angle bias $\sigma_{\theta b}$:	20	6 μrad
Range-difference fluctuation $\sigma_{\Delta rf}$ (Fig.2-7)	.014	.06 ft
Angle fluctuation $\sigma_{\theta f}$ (Fig. 2-7):	14	6 μrad

Table 4-3 (continued)

	Elevation	Azimuth
Effective baseline b' (velocity data):	10,000	100,000 ft
Range-rate difference fluctuation $\sigma_{\Delta \dot{r} f}$:	.006	.0014 ft/sec
Angle rate fluctuation $\sigma_{\dot{\theta} f}$ (Fig. 4-6):	0.6	0.14 μrad/sec

B. Ionospheric Components (normal ionosphere, f=10,000 mc)

Range bias Δr^i (Fig. 2-15):	0.2 ft	
Range fluctuation σ_{ri} (Fig. 2-15):	.001 ft	
Angle bias δ^i (Fig. 2-16):	0.16 μrad	
Ray error $\Delta\alpha_i$ (Fig. 4-4):	1.0 μrad	
Range rate error $\sigma_{\dot{r}i}$:	.01 ft/sec	
Ray difference error	0.1	0.3 μrad
Range rate difference error	.001	.003 ft/sec
Angle rate error	0.1	0.03 μrad/sec

C. Total Error

Range error σ_r	0.35 ft
Angle error σ_θ	25 μrad
RMS target position σ_p	100 ft
RMS target velocity σ_v	2.4 ft/sec

Significant error sources:
Tropospheric range bias
Tropospheric angle bias and fluctuation

Table 4-4. Typical Atmospheric Errors

Wide-Baseline Trilateration System on Satellite Track

A. Tropospheric Components (average weather)

Range bias ΔR_e (Fig. 2-2):	60 ft
Residual range bias σ_{rb} (Table 3-1):	0.3 ft
Range fluctuation σ_{rf} (Fig. 2-9):	0.1 ft
Geometrical dilution factor:	3
Equivalent angle bias $\sigma_{\theta b}$:	0.33 μrad
Equivalent angle fluctuation $\sigma_{\theta f}$:	0.11 μrad
Ray error bias $\sigma_{\alpha b}$:	2.5 μrad
Range rate bias $\sigma_{\dot{r}b}$:	.025 ft/sec
Equivalent angle rate bias $\sigma_{\dot{\theta}b}$:	.027 μrad/sec
Ray error fluctuation $\sigma_{\alpha f}$:	1.4 μrad
Range-rate fluctuation $\sigma_{\dot{r}f}$:	.014 ft/sec
Equivalent angle rate fluctuation $\sigma_{\dot{\theta}f}$:	.015 μrad/sec

B. Ionospheric Components (normal ionosphere)

	2000 mcps	6000 mcps
Range bias Δr^i (Fig. 2-15):	4.5	0.5 ft
Range fluctuation σ_{ri} (Fig. 2-25):	.03	.0033 ft
Equivalent angle bias $\sigma_{\theta b}$:	4.8	0.53 μrad
Equivalent angle fluctuation $\sigma_{\theta f}$:	.032	.0035 μrad
Ray error bias $\Delta\alpha_i$ (Fig. 4-4):	20	2.2 μrad
Range-rate bias $\sigma_{\dot{r}b}$:	0.2	.022 ft/sec
Equivalent angle rate bias $\sigma_{\dot{\theta}b}$:	0.22	.024 μrad/sec

Table 4-4 (continued)

C. Total Error

Frequency	2000 mcps	6000 mcps
Range error σ_r	4.5	0.6 ft
Equivalent angle error σ_θ	4.8	0.64 μrad
RMS target position σ_p	19	2.5 ft
RMS target velocity σ_v	0.9	0.15 ft/sec

Significant error components:

At 2000 mcps: Ionospheric range bias and ray error
At 6000 mcps: Ionospheric and tropospheric range bias and ray error (tropospheric is slightly greater than ionospheric at this frequency)

4.4 References

Barton, D. K., The Future of Pusle Radar for Missile and Space Range Instrumentation, IRE trans. MIL-5 No. 4, October 1961

Brown, D. C., On the Accuracies Attainable from Range Instrumentation for the Burnout Conditions to a Ballistic Missile, RCA (Patrick AFB) Data Reduction Report No. 44, March 21, 1958 (Astia AD 134276)

Iliff, W. R., and J. M. Holt, The Prediction of Total Atmospheric Refraction at Low Elevation Angles, URSI-IRE Meeting, April 30-May3, 1962, Washington, D. C.

McGavin, R. E., A Survey of the Techniques for Measuring the Radio Refractive Index, National Bureau of Standards Technical Note 99, May 1962.

5. CONCLUSIONS

5.1

Tropospheric bias errors are highly predictable using radiosonde or refractometer profiles; residual errors from 1% to 3% of the initial bias levels are commonly attained using procedures described in Section 3. Data to within one-half foot in range and 20 to 70 μradians in angle can be expected at elevation angles above five degrees.

5.2

Tropospheric fluctuation errors are not correctable using any known procedure, and will amount to a few tenths of a foot in range, and 10 to 50 μradians in angle (depending on the baseline or aperture used for measurement), under normal weather conditions.

5.3

The relationship between temporal and spatial correlation of tropospheric fluctuations has been investigated, based on data obtained by the National Bureau of Standards. The effect of short-period fluctuations is described by Figs. 2-7 and 2-8, and is consistent with a drift of tropospheric anomalies across a fixed measurement path at the speed of the prevailing wind.

5.4

In range instrumentation applications, where the beam is not fixed, the residual "bias" and long-term error components will change as the beam moves, and additional atmospheric rate errors will be generated, as shown in Fig. 4-6. These errors will be proportional to the tangential velocity of the missile, and will typically be five to fifty times the errors measured for a fixed beam.

5.5

The uncertainty in tropospheric path leads to errors equivalent to motion of the instrument on the ground. The

motion of the "virtual source" typically amounts to several feet normal to the path and a few tenths of a foot along the path.

5.6

Ionospheric errors are essentially unpredictable, and will exceed the residual tropospheric errors when operating frequencies below 3000 mcps are used. Even in the 5000-6000 mcps band the ionospheric errors will contribute to overall atmospheric error during daytime operation.

5.7

Redundant measurements performed at two frequencies below 3000 mcps can be used to correct for ionospheric error in both range and angle.

5.8

The lowest atmospheric errors are found in trilateration systems using very long baselines. Total position and velocity errors for a typical satellite track (660 miles range, 100 miles altitude) through average weather, are as follows:

	RMS Position Error (feet)	RMS Velocity Error (ft/sec)
Range-angle tracker at 6000 mcps	310	16
Interferometer, 10,000 mcps (Mistram)	100	2.4
Trilateration system,		
2000 mcps	19	0.9
6000 mcps	2.5	0.15

The above errors may be increased or decreased by a factor of two or three for different weather conditions (and at 2000 mcps for different ionospheric conditions). The trilateration errors shown are dependent upon perfect survey of station location, as well as instrumental errors below one-half foot in range and 0.02 ft/sec in range-rate.

6. RECOMMENDATIONS FOR ACHIEVING INCREASED ACCURACY TODAY

6.1

Since ionospheric refraction cannot at present be predicted to within better than about 50% of any instantaneous value, the use of microwave bands or of dual-frequency measurements is necessary in precision tracking of targets above 100 miles. Single frequency systems requiring velocity data better than one foot per second should operate above 3000 megacycles to minimize the ionospheric refraction effect.

6.2

A continuing program of data analysis at the various ranges should be instituted to evaluate and improve the atmospheric correction procedures described in Section 3. of this report. Some of this work is being done at AMR now (and perhaps at other Ranges) in connection with other activities. However this work is so important that it should be supported as a separate function; this is the only way it will receive the attention which it deserves. Data is available at all of the Ranges; it is only necessary that qualified people be assigned to an analysis of it. This work should be fully supported by the Air Force at its Ranges and by the other services at their respective Ranges. This data analysis conducted at each particular Range should be fully coordinated among the Ranges and with the NBS measurement program. Other interested agencies, such as NASA, should also be invited to participate. The Inter Range Instrumentation Group has done an excellent job in the past of providing coordination and dissemination of technical information among the Ranges on an informal basis and is well qualified to do so in this case. This coordination of effort, especially among the National Ranges, should receive the full support of DOD.

6.3

Standard procedures for atmospheric correction of tracking data should be adopted by all of the Ranges and Range users and estimates of residual bias errors agreed

upon for each procedure. The methods discussed in Section 3 of this Report are suggested as a basis for such Standards and are consistent with efforts now underway by the Electromagnetic Propagation Working Group of the Inter Range Instrumentation Group. The EPWG is currently working on a range instrumentation manual which it hopes will lead to more standardization. The work of the individual members of EPWG on this project should be given the full support of each particular Range where they are located and the project as a whole should have the complete support of DOD on an inter-range basis.

7. RECOMMENDED RESEARCH FOR FUTURE INCREASE IN ACCURACY

7.1

Future tracking systems should be designed to tolerate the unpredictable fluctuations of the measurement ray paths in the atmosphere. When targets of high velocity must be tracked with accurate three-coordinate velocity measurements, the measurement systems baselines should be as long as possible they should be consistent with target altitude. Systems which require that instrumentation sites be located with an accuracy on the order of one foot or better do not appear to be consistent with our ability to predict the ray paths in the troposphere.

7.2

A specific procedure for measuring and correcting tropospheric errors on a real-time basis has been proposed to the Panel. A brief discussion of this technique is given in Appendix B. Theoretically this technique appears very promising. It is now a question of determining whether experimental verification can be obtained. This work should receive full support from the Air Force.

7.3

The National Bureau of Standards (Boulder) has outlined a program of atmospheric measurements which it is attempting or would like to attempt. This program is discussed in Appendix C. These measurements would provide much needed data on spatial and temporal correlation of tropospheric range (or phase) errors. The Panel recommends that this program be pressed as rapidly as possible and fully supported by the Air Force to provide much needed information for both the interferometer systems and the longer baseline systems using range and range-rate data.

7.4

When tracking at interplanetary distances the errors imposed by the atmosphere become proportionally less. Consequently one limiting factor to tracking accuracy at such distances would appear to be the precision with which we

know the velocity of light, currently felt to be about 1 part per million. (A discussion of our knowledge of the velocity of light is given in the Report of the Ad Hoc Panel on Basic Measurements.) The efforts by the National Bureau of Standards to better determine this value should be fully supported.

7.5

With our current tracking techniques for interplanetary distances an even more critical need than a better determination of "c" is that of a better frequency standard. For doppler tracking a target over such distances a frequency standard or clock having a short time stability of 1 part in 10^{13} is needed now. (At the present time we can measure time with an accuracy of about 1 part in 10^{11}. This is discussed in the Report of the Ad Hoc Panel on Basic Measurements.) The continuing efforts of the National Bureau of Standards to develop more stable frequency standards should receive full support.

7.6

Since the accuracy limits of current tracking instruments and propagation correction procedures are on the order of about one foot, there is a definite need for geodetic systems or procedures capable of locating our tracking instruments or systems to this same accuracy over intercontinental distances It is recommended that a study group be convened to determine what are the most fruitful areas for investigation which could lead to a better determination of locations on a global basis and which ultimately perhaps might lead to the accuracy mentioned above.

8. FURTHER RECOMMENDATIONS

8.1

The Ranges should make the systems designers and/or Range users familiar with the basic limitations on tracking accuracy imposed by the atmosphere as described in this Report. It is futile for Range users to request accuracies which cannot be obtained for reasons discussed herein. And the Panel does not anticipate that significant improvement over the potential accuracies discussed here will be attained in the near future, although more consistent use of correction techniques will improve on past performance. However, if the research recommended in this Report is undertaken and adequately supported it may disclose means of reducing the basic uncertainties connected with propagation through the atmosphere which could be applied within the next decade.

8.2

In order to make the best use of the available resources for the development of instrumentation systems and techniques for propagation correction, the responsible agencies should arrive at consolidated requirements for missile and satellite measurement accuracies instead of new and different requirements for each individual program. The consolidated requirements should be stated and published in such a manner as to encourage scientific work on the most fundamental instrumentation problems, and should not be hampered by the security restrictions and "need-to-know" of any particular weapon or weapon system. This is a DOD wide problem and DOD should take the lead in trying to implement this. However, the Air Force could do much along this line with those programs under its cognizance.

Appendix A

OBSERVED ELEVATION ANGLE ERRORS

by

Dr. John B. Smyth
Smyth Research Associates

The smooth gross structure of the N profile causes errors which can be corrected if one knows the shape of the N profile, but the inhomogeneities cause an indeterminancy in the actual vehicle location which cannot be resolved. The principle concern in precision tracking is to correct for the gross effects (the bias errors) and to estimate as well as possible the magnitude of the random errors.

Smyth Research Associates, under contract to the Air Force*, are using a sea interferometer technique to measure the apparent position of satellites as they arise above the horizon over the Pacific Ocean. This experimental facility offers a high degree of resolution for sources near the horizon. Figure A-1 shows the location, a picture of one of the 45' by 70' antennas and a schematic of the experimental arrangement. Data obtained at this site have been used to evaluate the refraction of the ionosphere and troposphere as a function of elevation angle, α_o. Figures A-2 and A-3 give information on the average error angle at frequencies from 150 to 400 Mc for elevation angles between zero and ten degrees. The spread in the data is several milliradians, more-or-less independent of elevation angle. The reason for this is not completely clear, although it appears that a large part of this spread is in the uncertainty of the location of the satellite.

A comparison of observed and predicted elevation angle errors is given in Figure A-4.

---

*AF30(602)2084, Rome Air Development Center.

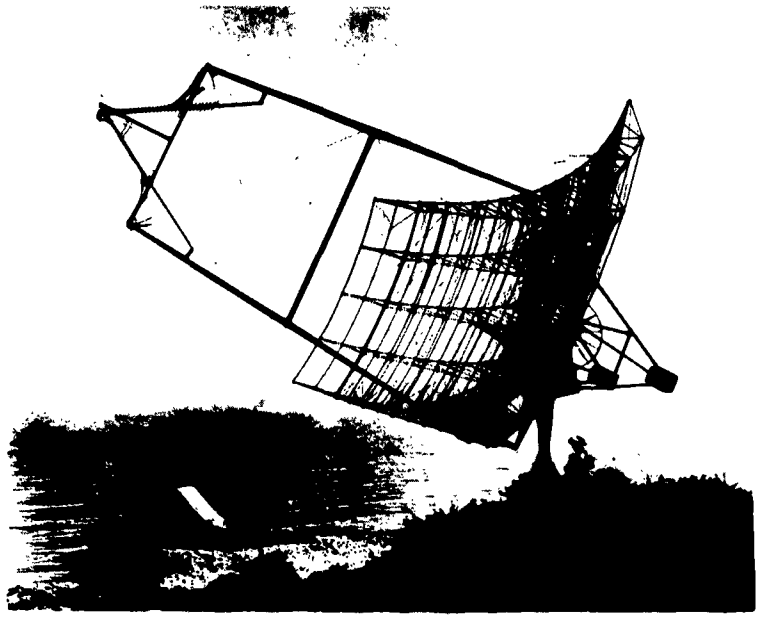

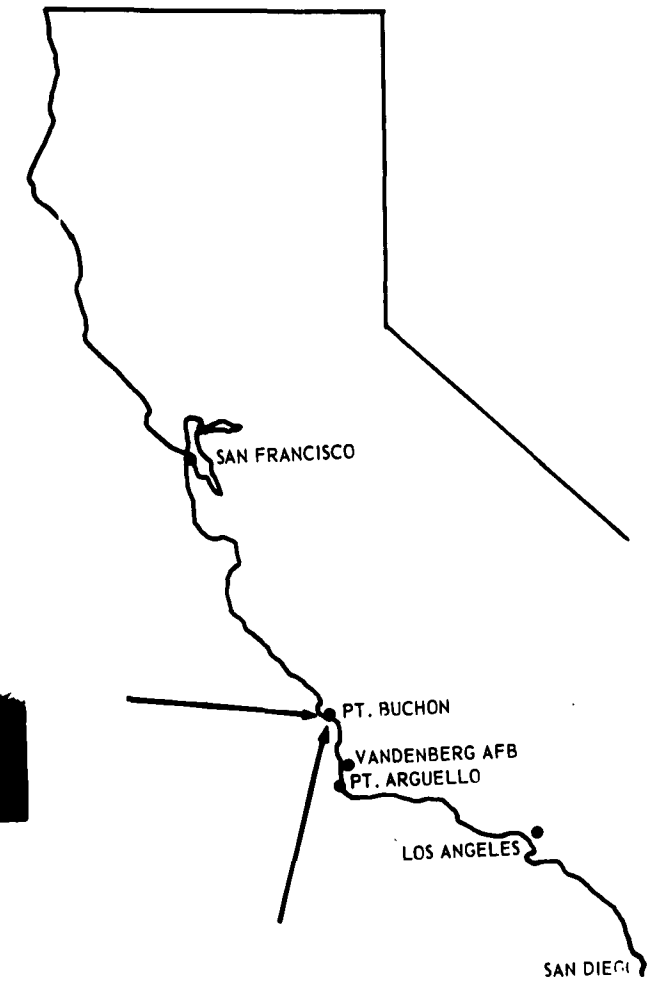

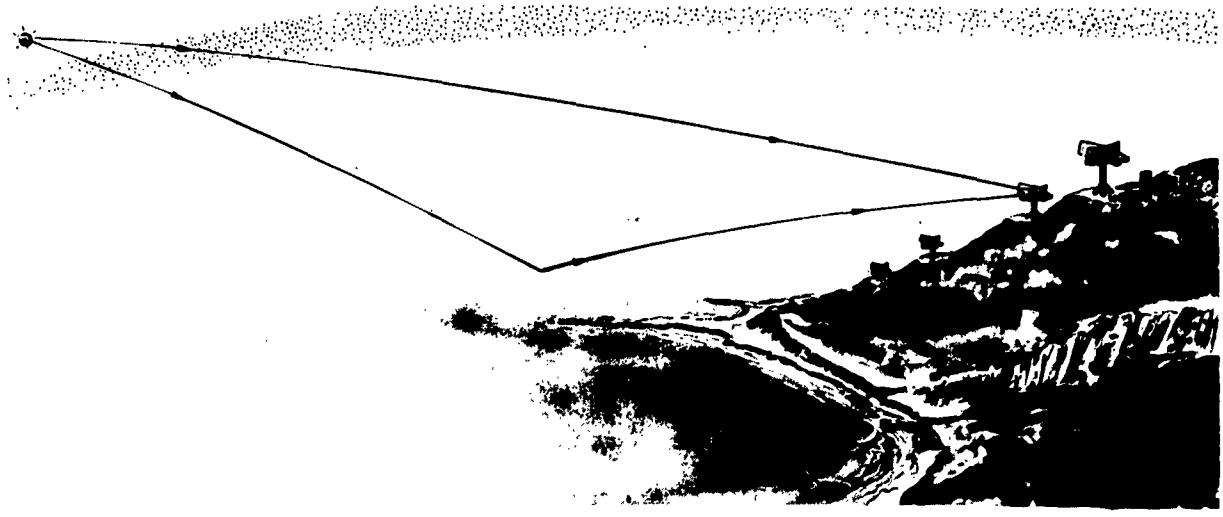

Figure A-1 Location of the SRA Point Buchon Field Station.

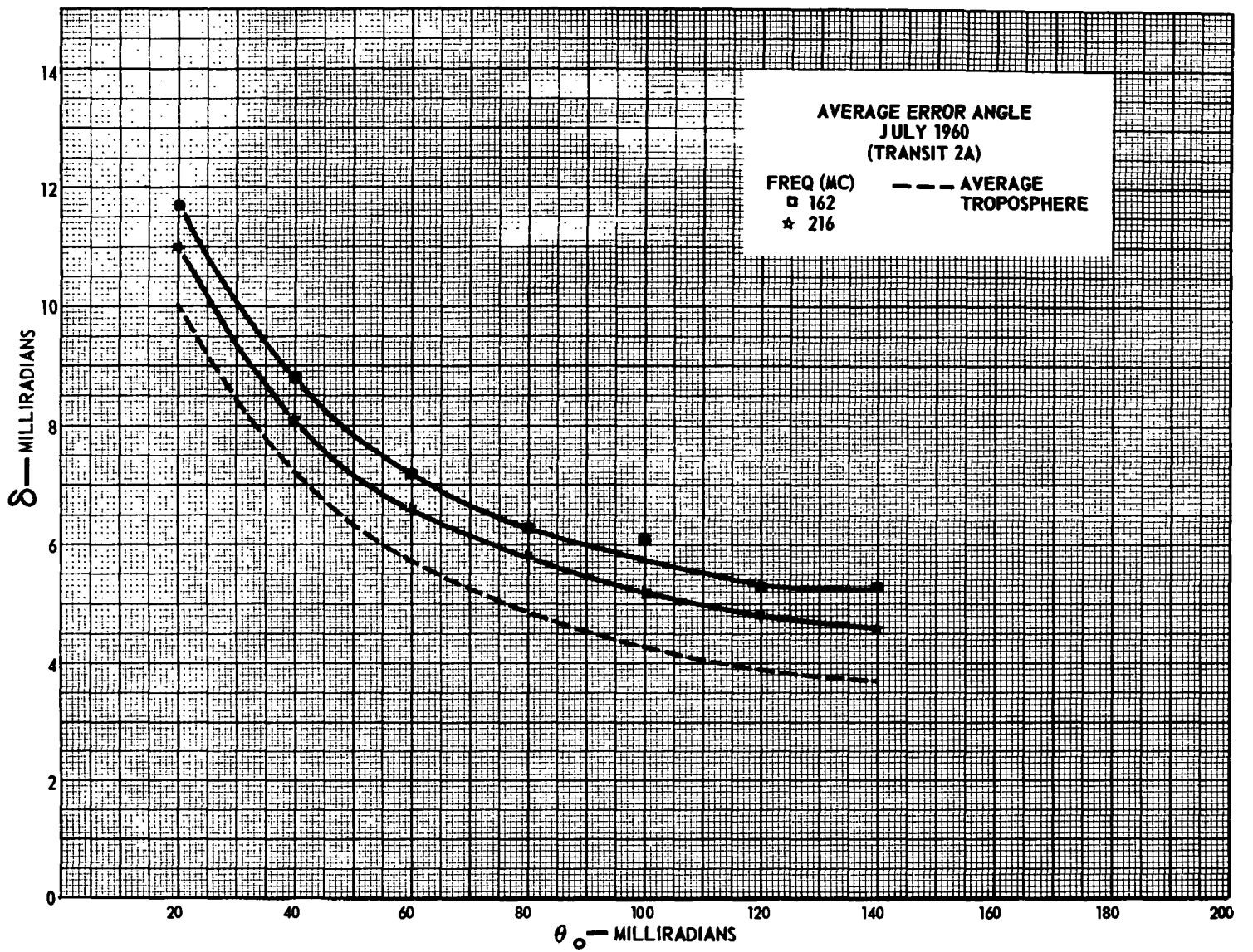

Figure A-2 Average error angle July 1960.

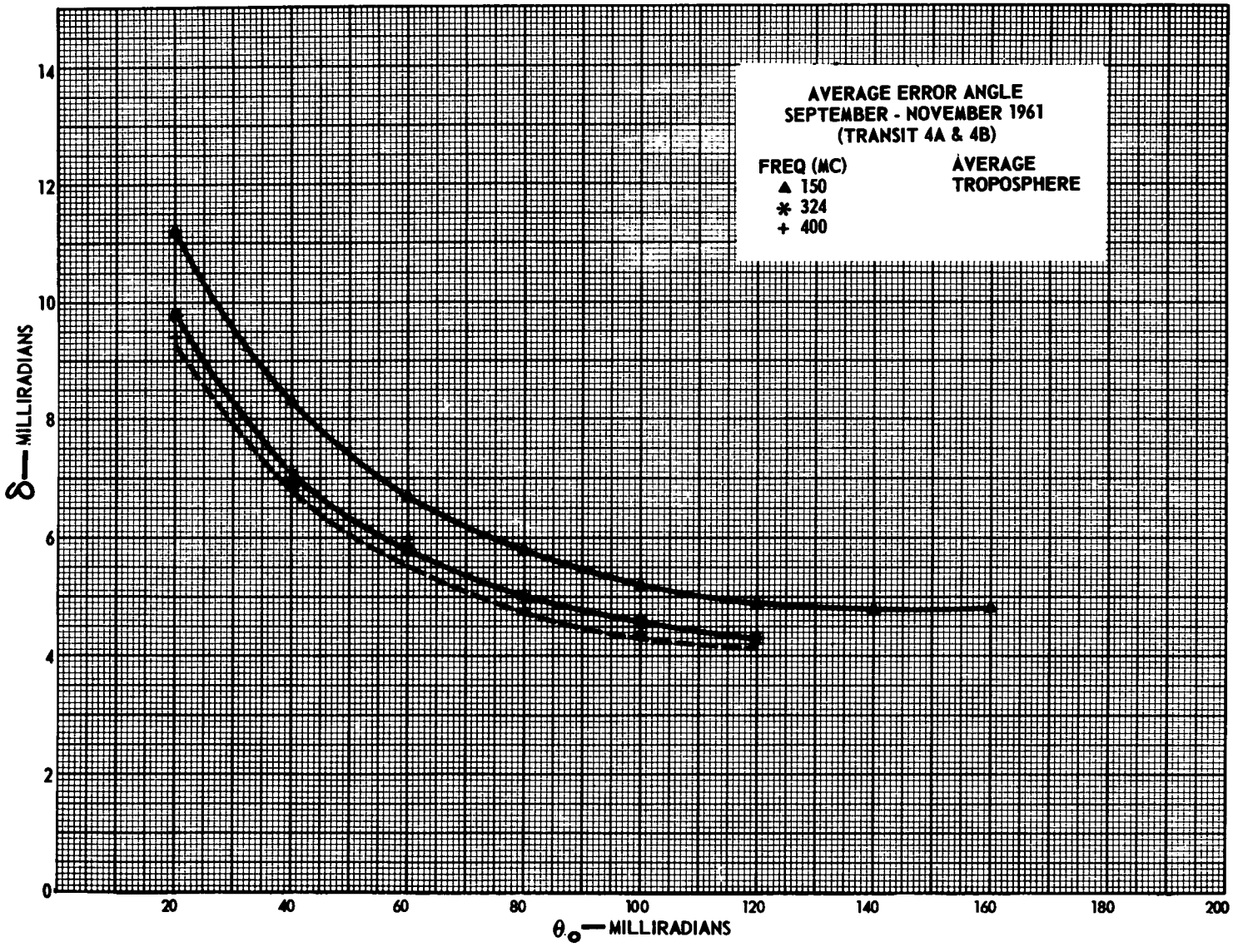

Figure A-3 Average error angle September and November 1961.

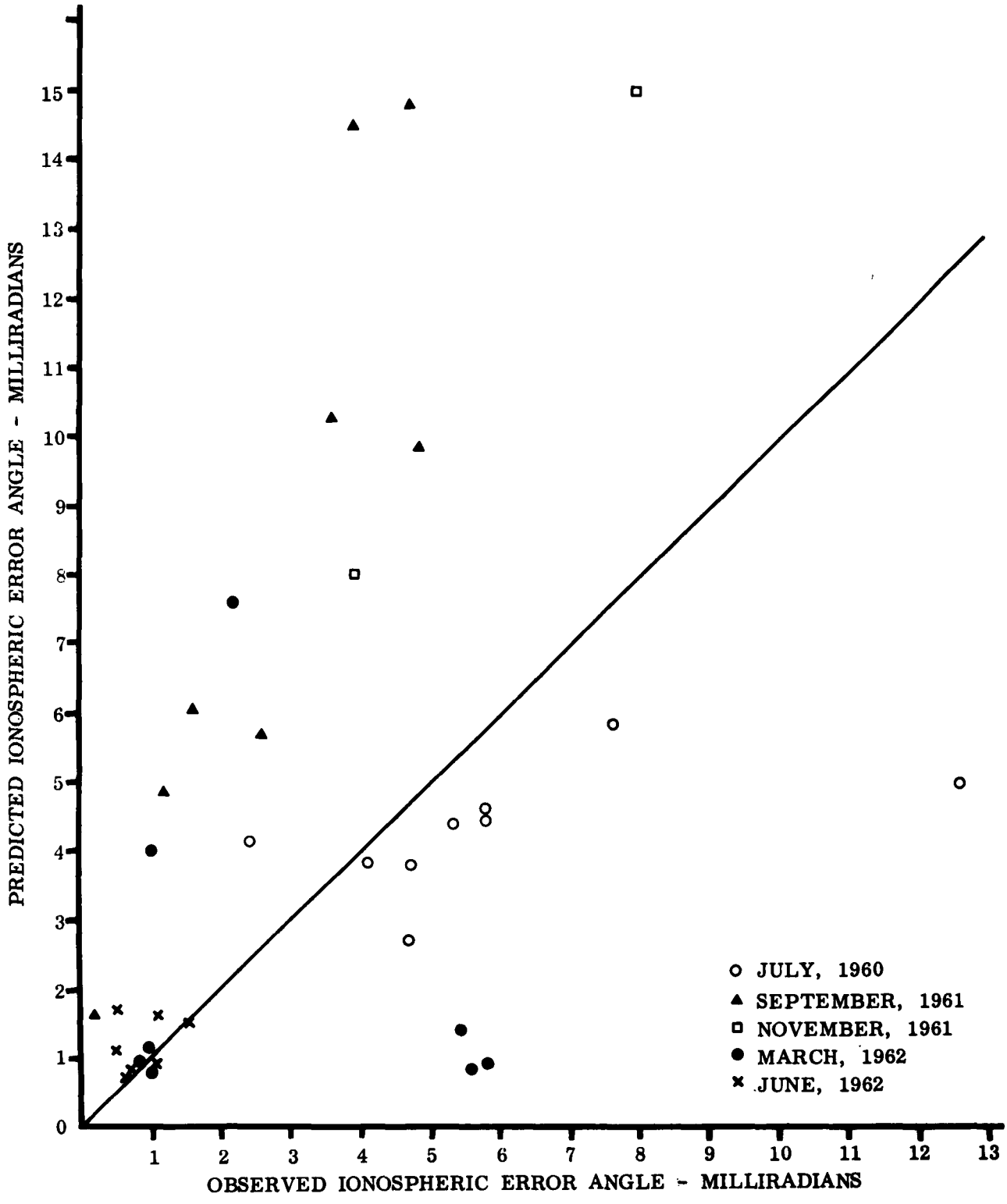
PREDICTED IONOSPHERIC ERROR ANGLE - MILLIRADIANS
OBSERVED IONOSPHERIC ERROR ANGLE - MILLIRADIANS
0
1
2
3
4
5
6
7
8
9
10
11
12
13
14
15
JULY, 1960
SEPTEMBER, 1961
NOVEMBER, 1961
MARCH, 1962
JUNE, 1962

Figure A-4

Appendix B

A LINE INTEGRAL REFRACTOMETER

by

John F. Sullivan
The Mitre Corporation

Introduction

This paper was prepared for the National Academy of Sciences Ad Hoc Panel on Electromagnetic Propagation, and is a report on the status of certain studies by the MITRE Corporation of the ultimate limitations on the accuracy and precision of microwave measurements imposed by the troposphere, and of techniques for correcting for its effect. The report is somewhat premature in that no experimental confirmation of the analyses is available, but since the subject is the committee's "raison d'etre" and the conclusions are somewhat at varience with current practice in this field, it is felt that a report should be presented for consideration.

Discussion of Problem

Essentially, the conclusion reached is that a measurement can be made in real time, over the path of interest, which will allow for the correction of the effects of a real turbulent atmosphere on position determinations. Residual errors remaining after such a correction have been estimated to be at least an order of magnitude down from present limitations in accuracy due to imperfectly known inhomogeneities and turbulence.

To illustrate this consider a ray traversing a path S between points P_1 and P_2 in a turbulent, inhomogeneous atmosphere, whose index of refraction is described by some scalar function, $n(x,y,z,t)$, of space and time. The elemental time (dt) required for a wave to traverse an elemental arc length (ds) along the ray is given by the expression:

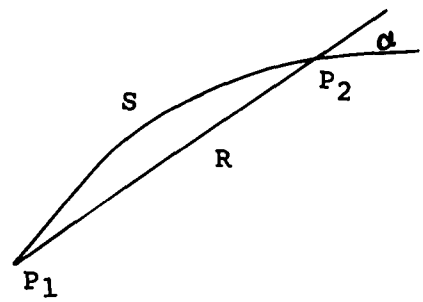

$$\frac{ds}{dt} = \frac{C}{n(x,y,z,t)} \qquad \text{(B-1)}$$

where C is the velocity of light in vacuum.

It is convenient to work with refractivity N defined by:

$$N(s,y,z,t) = n(x,y,z,t) - 1 \qquad \text{(B-2)}$$

By combining these expressions and integrating their results

$$S = C\Delta t - \int_s N(x,y,z,t)\,ds \qquad \text{(B-3)}$$

where Δt is the transit time as conventionally measured by electronic techniques.

This expression indicates that in order to know the arc length between two points in such an atmosphere, it is necessary to measure the transit time, multiply this by the vacuum velocity of light, and diminish the result by a quantity which represents the integrated effect of the slowing of the wave by the material atmosphere.

It is this latter quantity $\int_s N(x,y,z,t)\,ds$ which we propose to measure. Before discussing the method of measurement, however, it would be useful to examine the following implications of such a measurement:

1. To correct for the effect of a turbulent inhomogeneous atmosphere on an estimate of arc length (ds) from a conventional transit time measurement (Δt) it is only necessary to know this one time varying quantity ($\int_s N ds$). Present correction techniques assume some simple average spatial functional relationship of N(x,y,z). More or less sophisticated attempts are made to account for inhomogeneities and temporal variations of the medium by using this relationship to extrapolate from one or

interpolate between a relatively few measurements of point index of refraction. The estimate of $N(x,y,z,t)$ is based on previously measured data which becomes increasingly more expensive to obtain as the time and space intervals between data points is reduced. From this estimate, and its estimated gradient, rays are traced, and the quantity $\int_s N(x,y,z,t)ds$ is computed by some more or less complicated program. Here again, as the time interval between computer points decreases, the time and expense of the calculations required rapidly increases. It is, therefore, at least intuitively preferable to make a single measurement of the quantity $\int_s Nds$ in real time which can be simply subtracted, again in real time, from the transit time measurement multiplied by the velocity of light. No more sophisticated computation is necessary.

Until some experimental data upon which to base an error analysis is available, the above statements cannot be proven but the intuitive argument at least provides an incentive for looking for such a measurement technique. We are thinking in terms of an exceedingly accurate (about 1 part in 10^6) measurement of arc length. The basic measurement of transit time is more than capable of this kind of accuracy. It should be noted, however, that the measurement of the correction necessary to account for refraction need not be made to anything like this kind of percentage accuracy. Since refraction corrections typically amount to a few hundred parts per million, a measurement accuracy of slightly better than 1% is adequate.

2. Gradients in the index of refraction structure have the effect of bending the ray path. This bending causes the arc length S to differ from the straight line distance R between P_1 and P_2. It can be readily shown that this difference in length is completely negligible ($<1\times10^{-7}$) under normal atmospheric conditions unless the ray becomes trapped in a duct.

Thus, a direct measurement of the line integral of refractivity can give a significant improvement to measurements of range, and angles derived from range sum or range difference measurements, without a detailed knowledge of the refractive index structure.

3. From examination of the mathematical rules for the differentiation of an integral whose limits are functions of the variable of differentiation, one may conclude that from

a time derivative of this measurement $(\frac{d}{dt}\int_s N(x,y,z,t)ds$ one may obtain a real time correction for all of the refractive effects of the troposphere on the magnitude of doppler measurements. This correction would include the effect of turbulent variations of the medium, the effect of apparent variation in path length due to motion through a inhomogeneous medium, as well as the effect of the refractive index at the moving body. An angle (α) between the ray S and the straight line $P_1 P_2$ results from gradients in the refractive structure. From this measurement alone, however, one obtains no information on the effects of refraction on direction of the ray at the moving vehicle. The uncertainty in this angle is of significance in precision velocity determinations. Thus, for velocity measurements, this measurement alone does not completely account for refractive effects.

From the above considerations, it can be concluded that a device which would measure in real time the integrated effect of the slowing of electromagnetic waves by the troposphere could be useful in significantly reducing the effects of present limitations of knowledge of this region. This does not mean that there are no further limitations to the accuracies attainable, merely that they are different, and from our examination appear smaller. These include the difference between arc length and range previously noted and the deviations from simple ray theory upon which the foregoing discussion is based.

It would be rather fruitless to describe the improvements possible by means of a measurement without some conviction that such could be accomplished. We are working on a technique which we believe will ultimately provide the desired information. This work is in its early stages and much remains to be proven by means of equipment design as well as laboratory and field tests of the device. A number of detailed calculations have been performed which have led us to the conclusion that such an effort would be fruitful. While they have no place in this report, we would be happy to discuss them with those members who are interested in the details. What follows is intended to be descriptive of the technique proposed.

Proposed Technique

The radio index of refraction in any elemental volume of the atmosphere is considered as the sum of two parts; the dry,

or optical, part arising from the atomic refractivities of the gaseous constituents (N_2, O_2, A, etc.) weighted in accordance to their relative abundance; and the wet part, applicable only to radio and microwaves, arising from the permanent electric dipole moment of the uncondensed water vapor molecules present. At sea level and normal humidity the total index is about 300 N units ($N = (n-1) \times 10^6$) with about 60 N units of this total representing the "wet" contribution. The relative abundance of the various dry components is relatively constant throughout the atmosphere, while the water vapor density is quite erratic.

In the millimeter wave region molecular reasonances of water vapor and oxygen occur producing high absorption in the frequency region associated with the spectral lines. Because of the interest in microwave propagation, and the basic information on the structure of the molecules inherent in its parameters, this attenuation has been well explored both theoretically and experimentally. Associated with the resonances there is also a dispersion or variation of refractive index with frequency. These dispersions are extremely small (theoretically calculable to about .03 N units differential index across the 1.35 cm water vapor line, and 1.97 N units across the 60 kmc oxygen line, at sea level and normal temperatures and humidity). These values of dispersion are theoretical and have never been experimentally measured precisely. Measurements by Essen of total refractivity have been made at 9 kmc and 24 kmc and confirmed that the difference is less than .12 N units.

Assume that the small differential index of refraction between two frequencies (f_1 and f_2 for HOH, f_3 and f_4 for O_2) on either side of these spectral lines is proportional (at every point in the atmosphere) to the contributions of the wet and dry atmospheric constituents to the total refractive index. This assumption is valid if the frequencies involved are far enough away from the resonances so that collision broadening effects are negligible and temperature correction techniques (dependent upon the application) are emplyed.

This assumption can be expressed as:

$$N_1 - N_2 = K_{HOH} N_{HOH} \qquad N_3 - N_4 = K_{dry} N_{dry} \qquad \text{(B-4)}$$

where

N_1 = refractivity at f_1

N_2 = refractivity at f_2

N_3 = refractivity at f_3

N_4 = refractivity at f_4

K_{HOH}, K_{dry} = proportionality constants under assumption

N_{HOH} = Wet component of total refractivity

N_{dry} = Dry component of total refractivity

Consider, then, a system consisting of a transmitter which may be placed on a moving vehicle and a remote ground receiver

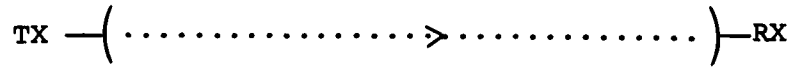

The transmitter radiates a CW wave which at some point in its plumbing may be expressed as:

$$A = A_1 \sin (2\pi f_1 t) + A_2 \sin (2\pi f_2 t) \qquad \text{(B-5)}$$

where f_1 and f_2 are harmonically related and locked in phase. At a remote receiver the phases of the two components of the wave received may be written from the wave equation:

$$\theta_1 = 2\pi f_1 \left(t - \int_s \frac{n_1(t,s)\ ds}{C}\right) \qquad \text{(B-6)}$$

$$\theta_2 = 2\pi f_2 \left(t - \int_s \frac{n_2(t,s)\ ds}{C}\right)$$

n_1 is very nearly equal at all points to n_2 so that both rays traverse essentially the same path. In the receiver the two components are separated, one component is multiplied by the frequency ratio, and the resultant phases compared in a phase detector. A voltage e_{HOH} will be produced.

$$e_{HOH} = \frac{K_1 C}{2\pi f_1}\left(\theta_1 - \frac{f_1}{f_2}\theta_2\right) = K_1 \int_s \left[N_1(t,s) - N_2(t,s)\ ds\right] \qquad \text{(B-7)}$$

where K_1 is the phase detector constant.

But, by the preceding assumption,

$$N_1(t,s) - N_2(t,s) = K_{HOH} N_{HOH}(t,s) \qquad \text{(B-8)}$$

$$\therefore e_{HOH} = K_1 K_{HOH} \int_s N_{HOH}(t,s)\, ds \qquad \text{(B-9)}$$

If a similar procedure is undertaken at frequencies f_3 and f_4 about the Oxygen line and the two voltages summed the result will be:

$$e_{TOT} = K_1 K_{HOH} \int_s N_{HOH}(t,s)\, ds + K_2 K_{dry} \int_s N_{dry}(t,s)\, ds \qquad \text{(B-10)}$$

$$e_{TOT} = K_3 \int_s N_{TOT}(t,s)\, ds \text{ (Upon proper adjustment of } K_1 \text{ and } K_2) \qquad \text{(B-11)}$$

This voltage is then directly proportional to the correction to the transit time measurement required to account for the effects of refractivity in the atmosphere over that particular path and at that particular time required by equation B-3

It should be noted that the transmission is unidirectional. The measurement is made of the quantity $\int_s N(x,y,z,t)$. A separate two-way transmission is required for the basic transit time measurement. (The treatment here represents an attack on the problem of clear air inhomogeneities and turbulence. Condensed water vapor in the form of rain and clouds will attenuate these frequencies and, more significantly, lack the gaseous in wave absorption lines. Analysis of this latter problem is continuing, but a solution to the clear air problem seems enough of a step forward to implement the necessary equipment.)

There are a number of equipment problems associated with the proposed measurement technique described, but a conclusion has been made that with care in design, a measurement of the extremely small phase differences can be accomplished. It would be well to state here, however, that the reason that the measurement is only formidable and not impossible is the fact

that it is a differential measurement. The same atmospheric path is traversed by the rays of both f_1 and f_2. Insofar as possible, f_1 and f_2 will traverse the same paths of the antennae, plumbing, transmitter, and receiver elements which will be designed to provide phase shifts linear with frequency (calibration techniques are anticipated to be required). Doppler effects (neglecting relativity) are proportional to frequency and cancel. Care must be exercised in the design of the antennae to reduce multipath to negligible proportions and preclude errors due to slight misalignment of antennae boresight.

Conclusion

An instrument can, therefore, be developed which will directly measure the integrated effect of the slowing of a radio wave through a real turbulent inhomogeneous atmosphere. This can be accomplished by the measurement of the small difference in one-way transit time between frequencies on either side of the microwave water vapor and oxygen absorption lines by the phase detector technique described. While a single measurement gives no indication of the bending of the ray which has occured, this can be shown to be a second order effect in the estimation of position.

Appendix C

PROPOSED EXPERIMENTAL STUDIES OF ATMOSPHERIC LIMITATIONS ON RADIO TRACKING ACCURACY

by

Harris B. Janes
National Bureau of Standards, Boulder

The following is an outline of some experimental research that should be undertaken to study the limitations imposed by the troposphere on line-of-sight radio ranging and tracking systems. This is not intended to be an exhaustive list of projects. In fact it is heavily weighted in the direction of those projects which constitute an extension of work performed by the National Bureau of Standards over a period of several years, and hence for which specialized equipment, techniques and personnel are available.

The proposed experimental work should be divided into two categories; "basic" and "applied". The basic atmospheric research consists of studying the four-dimensional statistics of the radio refractive index in the turbulent troposphere. This will be done first on a relatively modest scale with microwave refractometer sensors mounted on an orthogonal three-dimensional array on a very flat mesa near Boulder, Colorado. The purpose is to describe atmospheric turbulence in terms of the cross spectra between separated sensors as a function of separation, and the corresponding spatial correlation functions and wave number spectra for various conditions of wind velocity, solar radiation, etc. Future extensions of this work would include flying an array of refractometer sensors on a light aircraft to study the spatial structure as a function of altitude.

It is the second or "applied" research category that will probably be of most immediate interest to people concerned with missile tracking systems. In general it deals with tropospheric turbulence in terms of its effects on the accuracy of line-of-sight microwave ranging and angle measuring systems.

The experimental work in this category which we at NBS hope to undertake consists of three tasks; 1) the study of "bias" errors in range and range difference (angle) measurements, 2) the systematic study of atmospheric effects on baseline system accuracy as a function of baseline length, 3) the extension of these studies from the present X-band region (9.4 Gc/s) to K-band (22-24 Gc/s).

1. Although we have developed precision equipment to measure variations in the phase-of-arrival of X-band signals on the order of 0.1 degree (corresponding to a change in apparent range of .01 mm) relative to an arbitrary reference value, we cannot at present make absolute range or range difference measurements. Hence, although we have gathered a considerable amount of data at the upper end of the power spectrum (from about 1 cycle per hour to 10 c/s) we have not been able to look at the low frequency end of the spectrum, i.e., to measure the "biases" caused by relatively persistent atmospheric characteristics such as the vertical gradient of refractive index. The existing equipment should be modified to remove phase ambiguities so that the bias errors and short-term errors would be recorded simultaneously.

2. In designing a baseline tracking system, the baseline length is a parameter of utmost importance. However, except for the experiment performed by NBS in Hawaii in 1956, little has been done to study the atmospheric errors in range difference measurements as a function of baseline length. The Hawaii data lacked the long-term continuity necessary to study adequately the crucial low frequency end of the power spectrum of range difference variations. Subsequent improvements in the equipment make it possible to record range difference variations simultaneously on several baselines and continuously for periods of several days. This should be done systematically for baselines ranging in length from, say, two feet (of interest in geodetic angle-measuring applications) to as long as the experimental setup (terrain, target distance, etc.) will permit. The objective of this study would be a determination of the expected rms angular error versus baseline length with the possibility of determining optimum baseline lengths for various averaging times. It should be noted that refractometer measurements made at each end of the baseline may be used to reduce substantially the rms angular errors on the longer baselines. Measurement of the extent of this possible reduction is another objective of

the program. This study should include vertical (tower mounted) baselines as well as horizontal baselines to determine the relative merits of the two configurations, especially for measuring very small elevation angles.

3. Over the past several years, we have been gradually accumulating the necessary equipment to make range and range difference measurements at frequencies around 20 to 24 Gc/s. Such measurements would be potentially useful in determining the extent to which this frequency range with its higher phase resolution and greater immunity to multipath can be utilized in tracking systems. Also, it is contemplated that measurements will be made on a frequency in the range 10 to 12 Gc/s and simultaneously on its harmonic which will lie in the range 20 to 24 Gc/s. In this way it is hoped that some experimental data on the dispersive effect of water vapor can be obtained. It is also hoped that a refractometer can be developed for use in this higher frequency range. Such a refractometer would have a smaller cavity and thus be potentially useful for smaller-scale turbulence studies.